Effect of water and oxygen fugacity on tholeiitic basalt phase equilibria – an experimental study

Von der Naturwissenschaftlichen Fakultät

der Gottfried Wilhelm Leibniz Universität Hannover

zur Erlangung des Grades eines

DOKTORS DER NATURWISSENSCHAFTEN

Dr. rer. nat.

genehmigte Dissertation

von

Dipl.-Geow. Sandrin Tilman Feig

geboren am 25.05.1976 in Freiburg

2007

Referent: PD Dr. Jürgen Koepke

Korreferent: Prof. Dr. Jonathan E. Snow

Tag der Promotion: 13. April 2007

Erklärung zur Dissertation

Hierdurch erkläre ich, dass die Dissertation „Effect of water and oxygen fugacity on tholeiitic basalt phase equilibria – an experimental study" selbstständig verfasst und alle benutzten Hilfsmittel sowie evtl. zur Hilfeleistung herangezogene Institutionen vollständig angegeben wurden.

Die Dissertation wurde nicht schon als Diplom- oder ähnliche Prüfungsarbeit verwendet.

Hannover, den 11.01.2007

Sandrin Tilman Feig

Abstract

To investigate the effect of water on phase relations and compositions in a basaltic system, crystallization experiments in internally heated pressure vessels at pressures of 100, 200 and 500 MPa in a temperature range of 940 to 1220°C were performed. In the experiments, the water content of the system was varied from "nominally dry" to water-saturated conditions. Depending on the water activity, the oxygen fugacity varied between 1 and 4 log units above the quartz-magnetite-fayalite buffer (QFM+1 to QFM+4). To investigate the influence of oxygen fugacity and the interplay between redox conditions and water activity on the phase equilibria of the system, two additional sets of experiments with different nominal oxygen fugacities (QFM-1 to QFM+2 and QFM-3 to QFM) at a pressure of 200 MPa were performed. Thus, the whole investigated range in oxygen fugacity covers ~ 7 log units. The oxygen fugacity of the experiments was measured using the H_2-membrane technique.

Addition of water to the dry system shifts the solidus > 250°C to lower temperatures and increases the amount of melt drastically. For instance, at 1100°C and 200 MPa, the melt fraction increases from 12.5 wt% at a water content of 1.6 wt% to 96.3 % at a water content of 5 wt% in the melt. The compositions of the experimental phases also show a strong effect of water. Plagioclase is shifted to higher anorthite contents by the addition of water. Olivine and clinopyroxene show generally higher MgO/FeO ratios with added water, which is mainly related to the increasing in melt fraction with water. The addition of water could also change the crystallization sequence in a basaltic system. At 100 MPa, plagioclase crystallizes before clinopyroxene at all water contents. At pressures > 100 MPa, plagioclase crystallizes before clinopyroxene at low water contents (e.g. < 3 wt%), but after clinopyroxene at H_2O in the melt > 3 wt%. Moreover, water affects the partitioning of certain elements between minerals and melts, e.g., the Ca partitioning between olivine and melt.

Beside the effect of water, systematic effects of the oxygen fugacity on the stability and composition of the mafic silicate phases, Cr-spinel and Fe-Ti oxides under varying water contents were recorded. The Mg# of the melt, and therefore also the Mg# of olivine and clinopyroxene changes systematically as a function of oxygen fugacity. An example for the interplay between oxygen fugacity and water activity is the change in the crystallization sequence (olivine and Cr-spinel) due to a change in the oxygen fugacity caused by an increase in the water activity. The stability of magnetite is restricted to highly oxidizing conditions. The absence of magnetite in most of the experiments allows determining differentiation trends as a function of oxygen fugacity and water content demonstrating that in an oxide-free crystallization sequence water systematically affects the differentiation trend, while oxygen fugacity seems to have a negligible effect.

The characteristic change in the order of crystallization with water (plagioclase/clinopyroxene) may help to explain the formation of wehrlites intruding the lower oceanic crust (e.g., in Oman, Macquarie Island). This change in crystallization order indicates that a paragenesis typical for wehrlites (olivine - clinopyroxene - without plagioclase) is stabilized at low pressures typical of the oceanic crust only at high water contents. This opens the possibility that typical wehrlites in the oceanic crust can be formed by the fractionation and accumulation of olivine and clinopyroxene at 1060 °C and > 100 MPa in a primitive tholeiitic basaltic system containing more than 3 wt% water.

The comparison of the experimental results with evolution trends calculated by the thermodynamic models "MELTS" and "Comagmat" shows that neither model predicts the experimental phase relations with sufficient accuracy.

Zusammenfassung

In dieser Arbeit wurde der Einfluss von Wasser und Sauerstofffugazität (fO$_2$) auf die Phasenbeziehungen und die Phasenchemie eines tholeiitischen Basalts experimentell untersucht. Zur Bestimmung des Einflusses von Wasser wurden Kristallisationsexperimente in einer intern beheizten Gasdruckanlage bei Drücken von 100, 200 und 500 MPa in einem Temperaturbereich von 940-1220°C durchgeführt. Für jede untersuchte Temperatur wurden Wassergehalte von nominell trocken bis wassergesättigt eingestellt. Die fO$_2$ in diesen Experimenten variiert, in Abhängigkeit von der eingestellten Wasseraktivität, zwischen 1 und 4 log Einheiten oberhalb des Quarz-Magnetit-Fayalit Puffers (QFM+1 bis QFM+4). Zur Untersuchung des Einflusses verschiedener fO$_2$ und der Wechselwirkungen zwischen Redox-Bedingungen und Wasseraktivität auf die Phasengleichgewichte wurden zwei weitere experimentelle Reihen bei unterschiedlichen fO$_2$ (QFM-1 bis QFM+2 und QFM-3 bis QFM) und einem Druck von 200 MPa durchgeführt. Damit umfasst der untersuchte Redox-Bereich 7 log Einheiten.

Die Zugabe von Wasser zu einem trockenen tholeiitischen Basalt senkt dessen Solidus um mehr als 250°C ab und erhöht den Schmelzanteil bei einer gegebenen Temperatur drastisch. Bei 1100°C und 200 MPa zum Beispiel steigt der Schmelzanteil von 12,5% bei einem Wassergehalt von 1,6 Gew% auf 96,3% bei einem Wassergehalt von 5 Gew% in der Schmelze. Zusätzlich zu dem Einfluss auf den Schmelzpunkt und den Schmelzanteil des Systems werden auch die Stabilität und die Zusammensetzungen der experimentellen Phasen sowie die Kristallisationsreihenfolge stark vom Wassergehalt beeinflusst. Plagioklas zeigt grundsätzlich höhere Anorthit-Gehalte mit Wasser im System. Olivin sowie Klinopyroxen und Orthopyroxen zeigen höhere MgO/FeO Verhältnisse bei einer gegebenen Temperatur, was jedoch hauptsächlich durch den höheren Schmelzanteil, sowie durch die Änderung der

fO$_2$ mit Wasser im System erklärt werden kann. Eine Änderung in der Kristallisationsreihenfolge von Plagioklas und Klinopyroxen kann beim Vergleich zwischen niedrigen und hohen Wassergehalten beobachtet werden. Während Plagioklas bei einem Druck von 100 MPa (maximale Wasserlöslichkeit 3 Gew%) sowie bei Wassergehalten unter 3 Gew% bei höheren Temperaturen als Klinopyroxen kristallisiert, ist es bei höheren Wassergehalten umgekehrt. Weiterhin wurde auch ein Effekt von Wasser auf Verteilungskoeffizienten, wie zum Beispiel der Verteilung von Calcium zwischen Olivin und der umgebenden Schmelze, nachgewiesen.

Neben dem Einfluss von Wasser konnten auch systematische Effekte, basierend auf einer Änderung der fO$_2$ sowie Wechselwirkungen zwischen den Redox-Bedingungen und der Wasseraktivität, auf die Stabilität und die Zusammensetzung mafischer Mineralphasen, Cr-Spinelle und Fe-Ti Oxide bestimmt werden. Die fO$_2$ beeinflusst die Mg# (molar, MgO/(MgO+FeO) $\times$ 100) der Schmelze und damit auch die Mg# von Olivin sowie Klinopyroxen und Orthopyroxen, die im Gleichgewicht mit ihr stehen. Die fO$_2$ verändert somit ihre Zusammensetzung. Die Wechselwirkungen zwischen Redox-Bedingungen und der Wasseraktivität führen hingegen zu einer Änderung in der Kristallisationsreihenfolge von Olivin und Cr-Spinell, hervorgerufen durch eine Änderung in der fO$_2$ durch eine Erhöhung der Wasseraktivität. Magnetit tritt in dem untersuchten tholeiitischen System als einzige Fe-Oxid Phase auf und ist nur unter oxidierenden Bedingungen stabil. Das Fehlen von Magnetit in einem Großteil der Experimente ermöglicht die Bestimmung von Differenzierungstrends in Abhängigkeit vom Wassergehalt und der fO$_2$ in einer Oxid-freien Kristallisationsabfolge. Die Experimente zeigen einen deutlichen Einfluss des eingestellten Wassergehalts auf den Differenzierungstrend. Ein Effekt durch die eingestellte fO$_2$ auf den Differenzierungstrend konnte nicht beobachtet werden.

Die charakteristische Änderung in der Kristallisationsreihenfolge von Plagioklas und Klinopyroxen durch Wasser im System könnte helfen, die Bildung von Wehrlit-Intrusionen in der ozeanischen Kruste zu erklären (z.B. im Oman oder Macquarie Island). Der Wechsel in der Kristallisationsreihenfolge zeigt, dass die Wehrlit-Paragenese (Olivin und Klinopyroxen ohne Plagioklas) unter Drücken, die typisch für die Bildung der ozeanischen Kruste sind (bis zu 500 MPa), nur bei hohen Wassergehalten möglich ist. Die Experimente zeigen, das typische Wehrlit-Intrusionen durch Akkumulation und Fraktionierung von Olivin und Klinopyroxen bei ~ 1060°C und einem Druck von mehr als 100 MPa von einem primitiven tholeiitischen Basalt, der mehr als 3 Gew% Wasser enthält, gebildet werden können. Ein Vergleich der experimentell bestimmten Phasengleichgewichte mit Entwicklungstrend, die mit Hilfe der thermodynamischen Modelle „MELTS" und „Comagmat" berechnet wurden, zeigen, dass keines der beiden Modelle die bestimmten Phasengleichgewichte mit ausreichender Genauigkeit vorhersagen kann.

Schlagworte: Tholeiitischer Basalt, Wasser, Sauerstofffugazität, Gleichgewichtskristallisation, Phasengleichgewichte

Danksagung

Die vorliegende Arbeit wurde am Institut für Mineralogie der Gottfried Wilhelm Leibniz Universität Hannover unter der Leitung von Herrn PD Dr. Jürgen Koepke und Herrn Prof. Dr. Jonathan E. Snow (Department of Geosciences, University of Houston) angefertigt. Beiden möchte ich für die hervorragende Zusammenarbeit und Betreuung danken.

Ein großes Dankeschön geht an Otto Diedrich für die hervorragende Präparation der zahlreichen Dünnschliffe, sowie an Willi Hurkuck und Bettina Aichinger für die technische Unterstützung.

Bei Prof. Dr. Marcus Nowak, Prof. Dr. Francois Holtz, meinem „Mitbewohner" Kai Spickenbom, Holger Strauß und Dr. Renat Almeev möchte ich mich für viele hilfreiche Diskussionen und Tipps bedanken. Außerdem geht mein Dank an Prof. Dr. Harald Behrens, Dr. Roman Botcharnikov, Dr. Fleurice Parat, Jan St, Magnus, Jan Sc, Olli, Severine, Francesco und Piero.

Großer Dank geht auch an meine Familie, die durch ihre Unterstützung diese Arbeit erst ermöglicht hat, sowie an Bettina und Maja deren langjährige Freundschaft mir sehr viel bedeutet.

Table of Contents

1. Effect of water on tholeiitic basalt phase equilibria – an experimental study under oxidizing conditions*

1.1. Introduction

Water plays an important role in several aspects of seafloor magmatic processes. For a long time, it was considered that crystallization at mid-ocean ridges takes place under nearly "dry" conditions. During the last decade, improvements in analytical techniques have made it possible to determine small amounts of water in quenched MORB glasses (e.g., Kovalenko et al. 2000), in glass inclusions (e.g., Danyushevsky et al. 2000; Saal et al. 2002; Sobolev and Chaussidon 1996) and even in nominally dry minerals of the upper mantle (e.g., Bell and Rossman 1992; Hirschmann et al. 2005). Small amounts of water (< 1 wt %) may have a significant effect on MORB petrogenesis (Danyushevsky 2001), from partial melting of the mantle to fractionation (Asimow and Langmuir 2003). Moreover, it is well-known that water plays a significant role in late-stage magmatic processes during ocean crust formation, since water can be enriched during differentiation resulting in the formation of typical interstitial amphiboles (e.g., Coogan et al. 2001; Tribuzio et al. 2000). Finally, recent papers show that very high temperature (1200°C) hydrothermal activity triggers hydrous melting processes (Boudier et al. 2005; Koepke et al. 2005c; Koepke et al. 2004; Nicolas et al. 2003). Therefore, it is important to quantify the role of water both on the phase equilibria and on the mineral and melt compositions in MORB-type systems.

In this study, we present new crystallization experiments on a tholeiitic basalt composition from the Southwest Indian Ridge (SWIR). We systematically varied the water content and the pressure from near-surface conditions to those expected in the upper mantle at a slow-spreading ridge (e.g. shipboard scientific party, 2004).

The experiments vary in oxygen fugacity (fO$_2$) between QFM+1 to QFM+4 (QFM: quartz-magnetite-fayalite buffer), which is in general more oxidized compared to typical mid-ocean ridge conditions. The oxygen fugacity of erupted primitive MORB melts vary between QFM +1 to QFM -2 (Bezos and Humler 2005; Christie et al. 1986). Thus, direct comparison between these results and cogenetic MORB suites is not straightforward. However it is true that in drilled cumulate sections, the abundance of oxide gabbros (e.g. Natland and Dick 2002; Natland et al. 1991) suggests that more oxidizing conditions may characterize the middle crust than the mantle sources. This experimental investigation shows for the first time the systematic effect on the water and shallow pressure dependence of phase equilibria in a primitive tholeiitic basaltic system under fO$_2$ conditions, corresponding to the upper level of redox conditions known from nature. A second phase equilibria study in the same system under more reducing conditions QFM+2 (QFM+2 to -1, depending on the water activity) and QFM (QFM+0 to -3, depending on the water activity) is in progress.

1.1.1. Previous experimental work

Most of the experiments in tholeiitic basaltic systems thus far were performed at 1 atm (e.g. Grove and Baker 1984; Grove and Bryan 1983; Juster et al. 1989; Sano et al. 2001; Thy et al. 1998; Thy et al. 1999), revealing the well-known crystallization sequence of MORB. Further experiments were performed in gas mixture furnaces at 1 atm to identify the effect of different redox conditions on the chemistry of the experimental products (e. g., Snyder et al. 1993; Toplis and Carroll 1995). These experiments show that mainly the stability and the composition of iron-bearing phases (e. g., olivine, clinopyroxene and magnetite) are affected by the oxygen fugacity.

On the other hand, experiments in water-bearing systems under shallow pressures are limited in number. The first water-bearing phase equilibria experiments on tholeiitic basalts under

pressures below 500 MPa showed that the formation of quench-crystals during cooling was almost unavoidable (e.g. Eggler and Burnham 1973; Hamilton et al. 1964; Helz 1973; Helz 1976; Holloway and Burnham 1972). Such experiments do not allow adequate analyses of the glass phase, and it is very difficult to distinguish between quench- and equilibrium-crystallization. To reach higher quenching rates, a rapid quench system was developed for internally heated pressure vessels (Berndt et al. 2002; Holloway et al. 1992; Roux and Lefevre 1992), which allowed the experimental melts to be quenched to homogeneous glasses.

Most experiments on water-bearing tholeiitic basalts are typically carried out at water-saturated conditions. Sisson and Grove (1993a; 1993b) conducted experiments in a calc-alkaline system under water-saturated conditions at 200 MPa. Spulber and Rutherford (1983) performed experiments in a MORB system from the Galapagos Spreading Center. There are also experiments at reduced water activities like Holloway and Burnham (1972) who studied a tholeiitic basalt from the Kilauea volcano and Kawamoto (1996) who performed experiments in a calc-alkaline system at a water activity < 1. All these authors observed a strong effect of water on phase relations in the system. Aside from general effects like the stability of water-bearing phases (e.g. amphibole), effects on element partitioning were observed as well (Sisson and Grove 1993a; Sisson and Grove 1993b). Gaetani et al. (1993; 1994) investigated experimentally a basaltic andesite system under dry and water-saturated conditions (200 MPa). They found that the crystallization order in a dry system is olivine – plagioclase – clinopyroxene, while it is changed in a water-saturated system to olivine – clinopyroxene – plagioclase.

Due to the fixed water content in most of the studies mentioned above, systematic effects of water on the phase equilibria and phase compositions could not be determined. The only experimental study where the water content was varied systematically under crustal pressure was conducted by Berndt et al. (2005). In their study, they added different amounts of water to a synthetic glass corresponding to a primitive MORB and constructed phase diagrams for

the system at 200 MPa. With decreasing temperature the water content in the melt increases dramatically, due to ongoing crystallization. At low temperatures all experiments were water-saturated. They observed a strong effect of the water activity and the water content of the system on the phase relations, phase chemistry and on the element partitioning. Furthermore, they showed that water has the ability to control differentiation trends.

1.2. Experimental techniques

As capsule material, gold (at temperatures <1060°C) and $Au_{80}Pd_{20}$ (at higher temperatures) were used. XH$_2$O [molar H$_2$O/(H$_2$O+CO$_2$)] of the fluid phase was varied. In each experimental run, four different XH$_2$O were applied: 0.0 (nominally dry), 0.2, 0.6, and 1.0 (water-saturated). All experiments except the nominally dry were fluid-saturated. XH$_2$O of 0.2 and 0.6 are fixed via mixtures of water and silver oxalate ($Ag_2C_2O_4$). We assume that CO_2 does not play an important role as chemical component in this system. For each run 10 to 40 mg of starting glass powder (pre-dried), and the desired amounts of water (using a micro syringe) and silver oxalate were transferred into the capsule. For the "nominally dry" runs, only glass powder was inserted into the capsule. These filled capsules were dried at 500°C for ten minutes.

All experiments were performed in a vertically mounted internally heated pressure vessel (IHPV), equipped with a rapid quench system to prevent the formation of quench-crystals (Berndt et al. 2002; Holloway et al. 1992; Roux and Lefevre 1992), using pure argon as pressure medium. A detailed description of the apparatus is given by Berndt et al. (2002). All experiments were performed at an oxygen fugacity corresponding to the MnO-Mn$_3$O$_4$ buffer. Depending on aH$_2$O, the fO$_2$ of the experiments varies between ~ QFM+1 and QFM+4.2, which is in the upper level of the redox conditions known from nature (Bezos and Humler

2005; Christie et al. 1986). To apply this study to magma chamber processes of mid-ocean ridges, pressure conditions of 100, 200 and, taking into account the thick lithosphere at slow spreading ridges, 500 MPa were selected in the study. Additionally, the experiments at three different pressures also allow determining the effect of water as a function of pressure. To construct phase diagrams, experiments in the temperature range 940 - 1220 °C were performed. The temperature was measured with four S-type thermocouples, showing a gradient of less than 4°C along the sample and an uncertainty less than ±10°C. The experimental conditions for each run are listed in Table 1.1.

After quenching, each capsule was weighed to check for leaks and then, punctured and immediately weighed again to check if CO_2 was present in the capsule. To check if water was present, the punctured capsule was dried at 130 °C and weighed again.

Table 1.1: Conditions and phases of the performed experiments

Run	Pressure [MPa]	Temperature [°C]	Duration [h]	H$_2$O in the melt [wt%][1]	aH$_2$O[2]	log fO$_2$[3]	ΔQFM	Phases[4]	ΣR²[2]	K$_D$ Ol-melt/Fe-Mg[5]
#1	203.1	1100±4	30	5.0	1.00	-5.21	+4.14	Ol(2.8), Cr-sp(0.9), glass(96.3)	0.13	0.33
#2	203.1	1100±4	30	2.9	0.49	-5.83	+3.52	Ol(9.9), Plag(24.6), Cpx(13.8), glass(51.8)	0.35	0.34
#3	203.1	1100±4	30	1.9	0.30	-6.26	+3.09	Ol(12.0), Plag(43.3), Cpx(21.2), Mag(0.7), glass(22.8)	0.02	0.35
#5	203.1	1100±4	30	1.6	0.23	-6.49	+2.86	Ol(12.3), Plag(51.4), Cpx(22.9), Mag(0.9), glass(12.5)	0.02	0.36
#6	200.5	1180±2	30	4.9	1.00	-4.19	+4.17	glass(100.0)	6)	
#7	200.5	1180±2	30	3.0	0.54	-4.72	+3.64	Cr-sp, glass		
#8	200.5	1180±2	30	2.1	0.31	-5.20	+3.16	Ol(1.7), Cr-sp(0.4), glass(98.0)	0.45	0.46
#9	200.5	1180±2	30	0.8	0.06	-6.65	+1.71	Ol(3.1), Cr-sp(1.6), glass(95.4)	1.89	0.38
#10	202.7	1060±3	30	5.1	1.00	-5.77	+4.13	Ol(6.2), Cpx(1.9), Cr-sp(0.7), glass(91.2)	0.01	0.34
#11	202.7	1060±3	30	2.8	0.48	-6.41	+3.49	Ol(11.4), Plag(31.9), Cpx(18.3), Mag(0.6), glass(37.9)	0.00	0.37
#12	202.7	1060±3	30	n.a.	--	--	--	Ol, Plag, Cpx, Opx, Mag, glass	6)	
#13	202.7	1060±3	30	n.a.	--	--	--	Ol, Plag, Cpx, Opx, Mag, glass	6)	
#14	201.9	1140±3	30	4.9	1.00	-4.68	+4.16	Cr-sp(1.3), glass(98.7)	0.36	
#15	201.9	1140±3	30	2.8	0.46	-5.35	+3.49	Ol(4.0), Cr-Sp(0.8), glass(95.2)	0.09	0.38
#16	201.9	1140±3	30	1.7	0.24	-5.91	+2.93	Ol(10.7), Plag(26.1), Cpx(8.8), glass(54.4)	0.09	0.39
#17	201.9	1140±3	30	1.5	0.20	-6.10	+2.75	Ol(11.2), Plag(31.8), Cpx(13.5), glass(43.4)	0.31	0.42
#18	203.0	1220±2	20	1.9	0.28	-4.82	+3.08	Cr-sp(0.6), glass(99.4)	0.10	
#19	203.0	1220±2	20	1.2	0.13	-5.47	+2.43	Cr-Sp(0.7), glass(99.3)	0.22	
#20	203.0	1220±2	20	0.6	0.04	-6.57	+1.33	Ol(1.4), Cr-Sp(1.0), glass(97.6)	0.94	0.33
#21	201.8	1160±2	24	4.9	1.00	-4.44	+4.16	Cr-sp(0.6), glass(99.4)	0.30	
#22	201.8	1160±2	24	3.1	0.55	-4.95	+3.64	Ol(2.9), Cr-sp(1.2), glass(95.9)	0.34	0.47
#23	201.8	1160±2	24	1.5	0.18	-5.94	+2.66	Ol(5.1), Plag(0.7), Cr-sp(0.9), Glass(93.3)	0.37	0.41
#24	201.8	1160±2	24	0.9	0.08	-6.64	+1.96	Ol(9.4), Plag(16.9), Cpx(4.4), glass(69.3)	1.38	0.37
#25	203.5	1020±2	42	5.1	1.00	-6.36	+4.11	Ol(9.7), Plag(14.0), Cpx(14.6), Mag(1.2), glass(60.5)	0.08	0.37
#26	203.5	1020±2	42	n.a.	--	--	--	Ol, Plag, Cpx, Mag, glass	6)	
#31	203.0	980±1	43	5.2	1.00	-6.99	+4.10	Ol(0.9), Plag(18.0), Cpx(10.1), Amph(36.7), Mag(1.3), glass(33.1)	0.00	0.34

Table 1.1: Continued

Run	Pressure [MPa]	Temperature [°C]	Duration [h]	H_2O in the melt [wt%][1]	aH_2O[2]	log fO_2[3]	ΔQFM	Phases[4]						ΣR^2	K_D Ol-melt/Fe-Mg[5]
#32	203.0	940±4	68	5.3	1.00	-7.66	+4.08	Plag(20.2)	Cpx(0.8)	Opx(1.9)	Amph(57.5)	Mag(0.7)	glass(18.9)	0.01	
#38	104.7	1180±2	22	3.4	1.00	-4.24	+4.18	Cr-Sp(0.7)	glass(99.3)					0.17	
#39	104.7	1180±2	22	1.5	0.30	-5.30	+3.12	Ol(2.4)	Cr-Sp(1.4)	glass(96.1)				0.77	0.45
#40	104.7	1180±2	22	1.2	0.20	-5.65	+2.77	Ol(3.5)	Cr-Sp(0.9)	glass(95.6)				0.74	0.45
#41	104.7	1180±2	22	0.7	0.08	-6.46	+1.96	Ol	Plag	Cr-Sp	glass			[7]	0.40
#42	102.2	1100±4	41	3.5	1.00	-5.26	+4.16	Ol(5.3)	Cr-Sp(1.0)	glass(93.8)				0.10	0.43
#44	102.2	1100±4	41	1.7	0.41	-6.03	+3.39	Ol(14.4)	Plag(46.8)	Cpx(18.7)	glass(20.1)			0.78	0.47
#45	102.2	1100±4	41	1.9	0.49	-5.89	+3.53	Ol(13.7)	Plag(42.2)	Cpx(16.7)	glass(27.4)			0.55	0.47
#46	101.5	1160±4	82	3.4	1.00	-4.48	+4.18	Cr-Sp(0.9)	glass(99.1)					0.39	
#47	101.5	1160±4	82	2.1	0.48	-5.11	+3.55	Ol(2.8)	Cr-Sp(1.3)	glass(95.9)				0.78	0.45
#48	101.5	1160±4	82	1.0	0.15	-6.14	+2.53	Ol(5.4)	Plag(3.1)	Cpx(0.2)	Cr-Sp(2.8)	glass(88.4)		0.65	0.40
#49	101.5	1160±4	82	0.8	0.10	-6.45	+2.21	Ol(7.2)	Plag(10.9)	Cpx(2.2)	Cr-Sp(2.6)	glass(77.2)		1.75	0.39
#50	103.8	1060±2	42	3.5	1.00	-5.83	+4.14	Ol(10.2)	Plag(14.0)	Cpx(9.8)	glass(66.0)			0.14	0.46
#51	103.8	1060±2	42	2.1	0.52	-6.39	+3.58	Ol(14.5)	Plag(40.1)	Cpx(17.6)	glass(27.8)			0.20	0.45
#52	103.8	1060±2	42	n.a.	--	--	--	Ol	Plag	Cpx	glass			[6]	
#53	103.8	1060±2	42	1.8	0.34	-6.77	+3.20	Ol(15.5)	Plag(48.5)	Cpx(21.0)	glass(15.1)			0.33	0.41
#54	104.0	1140±2	22	3.4	1.00	-4.74	+4.17	Ol(2.2)	Cr-Sp(0.9)	glass(96.9)				0.11	0.39
#55	104.0	1140±2	22	2.0	0.44	-5.45	+3.46	Ol(5.4)	Plag(0.3)	Cr-Sp(0.5)	glass(93.8)			0.27	0.42
#56	104.0	1140±2	22	1.1	0.20	-6.14	+2.77	Ol(12.0)	Plag(30.3)	Cpx(8.6)	glass(49.1)			0.25	0.38
#57	104.0	1140±2	22	1.3	0.27	-5.89	+3.02	Ol(12.1)	Plag(31.7)	Cpx(8.9)	glass(47.3)			0.60	0.41
#58	100.9	980±3	70	n.a.	--	--	--	Ol	Plag	Cpx	Opx	Amph	Mag	[6]	
#67	501.0	1160±1	39	4.4	0.44	-4.98	+3.42	Ol(1.1)	Cr-Sp(0.8)	glass(98.1)				0.11	0.35
#68	501.0	1160±1	39	3.8	0.37	-5.13	+3.27	Ol(1.0)	Cr-Sp(1.1)	glass(97.9)				0.10	0.35
#69	501.0	1160±1	39	1.3	0.07	-6.56	+1.84	Ol(10.4)	Plag(35.6)	Cpx(20.1)	glass(33.9)			0.38	0.34
#70	502.0	1100±6	68	9.1	1.00	-5.05	+4.10	Ol(0.8)	Cr-Sp(0.7)	glass(98.5)				0.15	0.36
#71	502.0	1100±6	68	3.6	0.31	-6.05	+3.09	Ol	Plag	Cpx	Opx	glass		[7]	0.40

Table 1.1: Continued

Run	Pressure [MPa]	Temperature [°C]	Duration [h]	H_2O in the melt [wt%][1]	aH_2O[2]	$\log fO_2$[3]	ΔQFM	Phases[4]	ΣR^2	K_D Ol-melt/Fe-Mg[5]
#72	502.0	1100±6	68	2.8	0.22	-6.35	+2.80	Ol Plag Cpx Opx glass	[7]	0.38
#73	502.0	1100±6	68	n.a.	--	--	--	Ol Plag Cpx Opx Mag glass	[6]	
#74	501.7	1130±4	42	9.2	1.00	-4.65	+4.12	Cr-Sp(0.8) glass(99.2) glass	0.41	
#75	501.7	1130±4	42	4.4	0.41	-5.42	+3.34	Ol(3.4) Cpx(3.3) Cr-Sp(0.8) glass(92.5)	0.04	0.34
#76	501.7	1130±4	42	2.7	0.22	-5.98	+2.79	Ol Plag Cpx Opx glass	[7]	0.38
#77	501.7	1130±4	42	n.a.	--	--	--	Ol Plag Cpx Opx glass	[6]	
#78	501.5	1060±6	64	9.0	1.00	-5.60	+4.09	Ol Cpx Cr-Sp glass	[6]	0.35
#79	501.5	1060±6	64	6.3	0.57	-6.08	+3.60	Ol(6.8) Plag(16.1) Cpx(27.4) Cr-Sp(1.0) glass(48.8)	0.01	0.42
#80	501.5	1060±6	64	n.a.	--	--	--	Ol Plag Cpx Opx Mag glass	[6]	
#81	501.5	1060±6	64	n.a.	--	--	--	Ol Plag Cpx Opx Mag glass	[6]	
#82	503.2	980±10	91	8.8	1.00	-6.81	+4.05	Cpx(6.2) Amph(40.8) glass(53.0)	0.01	
#83	503.2	980±10	91	n.a.	--	--	--	Plag Cpx Opx Amph Mag glass	[6]	

Abbreviations: ol - olivine; plag - plagioclase; cpx - clinopyroxene; opx - orthopyroxene; cr-sp - Cr-rich spinel; mag - magnetite; amph - amphibole

[1] water content determined with "by-difference" method (e.g., Devine et al. 1995)
[2] aH_2O calculated after Burnham (1979)
[3] $\log fO_2$ was calculated following the procedure of Scaillet et al. (1995) with values of: Robie et al. (1978; Kw), Pitzer and Sterner (1994; water fugacity), Burnham (1979; water activity), Chou (1987; oxygen buffer, water-saturated) using values of Schwab and Küstner (1981) and Huebner and Sato (1970), Shaw and Wones (1964; hydrogen fugacity)
[4] Phase proportions calculated by mass balance
[5] calculated after Roeder and Emslie (1970), with Fe^{2+}-Fe^{3+} calculation after Kress and Carmicheal (1991)
[6] At least one phase is too small for reliable analyses
[7] a negative value is calculated for at least one phase

Table 1.2: Compositions of the experimental phases in wt%, starting material: R6a

Run	Temp. (°C)	Phase	n[1]	SiO_2	TiO_2	Al_2O_3	FeO^{tot}	MnO	MgO	CaO	Na_2O	K_2O	NiO	Cr_2O_3	P_2O_5	Total	X[2]
starting composition R6a				50.43	0.35	17.18	6.50	0.16	10.12	11.54	2.84	0.04			<0.03	99.16	
starting material: R6a (100 MPa)																	
#58	980	ol	4	41.97 (.12)		0.96 (.40)	9.24 (.13)	0.33 (.03)	47.82 (.72)	0.80 (.34)	0.15 (.06)		0.13 (.02)			101.40	90.2 (.1)
		plag	5	53.83 (.24)	0.05 (.01)	28.22 (.29)	1.11 (.12)		0.48 (.28)	12.03 (.19)	4.61 (.17)	0.04 (.00)				100.37	58.9 (.7)
		cpx	6	51.41 (.14)	0.55 (.05)	4.30 (.30)	6.05 (.22)	0.22 (.03)	16.61 (.36)	20.81 (.43)	0.61 (.05)					100.55	83.0 (.7)
		opx	2	55.99 (.04)	0.15 (.00)	7.57 (1.07)	6.34 (.27)	0.26 (.03)	27.74 (.34)	3.32 (.21)	0.80 (.11)					102.18	88.6 (.6)
		amph	7	43.45 (.23)	2.15 (.09)	11.70 (.16)	8.49 (.19)	0.12 (.02)	17.24 (.19)	11.63 (.17)	2.99 (.04)	0.09 (.01)	0.20 (.06)			97.86	78.4 (.5)
		mag	5	0.16 (.03)	2.03 (.03)	5.00 (.06)	75.48 (.97)	0.42 (.06)	7.58 (.16)	0.36 (.04)				1.52 (.55)		92.75	
#50	1060	ol	10	41.18 (.19)		0.10 (.11)	11.01 (.10)	0.24 (.05)	48.19 (.31)	0.36 (.11)			0.12 (.06)			101.20	88.6 (.1)
		plag	7	47.02 (.54)	0.04 (.02)	32.42 (.64)	1.12 (.14)	0.11 (.05)	0.40 (.15)	17.04 (.50)	1.74 (.27)					99.78	84.4 (2.4)
		cpx	6	50.59 (.87)	0.29 (.04)	4.98 (.81)	5.69 (.54)	0.13 (.10)	15.53 (.50)	22.30 (.52)	0.37 (.05)			0.49 (.14)		100.34	83.0 (1.7)
		glass	8	51.93 (.44)	0.41 (.04)	18.08 (.15)	6.56 (.33)		5.67 (.13)	10.30 (.17)	3.72 (.18)	0.06 (.02)				96.86	78.4
#51	1060	ol	7	39.81 (.20)		0.10 (.04)	16.70 (.15)	0.32 (.06)	43.25 (.21)	0.38 (.06)			0.12 (.04)			100.69	82.2 (2)
		plag	6	51.69 (.38)	0.06 (.02)	29.46 (.28)	1.15 (.07)		0.25 (.05)	13.49 (.27)	3.80 (.08)					99.90	66.2 (.9)
		cpx	6	51.19 (.54)	0.43 (.05)	3.68 (.43)	6.89 (.35)	0.18 (.04)	15.89 (.38)	21.10 (.31)	0.42 (.05)			0.28 (.05)		100.06	80.4 (1.0)
		glass	5	54.83 (.37)	0.80 (.06)	17.00 (.26)	7.57 (.37)	0.11 (.08)	4.36 (.30)	8.39 (.27)	4.80 (.34)	0.12 (.03)				97.98	67.7
#52	1060	ol	4	40.02 (.59)	0.06 (.03)	1.29 (.63)	20.93 (.63)	0.34 (.07)	37.44 (.92)	1.28 (.62)	0.16 (.07)		0.12 (.05)			101.63	76.1 (.4)
		plag	5	53.40 (.15)	0.11 (.02)	26.60 (.47)	1.40 (.17)		1.56 (.44)	11.55 (.37)	4.55 (.08)	0.04 (.01)				99.22	58.2 (1.1)
		cpx	4	50.72 (1.18)	0.81 (.03)	4.52 (1.73)	8.72 (.75)	0.23 (.02)	16.44 (1.72)	16.93 (1.63)	0.59 (.19)			0.19 (.03)		99.15	77.1 (1.0)
		glass	n.a.[4]														
#53	1060	ol	5	39.62 (.51)	0.07 (.02)	0.23 (.17)	19.10 (.35)	0.37 (.06)	40.98 (.21)	0.51 (.11)						100.80	79.3 (.3)
		plag	5	53.26 (.44)		27.99 (.47)	1.16 (.09)		0.35 (.22)	12.10 (.23)	4.68 (.16)	0.03 (.01)				99.63	58.7 (1.3)
		cpx	6	51.93 (.37)	0.56 (.05)	3.10 (.36)	7.63 (.27)	0.22 (.05)	16.33 (.34)	20.01 (.36)	0.41 (.03)			0.22 (.03)		100.40	79.2 (.6)
		glass	4	55.28 (.46)	1.01 (.14)	19.55 (.86)	7.42 (.30)	0.16 (.08)	3.53 (.33)	8.85 (.21)	4.71 (.23)	0.12 (.03)				100.65	61.2
#42	1100	ol	7	41.67 (.18)	0.29 (.02)	0.05 (.03)	7.40 (.13)	0.15 (.05)	51.12 (.24)	0.29 (.02)			0.16 (.05)			100.83	92.5 (.1)
		cr-sp	5	0.53 (.26)	0.34 (.03)	23.68 (.27)	30.02 (.41)	0.18 (.03)	16.11 (.21)	0.45 (.04)			0.18 (.06)	24.12 (.39)		95.56	0.41
		glass	7	50.05 (.30)		17.51 (.16)	5.96 (.30)	0.18 (.11)	7.54 (.18)	11.74 (.31)	2.90 (.23)	0.03 (.01)				96.26	84.1
#44	1100	ol	8	39.74 (.19)		0.13 (.06)	17.26 (.23)	0.32 (.02)	42.57 (.19)	0.42 (.04)						100.45	81.5 (2)
		plag	7	52.84 (.27)	0.05 (.01)	28.43 (.40)	1.04 (.10)		0.37 (.14)	12.46 (.21)	4.12 (.04)	0.02 (.01)				99.31	62.5 (.6)
		cpx	6	52.03 (.20)	0.50 (.04)	3.14 (.12)	7.12 (.17)	0.22 (.05)	16.58 (.23)	19.96 (.40)	0.41 (.03)			0.27 (.03)		100.22	80.6 (.4)
		glass	6	53.96 (.75)	1.11 (.08)	15.98 (.42)	8.57 (.39)	0.15 (.11)	5.25 (.08)	8.57 (.35)	4.23 (.18)	0.14 (.04)				97.96	67.5
#45	1100	ol	8	40.03 (.14)		0.11 (.06)	15.81 (.27)	0.29 (.06)	43.66 (.24)	0.43 (.04)						100.33	83.1 (.2)
		plag	5	52.32 (.50)	0.06 (.02)	29.10 (.31)	1.09 (.02)		0.34 (.09)	13.17 (.18)	3.88 (.11)	0.02 (.01)				99.98	65.2 (.9)
		cpx	8	51.58 (.35)	0.45 (.05)	3.18 (.25)	7.49 (.30)	0.20 (.06)	16.57 (.22)	19.96 (.41)	0.37 (.04)			0.26 (.05)		100.05	79.8 (.6)
		glass	7	53.86 (.30)	0.88 (.03)	16.08 (.26)	8.16 (.15)	0.16 (.08)	5.42 (.30)	9.16 (.38)	3.93 (.27)	0.10 (.03)				97.75	70.0

11

Table 1.2: Continued

Run	Temp. (°C)	Phase	n[1]	SiO₂	TiO₂	Al₂O₃	FeO[tot]	MnO	MgO	CaO	Na₂O	K₂O	NiO	Cr₂O₃	P₂O₅	Total	X[2]
#54	1140	ol	5	41.86 (.07)		0.05 (.03)	6.09 (.22)	0.13 (.02)	52.28 (.08)	0.30 (.03)			0.17 (.07)			100.88	93.9 (.2)
		cr-sp	4	0.25 (.17)	0.23 (.01)	23.71 (.65)	28.09 (.66)	0.15 (.04)	17.06 (.36)	0.37 (.04)			0.18 (.02)	24.97 (.72)		95.01	0.41
		glass	8	49.90 (.43)	0.36 (.04)	16.98 (.19)	6.06 (.24)	0.12 (.11)	8.83 (.18)	11.49 (.25)	3.04 (.09)	0.05 (.03)				96.83	85.8
#55	1140	ol	5	41.78 (.26)		0.06 (.02)	8.24 (.17)	0.17 (.04)	50.52 (.26)	0.33 (.02)						101.10	91.6 (.2)
		plag	5	47.32 (.40)		32.22 (.54)	1.01 (.05)		0.46 (.14)	16.89 (.45)	1.89 (.09)					99.79	83.1 (1.0)
		cr-sp	5	0.59 (.34)	0.21 (.03)	30.62 (.70)	22.48 (.37)	0.18 (.05)	17.16 (.05)	0.37 (.05)	0.06 (.06)			25.01 (.56)		96.68	0.35
		glass	5	50.75 (.15)	0.37 (.06)	17.77 (.23)	6.01 (.21)		7.76 (.12)	12.27 (.17)	3.37 (.28)	0.05 (.05)				98.35	82.1
#56	1140	ol	6	40.51 (.07)		0.09 (.03)	12.55 (.21)	0.24 (.02)	46.28 (.07)	0.43 (.05)						100.10	86.8 (.2)
		plag	6	51.31 (.30)	0.04 (.03)	29.67 (.54)	1.05 (.16)		0.42 (.18)	14.15 (.30)	3.62 (.08)	0.02 (.01)				100.28	68.3 (.9)
		cpx	7	51.76 (.52)	0.26 (.02)	3.50 (.32)	5.55 (.38)	0.12 (.04)	16.44 (.19)	20.89 (.28)	0.40 (.03)			0.50 (.07)		99.42	84.1 (1.0)
		glass	8	52.74 (.22)	0.62 (.05)	16.06 (.29)	7.86 (.47)	0.18 (.08)	6.43 (.28)	10.75 (.36)	3.76 (.22)	0.07 (.04)				98.47	71.3
#57	1140	ol	7	40.51 (.28)		0.06 (.01)	12.92 (.19)	0.25 (.04)	46.22 (.20)	0.43 (.04)						100.39	86.4 (.2)
		plag	7	51.63 (.42)	0.05 (.02)	29.24 (.55)	0.95 (.08)		0.58 (.26)	13.65 (.32)	3.67 (.11)	0.02 (.01)				99.79	67.2 (.9)
		cpx	5	52.03 (.33)	0.31 (.05)	3.30 (.24)	5.73 (.39)	0.17 (.07)	16.94 (.26)	20.42 (.27)	0.36 (.05)			0.37 (.04)		99.63	84.1 (.9)
		glass	7	53.06 (.31)	0.65 (.03)	16.04 (.40)	7.83 (.43)	0.12 (.12)	6.43 (.27)	10.91 (.41)	3.82 (.22)	0.07 (.02)				98.93	72.4
#46	1160	cr-sp	4	0.23 (.13)	0.20 (.02)	23.34 (.72)	22.69 (.23)	0.14 (.06)	17.52 (.23)	0.38 (.01)				30.49 (.86)		94.99	0.47
		glass	8	49.70 (.38)	0.31 (.03)	16.79 (.23)	5.57 (.28)	0.15 (.16)	9.80 (.16)	11.44 (.14)	2.72 (.12)	0.05 (.02)			0.06 (.08)	96.59	87.9
#47	1160	ol	9	41.75 (.21)		0.07 (.02)	7.06 (.30)	0.13 (.03)	51.27 (.33)	0.34 (.04)						100.62	92.8 (.3)
		cr-sp	5	0.38 (.24)	0.17 (.02)	28.78 (.51)	18.89 (.88)	0.18 (.03)	18.07 (.26)	0.38 (.05)				30.05 (.81)		96.90	0.41
		glass	7	51.03 (.35)	0.39 (.03)	17.53 (.24)	5.34 (.61)	0.13 (.07)	8.86 (.23)	11.81 (.50)	2.78 (.23)	0.05 (.02)			0.06 (.08)	97.98	85.5
#48	1160	ol	8	41.27 (.21)		0.10 (.09)	8.64 (.33)	0.17 (.05)	49.60 (.42)	0.44 (.08)						100.22	91.1 (.4)
		plag	8	49.54 (.36)		30.64 (.29)	0.67 (.06)		0.48 (.16)	15.19 (.20)	2.79 (.11)					99.31	75.0 (.9)
		cpx	8	51.82 (.31)	0.18 (.01)	3.71 (.17)	3.34 (.23)	0.21 (.05)	17.29 (.28)	22.05 (.21)	0.30 (.03)			1.31 (.07)		100.00	90.2 (.7)
		cr-sp	4	0.66 (.20)	0.25 (.01)	24.99 (.20)	17.16 (.36)		16.29 (.26)	0.48 (.08)				36.42 (.15)		96.46	0.49
		glass	5	52.79 (.53)	0.42 (.03)	17.38 (.46)	5.56 (.18)	0.14 (.17)	7.73 (.22)	12.20 (.24)	3.30 (.16)	0.05 (.02)				99.57	80.3
#49	1160	ol	7	41.20 (.17)		0.04 (.02)	8.63 (.22)	0.19 (.03)	49.89 (.26)	0.43 (.04)						100.38	91.2 (.2)
		plag	6	50.95 (.55)	0.05 (.02)	29.67 (.32)	0.73 (.09)		0.59 (.09)	14.35 (.20)	3.27 (.10)					99.61	70.8 (.9)
		cpx	5	52.40 (.04)	0.19 (.02)	3.22 (.33)	3.60 (.29)	0.11 (.03)	17.71 (.21)	21.58 (.14)	0.28 (.01)			0.86 (.15)		99.95	89.8 (.8)
		cr-sp	1	0.06	0.27	23.04	16.94	0.26	15.81	0.40				39.39		96.17	0.53
		glass	6	53.98 (.49)	0.47 (.02)	17.11 (.20)	5.23 (.19)	0.15 (.04)	7.57 (.15)	11.73 (.24)	3.35 (.21)	0.06 (.02)				99.65	80.1
#38	1180	cr-sp	5	0.79 (.54)	0.20 (.02)	22.12 (.32)	22.31 (.35)	0.17 (.03)	17.09 (.18)	0.48 (.10)	0.05 (.05)			33.02 (.59)		96.23	0.50
		glass	9	49.91 (.38)	0.32 (.03)	16.91 (.20)	6.10 (.17)	0.13 (.04)	9.70 (.20)	11.26 (.20)	2.90 (.19)	0.04 (.03)				97.27	86.6
#39	1180	ol	9	41.76 (.18)		0.06 (.03)	7.56 (.12)	0.13 (.02)	50.96 (.20)	0.34 (.02)	0.16					100.81	92.3 (.1)
		cr-sp	1	2.03	0.15	33.57	13.75	0.14	17.93	0.75				28.69		97.17	0.36
		glass	8	51.75 (.20)	0.34 (.02)	17.57 (.23)	5.54 (.17)		9.19 (.19)	12.20 (.23)	2.92 (.18)	0.06 (.02)				99.57	84.3

Table 1.2: Continued

Run	Temp. (°C)	Phase	n[1]	SiO_2	TiO_2	Al_2O_3	FeO^{tot}	MnO	MgO	CaO	Na_2O	K_2O	NiO	Cr_2O_3	P_2O_5	Total	X[2]
#40	1180	ol	9	41.60 (.15)	0.17 (.01)	0.07 (.03)	8.20 (.15)	0.16 (.05)	50.15 (.17)	0.39 (.03)	0.16 (.06)					100.57	91.6 (.1)
		cr-sp	4	1.84 (.48)		35.35 (1.24)	13.28 (.39)	0.10 (.03)	18.48 (.27)	0.55 (.07)				28.48 (1.35)		98.41	0.35
		glass	8	51.79 (.22)	0.39 (.04)	17.96 (.27)	5.54 (.22)	0.14 (.08)	8.87 (.23)	12.27 (.20)	3.11 (.26)	0.05 (.03)				100.12	82.9
#41	1180	ol	9	41.72 (.24)	0.03 (.02)	0.05 (.03)	7.74 (.19)	0.15 (.04)	50.59 (.16)	0.39 (.02)						100.64	92.1 (.2)
		plag	7	50.78 (.40)		29.85 (.29)	0.64 (.05)		0.70 (.13)	14.93 (.35)	3.07 (.17)					100.00	72.8 (1.5)
		cr-sp	5	0.75 (.41)	0.18 (.03)	31.13 (1.40)	12.40 (.25)	0.13 (.04)	18.19 (.28)	0.46 (.09)	0.05 (.03)			34.19 (1.82)		97.48	0.42
		glass	10	53.09 (.30)	0.39 (.03)	17.93 (.30)	5.03 (.42)	0.10 (.09)	8.77 (.17)	12.39 (.31)	3.16 (.15)	0.03 (.02)				100.89	82.3

starting material: R6a (200 MPa)

Run	Temp. (°C)	Phase	n[1]	SiO_2	TiO_2	Al_2O_3	FeO^{tot}	MnO	MgO	CaO	Na_2O	K_2O	NiO	Cr_2O_3	P_2O_5	Total	X[2]
#32	940	plag	7	51.13 (.35)	0.15 (.03)	30.19 (.52)	0.98 (.14)	0.30 (.06)	0.24 (.09)	14.17 (.29)	3.19 (.14)	0.02 (.01)				99.92	71.0 (.7)
		cpx	8	52.33 (.57)	0.06 (.02)	3.24 (.72)	6.81 (.26)	0.40 (.05)	16.97 (1.05)	20.22 (.87)	0.33 (.06)			0.09 (.06)		100.44	81.6 (1.3)
		opx	7	54.73 (.37)		2.83 (.27)	10.89 (.20)	0.40 (.05)	29.84 (.40)	1.41 (.27)						100.16	83.0 (.2)
		amph	8	45.35 (.44)	0.61 (.02)	11.24 (.36)	9.36 (.17)	0.16 (.04)	17.15 (.22)	11.40 (.19)	2.29 (.13)	0.03 (.01)		0.10 (.05)		97.69	76.6 (.4)
		mag	4	0.17 (.10)	1.08 (.01)	4.93 (.11)	78.36 (.27)	0.25 (.05)	4.05 (.16)	0.30 (.05)				1.82 (.31)		90.96	
		glass	8	59.33 (.47)	0.16 (.03)	17.04 (.45)	3.92 (.32)		2.27 (.45)	5.60 (.21)	3.09 (.31)	0.12 (.03)		0.09 (.13)	0.20 (.11)	91.82	70.6
#31	980	ol	5	41.53 (.24)		0.07 (.04)	7.78 (.29)	0.31 (.02)	51.11 (.13)	0.18 (.04)						100.98	92.1 (.3)
		plag	4	48.10 (.37)		32.01 (.28)	1.12 (.19)		0.22 (.05)	16.10 (.10)	2.16 (.14)	0.02 (.00)				99.73	80.4 (1.1)
		cpx	3	51.17 (.08)	0.22 (.03)	4.18 (.33)	6.60 (.21)	0.24 (.05)	17.40 (.39)	20.01 (.33)	0.32 (.04)	0.03 (.01)		0.12 (.04)		100.14	82.5 (.4)
		amph	9	43.79 (.23)	0.63 (.03)	12.38 (.34)	8.78 (.27)	0.17 (.05)	17.51 (.27)	11.65 (.34)	2.44 (.08)	0.03 (.01)		1.39 (.34)		97.50	78.0 (.7)
		mag	3	0.25 (.22)	0.61 (.02)	6.58 (.18)	73.83 (.45)	0.40 (.02)	8.49 (.09)	0.34 (.14)			0.19 (.07)			92.08	
		glass	7	57.13 (.47)	0.26 (.02)	18.07 (.16)	3.62 (.29)	0.11 (.09)	3.49 (.17)	6.56 (.10)	4.27 (.19)	0.10 (.02)			0.11 (.08)	93.72	80.1
#25	1020	ol	7	41.11 (.23)		0.04 (.04)	10.00 (.62)	0.22 (.08)	48.78 (.56)	0.23 (.03)			0.17 (.04)			100.55	89.7 (.7)
		plag	6	45.80 (.37)		33.43 (.37)	1.13 (.13)		0.20 (.09)	17.84 (.35)	1.50 (.10)					99.90	86.7 (.9)
		cpx	4	50.72 (.44)	0.26 (.01)	4.05 (.56)	5.63 (.33)	0.10 (.03)	16.49 (.22)	22.30 (.59)	0.21 (.18)			0.09 (.03)		99.85	83.9 (.9)
		mag	5	0.21 (.07)	1.11 (.05)	10.90 (.15)	69.38 (1.30)	0.29 (.04)	8.58 (.28)	0.35 (.10)			0.25 (.01)	2.42 (.98)		93.49	
		glass	8	50.26 (.78)	0.41 (.04)	18.14 (.41)	5.78 (.29)		4.49 (.19)	8.87 (.16)	3.62 (.29)	0.06 (.03)			0.05 (.07)	91.68	76.2
#26	1020	ol	5	39.67 (.19)	0.08 (.03)	0.08 (.02)	16.42 (.34)	0.32 (.04)	42.87 (.20)	0.28 (.03)			0.13 (.04)			99.77	82.3 (.3)
		plag	5	52.44 (.58)		28.45 (.73)	1.24 (.21)		0.51 (.31)	12.73 (.15)	4.43 (.12)	0.02 (.01)				99.90	61.3 (.9)
		cpx	6	50.48 (.67)	0.59 (.06)	4.61 (.80)	7.31 (.19)	0.26 (.04)	15.71 (.38)	20.28 (.44)	0.53 (.04)					99.77	79.3 (.7)
		mag	2	4.11 (.35)	3.55 (.09)	6.78 (.83)	71.47 (.65)	0.24 (.02)	5.87 (.44)	1.24 (.54)	0.21 (.24)		0.21 (.00)	1.71 (.01)		95.39	
		glass	n.a.[4]														
#10	1060	ol	10	41.72 (.21)	0.17 (.02)	0.03 (.02)	6.54 (.25)	0.18 (.03)	51.32 (.31)	0.24 (.03)			0.21 (.05)			100.24	93.3 (.3)
		cpx	8	50.77 (.41)	0.41 (.02)	4.08 (.51)	4.56 (.21)	0.10 (.05)	16.20 (.38)	23.03 (.40)	0.25 (.05)			0.35 (.08)		99.51	86.3 (.7)
		cr-sp	5	0.42 (.23)	0.41 (.02)	16.85 (.13)	48.63 (.31)	0.21 (.09)	13.72 (.24)	0.41 (.04)			0.28 (.11)	13.04 (.30)		93.98	0.34
		glass	11	49.22 (.46)	0.34 (.03)	17.77 (.28)	5.96 (.35)	0.11 (.08)	6.86 (.18)	11.60 (.28)	2.99 (.23)	0.05 (.04)				94.90	82.8

Table 1.2: Continued

Run	Temp. (°C)	Phase	n[1]	SiO2	TiO2	Al2O3	FeO[tot]	MnO	MgO	CaO	Na2O	K2O	NiO	Cr2O3	P2O5	Total	X[2]
#11	1060	ol	9	40.43 (.20)	0.08 (.04)	0.08 (.05)	12.94 (.23)	0.28 (.04)	46.07 (.32)	0.33 (.03)			0.16 (.05)			100.29	86.4 (.2)
		plag	5	50.13 (.38)		28.78 (.48)	1.49 (.24)		0.66 (.23)	13.68 (.10)	3.39 (.14)					98.21	69.0 (.8)
		cpx	9	48.77 (.37)	0.41 (.02)	5.71 (.36)	7.20 (.28)	0.18 (.04)	15.27 (.25)	20.93 (.39)	0.36 (.17)			0.12 (.04)		98.95	79.1 (.5)
		mag	4	0.33 (.22)	1.39 (.02)	9.27 (.09)	67.60 (1.30)	0.23 (.07)	7.75 (.18)	0.28 (.11)			0.16 (.08)	4.55 (.26)		91.56	
		glass	7	53.74 (.39)	0.60 (.06)	17.56 (.21)	7.27 (.26)	0.13 (.09)	4.89 (.09)	8.45 (.30)	4.40 (.21)	0.07 (.03)			0.05 (.05)	97.16	70.2
#12	1060	ol	3	39.37 (.12)	0.13 (.05)	0.31 (.14)	17.20 (.11)	0.36 (.03)	41.69 (.26)	0.45 (.06)						99.38	81.2 (.1)
		plag	4	52.90 (.19)		27.52 (.37)	1.55 (.32)		0.53 (.10)	11.99 (.22)	4.56 (.09)	0.04 (.00)				99.22	59.1 (.8)
		cpx	7	50.33 (.53)	0.58 (.04)	4.00 (.79)	7.68 (.34)	0.23 (.05)	16.07 (.41)	19.32 (.41)	0.50 (.07)					98.71	78.9 (.6)
		opx	3	53.56 (.70)	0.31 (.03)	4.29 (.30)	11.39 (.43)	0.30 (.03)	26.60 (.23)	2.66 (.30)	0.29 (.05)					99.39	80.6 (.5)
		mag	n.a.[3]														
		glass	n.a.[4]														
#13	1060	ol	3	40.12 (.76)	0.03 (.02)	0.74 (.17)	16.53 (.21)	0.35 (.02)	41.04 (.31)	0.90 (.09)	0.12 (.04)		0.15 (.01)			99.98	81.6 (.1)
		plag	3	52.36 (.12)	0.07 (.03)	27.88 (.23)	1.32 (.12)		0.68 (.19)	12.22 (.16)	4.44 (.10)					98.97	60.2 (.5)
		cpx	5	50.55 (.19)	0.59 (.06)	4.40 (.73)	7.71 (.11)	0.23 (.04)	15.93 (.34)	19.40 (.46)	0.54 (.09)					99.35	78.6 (.3)
		opx	3	53.67 (.59)	0.33 (.03)	5.49 (1.65)	10.63 (.62)	0.29 (.02)	24.98 (1.16)	3.36 (.58)	0.51 (.27)					99.28	80.7 (.2)
		mag	n.a.[3]														
		glass	n.a.[4]														
#1	1100	ol	5	42.06 (.25)		0.05 (.03)	5.51 (.25)	0.16 (.02)	52.92 (.23)	0.22 (.02)			0.27 (.05)			101.19	94.5 (.2)
		cr-sp	5	0.68 (.38)	0.26 (.01)	15.29 (.32)	41.93 (.63)	0.24 (.02)	15.85 (.34)	0.42 (.10)			0.32 (.08)	20.21 (1.03)		95.20	0.47
		glass	11	48.79 (.48)	0.33 (.03)	16.66 (.22)	6.02 (.33)	0.10 (.11)	8.37 (.11)	11.43 (.14)	2.60 (.08)	0.04 (.03)				94.34	85.1
#2	1100	ol	5	40.83 (.27)	0.04 (.02)	0.04 (.02)	10.71 (.26)	0.27 (.02)	48.77 (.37)	0.28 (.03)						100.91	89.0 (.2)
		plag	5	49.54 (.18)		30.43 (.24)	1.37 (.25)		0.47 (.20)	14.41 (.21)	2.79 (.12)					99.05	74.0 (.9)
		cpx	4	50.55 (.59)	0.29 (.05)	4.74 (.37)	5.87 (.30)	0.16 (.05)	16.14 (.29)	20.78 (.21)	0.35 (.02)			0.45 (.04)		99.34	83.1 (.9)
		glass	7	52.31 (.36)	0.50 (.03)	17.12 (.20)	7.51 (.37)	0.13 (.06)	6.04 (.22)	9.51 (.31)	3.72 (.23)	0.06 (.02)				96.90	73.6
#3	1100	ol	5	40.17 (.11)	0.05 (.01)	0.11 (.06)	15.34 (.28)	0.28 (.04)	44.76 (.40)	0.38 (.10)			0.13 (.04)			101.16	83.9 (.1)
		plag	5	52.09 (.25)		29.25 (.21)	1.27 (.17)		0.22 (.05)	12.55 (.11)	3.96 (.14)					99.40	63.6 (.8)
		cpx	5	51.27 (.27)	0.38 (.04)	3.85 (.40)	7.16 (.22)	0.20 (.04)	16.45 (.20)	19.41 (.18)	0.44 (.09)			0.26 (.04)		99.42	80.4 (.6)
		mag	4	0.45 (.23)	1.99 (.04)	7.45 (.15)	74.92 (.45)	0.24 (.02)	6.58 (.12)	0.39 (.07)			0.14 (.09)	2.16 (.39)		94.32	
		glass	8	53.55 (.37)	0.88 (.08)	16.00 (.24)	9.21 (.39)	0.19 (.14)	5.35 (.18)	8.50 (.27)	4.06 (.24)	0.08 (.02)				97.82	64.5
#5	1100	ol	5	39.84 (.23)	0.09 (.07)	0.27 (.23)	16.92 (.17)	0.33 (.06)	42.90 (.29)	0.46 (.10)			0.14 (.03)			100.71	81.9 (.2)
		plag	6	52.59 (.18)		27.77 (.69)	1.64 (.46)		0.83 (.59)	11.84 (.32)	4.16 (.13)					98.92	61.1 (.9)
		cpx	4	51.45 (.31)	0.47 (.03)	3.43 (.22)	7.67 (.21)	0.24 (.03)	16.61 (.26)	18.99 (.43)	0.42 (.08)			0.25 (.03)		99.54	79.4 (.4)
		mag	5	0.44 (.19)	2.95 (.04)	6.49 (.10)	75.20 (.59)	0.26 (.04)	5.88 (.11)	0.38 (.08)			0.14 (.03)	1.67 (.25)		93.41	
		glass	6	53.81 (.44)	1.03 (.07)	16.11 (.57)	9.67 (.29)	0.22 (.07)	5.31 (.32)	8.38 (.81)	4.08 (.36)	0.12 (.03)			0.05 (.05)	98.78	62.1
#14	1140	cr-sp	1	0.78	0.23	19.77	30.70	0.13	17.59	0.50	0.06		0.20	27.52		97.49	0.48
		glass	10	49.12 (.40)	0.33 (.05)	16.57 (.23)	5.87 (.25)	0.14 (.09)	9.16 (.18)	11.21 (.29)	2.74 (.16)	0.05 (.04)				95.19	86.5

14

Table 1.2: Continued

Run	Temp. (°C)	Phase	n[1]	SiO2	TiO2	Al2O3	FeO^tot	MnO	MgO	CaO	Na2O	K2O	NiO	Cr2O3	P2O5	Total	X[2]
#15	1140	ol	6	41.19 (.31)		0.03 (.02)	7.41 (.09)	0.13 (.02)	51.01 (.22)	0.29 (.03)			0.19 (.03)			100.24	92.5 (.1)
		cr-sp	3	0.26 (.05)	0.22 (.02)	27.72 (.61)	25.09 (.18)	0.11 (.07)	17.42 (.13)	0.37 (.04)			0.20 (.04)	26.37 (.90)		97.76	0.39
		glass	9	50.73 (.23)	0.35 (.02)	17.56 (.12)	6.20 (.34)	0.11 (.09)	8.22 (.17)	11.76 (.24)	2.89 (.24)					97.82	82.2
#16	1140	ol	7	40.13 (.19)	0.03 (.01)	0.08 (.04)	12.20 (.23)	0.25 (.07)	46.71 (.13)	0.39 (.03)						99.75	87.2 (.2)
		plag	5	50.75 (.27)		30.13 (.26)	1.01 (.09)		0.41 (.09)	14.49 (.27)	3.28 (.06)					100.09	70.9 (.5)
		cpx	5	51.82 (.40)	0.24 (.02)	4.05 (.30)	5.95 (.20)	0.15 (.05)	17.25 (.39)	20.57 (.36)	0.36 (.00)			0.40 (.03)		100.79	83.8 (.3)
		glass	5	52.84 (.45)	0.56 (.04)	16.59 (.19)	7.81 (.19)	0.16 (.10)	6.65 (.35)	10.86 (.13)	3.67 (.21)	0.07 (.04)			0.07 (.05)	99.28	72.5
#17	1140	ol	6	39.65 (.19)		0.07 (.02)	13.76 (.12)	0.27 (.05)	45.34 (.28)	0.42 (.04)						99.51	85.5 (.1)
		plag	7	51.06 (.49)	0.04 (.01)	29.54 (.25)	0.97 (.06)		0.36 (.08)	13.53 (.18)	3.87 (.16)					99.36	65.8 (1.1)
		cpx	7	51.52 (.63)	0.34 (.03)	3.78 (.31)	6.91 (.30)	0.20 (.02)	16.95 (.36)	19.79 (.32)	0.40 (.04)			0.38 (.03)		100.28	81.4 (.8)
		glass	5	53.75 (.17)	0.68 (.06)	16.79 (.29)	7.79 (.24)	0.11 (.15)	6.53 (.29)	10.25 (.15)	3.82 (.23)	0.07 (.03)				99.79	71.4
#21	1160	cr-sp	4	1.06 (.21)	0.20 (.01)	22.65 (.78)	22.57 (.30)	0.14 (.02)	17.12 (.12)	0.50 (.03)	0.05 (.03)			34.09 (1.18)		98.38	0.50
		glass	6	48.17 (.46)	0.33 (.04)	16.26 (.15)	5.89 (.21)	0.10 (.09)	9.29 (.25)	11.31 (.21)	2.70 (.15)	0.02 (.03)		0.12 (.16)		94.19	86.6
#22	1160	ol	6	41.78 (.13)		0.04 (.01)	7.83 (.13)	0.13 (.05)	50.97 (.22)	0.29 (.04)						101.04	92.1 (.1)
		cr-sp	3	1.62 (.21)	0.17 (.01)	28.87 (.43)	18.24 (.06)		17.34 (.27)	0.57 (.03)	0.09 (.06)			32.08 (.60)		99.00	0.43
		glass	5	49.56 (.35)	0.34 (.04)	16.78 (.32)	5.68 (.38)	0.14 (.13)	8.52 (.23)	11.68 (.16)	2.92 (.20)	0.02 (.01)			0.06 (.05)	95.68	84.4
#23	1160	ol	7	41.84 (.30)		0.07 (.02)	8.92 (.19)	0.17 (.04)	49.90 (.10)	0.37 (.03)						101.27	90.9 (.2)
		plag	6	50.71 (.27)		30.71 (.16)	0.75 (.10)		0.38 (.07)	14.97 (.33)	3.28 (.09)					100.80	71.6 (.9)
		cr-sp	1	1.50	0.18	34.96	15.48		18.18	0.52	0.07			28.55		99.44	0.35
		glass	7	50.34 (.41)	0.36 (.04)	17.37 (.25)	5.78 (.32)	0.11 (.11)	7.88 (.21)	12.15 (.18)	3.11 (.18)	0.03 (.02)			0.06 (.08)	97.19	80.3
#24	1160	ol	7	40.88 (.38)	0.03 (.01)	0.08 (.04)	9.96 (.15)	0.21 (.02)	48.67 (.36)	0.42 (.05)						100.22	89.7 (.2)
		plag	4	51.11 (.44)		30.16 (.21)	0.63 (.03)		0.39 (.04)	14.24 (.05)	3.60 (.04)					100.16	68.6 (.3)
		cpx	6	51.51 (.55)	0.29 (.04)	3.83 (.47)	6.06 (.27)	0.15 (.05)	17.60 (.19)	19.71 (.31)	0.32 (.03)			0.41 (.04)		99.88	83.8 (.6)
		glass	5	52.06 (.46)	0.48 (.04)	16.83 (.09)	5.88 (.24)	0.14 (.09)	7.14 (.07)	11.42 (.17)	3.57 (.31)	0.06 (.05)				97.58	76.4
#6	1180	glass	8	46.93 (.44)	0.34 (.02)	16.00 (.17)	5.72 (.29)	0.11 (.13)	9.43 (.27)	10.37 (.33)	2.48 (.12)					91.38	86.8
#7	1180	cr-sp	n.a.[3]														
		glass	8	49.11 (.37)	0.35 (.03)	16.64 (.21)	5.69 (.35)	0.10 (.07)	9.66 (.20)	10.77 (.27)	2.72 (.18)	0.03 (.02)				95.06	85.7
#8	1180	ol	8	41.10 (.18)		0.09 (.09)	7.86 (.11)	0.10 (.05)	50.63 (.22)	0.33 (.03)						100.10	92.0 (.1)
		cr-sp	1	8.44	0.17	33.76	13.83	0.12	18.46	1.80	0.46			26.65		103.68	0.35
		glass	6	49.66 (.17)	0.35 (.04)	17.13 (.16)	5.61 (.20)	0.11 (.04)	9.21 (.30)	11.20 (.15)	2.98 (.34)	0.03 (.04)			0.05 (.03)	96.34	84.1
#9	1180	ol	9	41.41 (.21)		0.05 (.01)	6.90 (.16)	0.14 (.03)	51.76 (.22)	0.38 (.02)						100.64	93.0 (.2)
		cr-sp	3	2.78 (.31)	0.16 (.00)	31.35 (.83)	10.98 (.14)		19.00 (.52)	0.78 (.08)	0.22 (.04)			34.80 (.70)		100.06	0.43
		glass	9	51.70 (.62)	0.34 (.03)	18.10 (.20)	4.60 (.28)		9.10 (.18)	11.95 (.32)	3.00 (.24)					98.78	83.4

Table 1.2: Continued

Run	Temp. (°C)	Phase	n[1]	SiO_2	TiO_2	Al_2O_3	FeO^{tot}	MnO	MgO	CaO	Na_2O	K_2O	NiO	Cr_2O_3	P_2O_5	Total	$X^{2)}$
#18	1220	cr-sp	3	0.43 (.04)	0.17 (.00)	22.94 (.10)	24.70 (.34)	0.15 (.06)	18.34 (.10)	0.39 (.06)	0.05 (.02)		0.16 (.02)	30.25 (.25)		97.58	0.47
		glass	19	50.69 (.44)	0.32 (.04)	17.15 (.25)	6.32 (.23)		9.85 (.12)	11.56 (.29)	2.98 (.22)	0.04 (.03)				98.91	83.0
#19	1220	cr-sp	4	1.29 (.62)	0.14 (.01)	32.92 (.37)	16.56 (.20)	0.13 (.05)	19.12 (.18)	0.52 (.10)	0.11 (.05)			28.23 (.46)		99.02	0.37
		glass	17	51.13 (.32)	0.33 (.04)	17.29 (.29)	6.13 (.29)	0.10 (.08)	10.06 (.18)	11.93 (.25)	2.94 (.18)	0.04 (.04)				99.95	82.1
#20	1220	ol	7	41.42 (.19)		0.07 (.01)	7.22 (.20)	0.13 (.03)	51.50 (.31)	0.36 (.03)						100.70	92.7 (.2)
		cr-sp	3	0.35 (.10)	0.12 (.00)	35.30 (.58)	13.15 (.32)	0.13 (.06)	19.37 (.13)	0.36 (.03)				29.99 (.66)		98.77	0.36
		glass	16	52.02 (.49)	0.34 (.04)	17.80 (.17)	5.56 (.23)	0.11 (.11)	9.81 (.22)	12.11 (.33)	2.96 (.21)	0.04 (.03)			0.06 (.06)	100.81	81.0

starting material: R6a (500 MPa)

Run	Temp. (°C)	Phase	n[1]	SiO_2	TiO_2	Al_2O_3	FeO^{tot}	MnO	MgO	CaO	Na_2O	K_2O	NiO	Cr_2O_3	P_2O_5	Total	$X^{2)}$
#82	980	cpx	9	47.53 (.37)	0.32 (.03)	7.66 (.28)	7.41 (.25)	0.15 (.05)	13.48 (.23)	23.16 (.16)	0.35 (.03)	0.02 (.01)		0.11 (.04)		100.17	76.4 (.8)
		amph	13	43.00 (.37)	0.50 (.03)	13.93 (.36)	8.32 (.30)		16.89 (.18)	12.31 (.13)	2.52 (.07)	0.05 (.02)		0.09 (.04)		97.58	78.3 (.7)
		glass	16	51.54 (.32)	0.22 (.03)	19.02 (.26)	4.42 (.31)	0.14 (.09)	4.08 (.19)	8.71 (.24)	2.99 (.23)					91.17	78.5
#83	980	plag	6	52.58 (.15)		29.62 (.20)	0.90 (.06)		0.15 (.05)	12.82 (.14)	4.16 (.09)	0.02 (.00)				100.25	62.9 (.3)
		cpx	6	50.14 (.26)	0.31 (.03)	5.38 (.22)	7.71 (.17)	0.25 (.03)	14.77 (.17)	20.70 (.18)	0.65 (.02)					99.91	77.3 (.5)
		opx	8	53.81 (.40)	0.09 (.01)	4.24 (.26)	10.70 (.22)	0.29 (.04)	29.78 (.26)	1.23 (.15)	0.06 (.02)					100.20	83.2 (.3)
		amph	7	43.36 (.40)	1.04 (.05)	12.60 (.29)	9.59 (.29)	0.13 (.03)	16.18 (.26)	11.23 (.27)	2.75 (.06)	0.04 (.01)	0.22 (.03)	0.09 (.06)		97.01	75.0 (.7)
		mag	6	0.11 (.02)	0.98 (.03)	6.60 (.15)	77.04 (.65)	0.26 (.05)	5.44 (.08)	0.28 (.05)				1.61 (.37)		92.54	
		glass	n.a.[4]														
#78	1060	ol	9	41.94 (.32)	0.16 (.02)		6.43 (.16)	0.17 (.04)	51.30 (.17)	0.21 (.04)			0.22 (.06)			100.27	93.4 (.2)
		cpx	6	51.13 (.42)		4.10 (.43)	4.21 (.22)		15.94 (.32)	23.56 (.21)	0.26 (.02)			0.71 (.07)		100.07	87.1 (.8)
		cr-sp	n.a.[3]														
		glass	10	48.02 (.30)	0.33 (.03)	16.71 (.22)	5.91 (.16)		7.26 (.10)	11.33 (.26)	2.65 (.20)	0.10 (.02)				92.31	83.2
#79	1060	ol	8	40.40 (.20)	0.03 (.01)	0.06 (.04)	12.49 (.28)	0.20 (.03)	46.81 (.24)	0.23 (.05)			0.13 (.04)			100.32	87.0 (.2)
		plag	6	49.22 (.41)	0.35 (.03)	31.30 (.33)	0.97 (.05)		0.24 (.05)	14.18 (.28)	2.86 (.17)	0.02 (.01)				98.83	73.3 (1.5)
		cpx	7	48.63 (.36)		7.09 (.42)	7.01 (.23)	0.15 (.03)	14.99 (.31)	19.24 (.50)	0.51 (.02)			0.16 (.07)		98.13	79.1 (.4)
		cr-sp	1	1.51	0.40	38.30	37.51	0.19	15.29	0.37	0.14		0.28	3.35		97.35	0.06
		glass	10	51.55 (.57)	0.44 (.05)	19.20 (.39)	6.32 (.42)	0.11 (.10)	5.19 (.15)	7.67 (.23)	4.31 (.21)	0.06 (.02)				94.84	73.9
#80	1060	ol	3	40.01 (.37)	0.04 (.02)	0.59 (.41)	16.91 (.03)	0.40 (.05)	41.98 (.64)	0.52 (.20)	0.07 (.08)					100.52	81.6 (.2)
		plag	4	54.06 (.26)	0.06 (.01)	27.97 (.42)	0.99 (.09)		0.43 (.13)	11.68 (.07)	4.72 (.07)	0.05 (.02)				99.96	57.8 (.4)
		cpx	7	50.38 (.24)	0.65 (.04)	5.05 (.17)	8.03 (.28)	0.24 (.05)	15.48 (.19)	19.48 (.30)	0.73 (.03)					100.04	77.5 (.6)
		opx	6	53.40 (.35)	0.27 (.02)	4.29 (.15)	12.10 (.21)	0.29 (.06)	28.10 (.38)	1.59 (.16)	0.08 (.05)					100.12	80.6 (.4)
		mag	7	0.35 (.20)	4.12 (.05)	9.62 (.11)	70.14 (.49)	0.29 (.05)	6.17 (.18)	0.36 (.05)	0.10 (.15)		0.18 (.06)	1.31 (.15)		92.64	
		glass	n.a.[4]														

Table 1.2: Continued

Run	Temp. (°C)	Phase	n[1]	SiO_2	TiO_2	Al_2O_3	FeO^{tot}	MnO	MgO	CaO	Na_2O	K_2O	NiO	Cr_2O_3	P_2O_5	Total	X[2]
#81	1060	ol	1	39.98		0.21	16.87	0.27	42.82	0.34	0.04					100.53	81.9
		plag	5	54.84 (.28)	0.07 (.03)	27.96 (.18)	0.96 (.14)		0.14 (.06)	11.03 (.23)	5.20 (.11)	0.05 (.01)				100.25	54.0 (.9)
		cpx	8	50.13 (.38)	0.69 (.06)	5.59 (.22)	8.16 (.15)	0.21 (.04)	15.10 (.27)	19.45 (.34)	0.79 (.08)					100.12	76.8 (.3)
		opx	n.a.[5]														
		mag	6	0.22 (.05)	3.95 (.05)	9.85 (.14)	70.67 (.79)	0.28 (.03)	6.30 (.14)	0.37 (.03)			0.16 (.04)	1.46 (.26)		93.26	
		glass	n.a.[4]														
#70	1100	ol	24	42.26 (.17)			5.55 (.14)	0.14 (.04)	52.52 (.18)	0.17 (.02)			0.32 (.06)			100.96	94.4 (.1)
		cr-sp	4	0.55 (.24)	0.29 (.01)	16.48 (.20)	35.29 (.89)	0.19 (.03)	15.47 (.24)	0.46 (.05)			0.33 (.03)	25.28 (.76)		94.34	0.51
		glass	18	47.93 (.40)	0.34 (.05)	16.14 (.27)	5.98 (.31)	0.10 (.11)	9.12 (.16)	11.02 (.22)	2.47 (.18)	0.17 (.04)				93.27	85.7
#71	1100	ol	8	40.02 (.16)	0.04 (.02)	0.15 (.11)	15.79 (.27)	0.28 (.04)	43.45 (.39)	0.35 (.05)						100.04	83.1 (.3)
		plag	5	52.34 (.45)		29.59 (.26)	0.89 (.13)		0.19 (.07)	12.88 (.13)	4.22 (.09)	0.02 (.01)				100.17	62.7 (.7)
		cpx	6	50.90 (.29)	0.39 (.04)	4.97 (.38)	7.48 (.16)	0.19 (.07)	16.10 (.24)	19.10 (.21)	0.55 (.05)			0.22 (.05)		99.90	79.3 (.5)
		opx	6	54.21 (.69)	0.14 (.04)	3.47 (.76)	10.90 (.19)	0.25 (.06)	29.18 (.37)	1.74 (.07)	0.07 (.02)			0.12 (.03)		100.08	82.7 (.4)
		glass	6	52.66 (.27)	0.80 (.05)	17.76 (.15)	8.22 (.32)	0.20 (.12)	5.22 (.14)	8.04 (.22)	4.29 (.18)	0.11 (.02)				97.30	66.1
#72	1100	ol	6	39.84 (.26)	0.04 (.01)	0.12 (.13)	17.09 (.19)	0.26 (.04)	42.99 (.21)	0.33 (.07)						100.63	81.8 (.2)
		plag	6	52.91 (.30)		29.33 (.09)	0.86 (.04)		0.17 (.03)	12.53 (.10)	4.39 (.08)	0.02 (.01)				100.25	61.1 (.5)
		cpx	5	50.89 (.28)	0.44 (.04)	4.89 (.16)	8.39 (.31)	0.20 (.04)	16.36 (.23)	18.10 (.48)	0.59 (.04)			0.17 (.05)		100.03	77.7 (.6)
		opx	7	53.53 (.44)	0.20 (.02)	4.20 (.42)	12.16 (.28)	0.30 (.04)	28.42 (.18)	1.77 (.08)	0.07 (.02)			0.12 (.03)		100.77	80.6 (.4)
		glass	7	52.62 (.65)	0.95 (.06)	17.71 (.24)	8.66 (.25)	0.12 (.13)	5.14 (.13)	7.74 (.21)	4.56 (.28)	0.15 (.04)				97.65	63.3
#73	1100	ol	6	39.67 (.14)	0.03 (.01)	0.14 (.07)	18.75 (.50)	0.32 (.04)	41.82 (.16)	0.38 (.08)						101.11	79.9 (.5)
		plag	6	53.32 (.23)	0.04 (.03)	28.96 (.25)	1.05 (.10)		0.21 (.11)	12.12 (.16)	4.56 (.04)	0.03 (.01)				100.29	59.4 (.4)
		cpx	7	50.09 (.39)	0.61 (.05)	5.25 (.40)	8.60 (.32)	0.25 (.04)	15.56 (.22)	18.63 (.26)	0.63 (.03)			0.16 (.07)		99.78	76.3 (.8)
		opx	3	53.97 (.50)	0.30 (.08)	4.95 (1.54)	11.95 (.14)	0.27 (.05)	26.31 (1.35)	2.63 (.29)	0.26 (.12)	0.02 (.01)				100.66	79.7 (.7)
		mag	4	0.61 (.52)	3.51 (.12)	14.31 (.37)	62.27 (1.06)	0.28 (.04)	7.40 (.09)	0.39 (.11)			0.13 (.02)	5.45 (.64)		94.35	
		glass	n.a.[4]														
#74	1130	cr-sp	4	0.66 (.73)	0.21 (.02)	14.39 (.33)	34.13 (.54)	0.23 (.08)	16.36 (.25)	0.40 (.12)	0.06 (.04)		0.37 (.06)	26.88 (.39)		93.69	0.56
		glass	11	47.51 (.26)	0.32 (.04)	15.85 (.16)	5.94 (.40)	0.11 (.09)	9.16 (.18)	10.88 (.28)	2.30 (.18)	0.29 (.05)				92.36	85.8
#75	1130	ol	10	41.90 (.25)		0.06 (.06)	7.04 (.08)	0.16 (.03)	51.04 (.28)	0.26 (.04)			0.18 (.05)			100.64	92.8 (.1)
		cpx	9	50.13 (.38)	0.18 (.03)	5.89 (.50)	4.80 (.32)		16.10 (.26)	21.37 (.39)	0.41 (.04)			0.80 (.22)		99.68	85.7 (.8)
		cr-sp	5	0.68 (.37)	0.21 (.03)	29.35 (.35)	27.91 (.33)	0.16 (.07)	17.17 (.09)	0.42 (.10)	0.04 (.05)		0.19 (.06)	19.94 (.54)		96.07	0.31
		glass	18	49.86 (.45)	0.36 (.03)	17.57 (.21)	6.10 (.34)		8.14 (.18)	11.34 (.27)	3.01 (.22)	0.04 (.02)				96.42	81.5
#76	1130	ol	7	40.43 (.10)	0.03 (.01)	0.08 (.05)	13.72 (.16)	0.26 (.04)	45.54 (.21)	0.29 (.03)						100.32	85.5 (.2)
		plag	4	52.32 (.12)		29.21 (.31)	0.97 (.09)		0.22 (.03)	12.74 (.14)	4.09 (.10)	0.02 (.01)				99.60	63.2 (.6)
		cpx	5	50.11 (.35)	0.36 (.03)	5.48 (.33)	7.28 (.25)	0.16 (.04)	16.15 (.28)	19.01 (.69)	0.52 (.04)			0.31 (.05)		99.38	79.8 (.6)
		opx	1	53.70	0.11	4.44	9.90	0.14	29.90	1.84	0.06			0.15		100.24	84.3
		glass	10	52.10 (.36)	0.70 (.05)	17.48 (.22)	8.16 (.26)	0.17 (.08)	6.27 (.24)	8.82 (.24)	4.01 (.23)	0.08 (.04)			0.05 (.06)	97.84	69.0

Table 1.2: Continued

Run	Temp. (°C)	Phase	n[1]	SiO$_2$	TiO$_2$	Al$_2$O$_3$	FeO^{tot}	MnO	MgO	CaO	Na$_2$O	K$_2$O	NiO	Cr$_2$O$_3$	P$_2$O$_5$	Total	X [2]
#77	1130	ol	6	39.62 (.20)		0.10 (.05)	16.53 (.22)	0.30 (.04)	42.62 (.30)	0.35 (.02)						99.52	82.1 (.3)
		plag	4	52.69 (.32)	0.07 (.01)	28.62 (.53)	1.02 (.13)		0.30 (.14)	12.39 (.20)	4.51 (.03)	0.04 (.00)				99.64	60.1 (.4)
		cpx	6	50.67 (.65)	0.50 (.06)	4.91 (.50)	8.48 (.24)	0.26 (.06)	16.34 (.64)	17.60 (.58)	0.55 (.03)			0.20 (.06)		99.51	77.5 (.7)
		opx	6	52.79 (.39)	0.24 (.03)	4.29 (.37)	12.04 (.31)	0.26 (.05)	27.84 (.27)	1.92 (.16)	0.08 (.02)			0.13 (.05)		99.59	80.5 (.4)
		glass	n.a.[4]														
#67	1160	ol	6	41.92 (.20)		0.04 (.02)	6.38 (.10)	0.16 (.03)	51.90 (.20)	0.27 (.03)			0.18 (.06)			100.85	93.5 (.1)
		cr-sp	5	1.12 (.45)	0.17 (.01)	27.38 (.76)	24.00 (.18)	0.11 (.04)	17.85 (.24)	0.54 (.10)	0.07 (.02)		0.16 (.08)	24.74 (1.12)		96.14	0.38
		glass	8	49.66 (.40)	0.35 (.04)	16.76 (.23)	6.15 (.35)		9.30 (.24)	11.23 (.37)	2.88 (.18)	0.04 (.03)				96.37	83.4
#68	1160	ol	8	42.02 (.13)		0.06 (.05)	6.52 (.10)	0.11 (.01)	51.51 (.11)	0.27 (.03)			0.18 (.03)			100.56	93.4 (.1)
		cr-sp	3	0.47 (.27)	0.18 (.03)	27.60 (.21)	24.73 (.44)	0.12 (.09)	17.44 (.18)	0.40 (.10)	0.05 (.05)		0.15 (.06)	24.81 (.67)		95.94	0.38
		glass	9	49.95 (.28)	0.33 (.04)	16.67 (.16)	6.10 (.17)		9.35 (.24)	11.51 (.35)	2.85 (.16)	0.03 (.03)				96.91	83.2
#69	1160	ol	9	40.39 (.24)		0.07 (.01)	14.64 (.23)	0.21 (.09)	44.92 (.18)	0.34 (.03)						100.57	84.5 (.2)
		plag	7	52.96 (.40)	0.05 (.02)	29.01 (.31)	0.87 (.12)		0.37 (.16)	12.90 (.16)	4.23 (.09)	0.02 (.01)				100.41	62.7 (.5)
		cpx	10	51.50 (.40)	0.38 (.05)	4.84 (.42)	7.42 (.37)	0.18 (.05)	17.01 (.39)	18.31 (.68)	0.50 (.03)			0.20 (.05)		100.34	80.3 (.7)
		glass	9	52.70 (.31)	0.81 (.05)	17.46 (.37)	8.52 (.27)	0.20 (.10)	6.29 (.21)	9.24 (.42)	3.92 (.19)	0.09 (.03)				99.23	64.8

Abbreviations: ol - olivine; plag - plagioclase; cpx - clinopyroxene; opx - orthopyroxene; cr-sp - Cr-rich spinel; mag - magnetite; amph - amphibole

Missing values: below detection limit of the electron microprobe.

[1] Number of analyses; numbers in paratheses are standard deviations (1 σ).

[2] Compositional parameter in mol%: olivine - forsterite content (calculated without MnO); plagioclase – anorthite content (calculated without K$_2$O); pyroxene and amphibole $100 \cdot \mathrm{Mg}/(\mathrm{Mg} + \mathrm{Fe}^{2+})$ with Fetot as FeO; cr-rich spinel $\mathrm{Cr}/(\mathrm{Cr} + \mathrm{Al})$; glass $100 \cdot \mathrm{Mg}/(\mathrm{Mg} + \mathrm{Fe}^{2+})$ with Fe^{2+} calculated after Kress and Carmicheal (1991)

[3] The crystal phase in these runs is too small for reliable analyses.

[4] The glass pools in these runs are too small for reliable analyses.

18

1.2.1. Starting material

As a starting material for the experiments, we used a microgabbro from the Southwest Indian Ridge (SWIR). Microgabbros occur as small dikes with medium to fine-grained equigranular textures within the drilled gabbro section of the Southwest Indian Ridge. According to Dick et al. (2000) these microgabbros represent melt transport channels through crystallizing intrusions. We used the microgabbro "R6a" (ODP designation: 176-735B-178R-6:132-138; Snow, 2002), recovered from a depth of 1219 mbsf (meters below sea floor) on ODP Leg 176. This rock exhibits a fine-grained (< 0.5 mm), equigranular texture consisting of plagioclase (55 mol% anorthite; ~65 vol% in the mode), olivine (71 mol% forsterite; ~15 vol% in the mode), clinopyroxene (Mg# = 79 (molar $100 \times MgO/(MgO+FeO)$); ~ 15 vol% in the mode) and interstitial phases (pargasitic amphibole, orthopyroxene, ilmenite, Cr-rich magnetite, and pyrite; ~ 5 vol% in the mode in total). The chemical composition of the gabbro is close to a primitive tholeiitic basalt (Table 1.2), but K_2O, TiO_2, and P_2O_5 are nonetheless somewhat low for such a composition. Therefore, we believe that this rock also includes a certain cumulate character.

The starting glass was prepared by crushing the sample and regrinding it in a rotary mortar. The rock was totally fused at 1600°C in a platinum crucible and quenched with water. The homogeneity of the glass was confirmed by electron microprobe analyses. For the experimental runs, this glass was crushed to a grain size of <150μm and filled into noble metal capsules (10 to 40 mg for each run).

1.2.2. Loss of Iron

To avoid iron loss during the experiment Au was used as capsule material at temperatures ≤ 1020°C. At temperatures > 1020 °C $Au_{80}Pd_{20}$ was used instead of platinum due to its lower

Fe-solubility (Kawamoto and Hirose 1994). After the experiment, iron loss to the capsule was checked by electron microprobe and found to be negligible, in agreement with previous studies under relatively oxidizing conditions (e.g., Berndt et al. 2005). This conclusion is further supported by the compositions of the iron-bearing phases of the experimental runs. Olivine, for example, systematically increases in forsterite content with temperature and water in the coexisting melt. If iron loss had occurred, an increase in the forsterite content of olivine in runs with low water activities would be expected, which was not observed. Experiments with low water activity and thus low oxygen fugacity could have lost some iron. Mass balance calculations predict iron loss of up to 1.6 wt %, which does not significantly affect the results.

1.2.3. Calculation of Water activity and oxygen fugacity

With the help of the estimated water contents of the melts (see below), water activities for each run were calculated according to the model of Burnham (1979). This model works well up to 200 MPa (e.g., Berndt et al. 2005), but is not correct for higher pressures. A correction term was introduced for calculating those water activities for 500 MPa, assuming that the model calculates the relative values for different water contents correctly. Based on this assumption, the water-saturated experiments were defined as $aH_2O=1$ and the relative deviation, calculated by the model, was subtracted from the experiments performed at the same conditions but with reduced water activity.

The experimental runs were conducted under "intrinsic" fO_2 condition of the IHPV, which was measured by Berndt et al. (2002) at four temperatures using solid redox sensor and corresponds to QFM +4.2 (4.2 log units above the quartz-fayalite-magnetite oxygen buffer) for water-saturation. Since the fO_2 in a given run is strongly affected by the water activity (aH_2O; e.g., Berndt et al. 2005; Scaillet et al. 1995) the fO_2 of our experiments varied between ~ QFM +1.0 for "nominally dry" runs (near liquidus) and QFM +4.2 for water-saturated runs.

The prevailing oxygen fugacity for each experiment with reduced aH₂O was calculated according the procedure outlined by Scaillet et al. (1995). The water fugacity was calculated from aH₂O using the equation of Pitzer and Sterner (1994) with a K_W of Robie et al. (1978). Finally, the oxygen fugacity was determined after Chou (1987) using the values of Schwab and Küstner (1981) and Huebner and Sato (1970) and a fH_2 after Shaw and Wones (1964) which is imposed by the vessel and corresponds to QFM +4.2 (Berndt et al. 2002).

1.2.4. Difficulties reaching "dry" conditions in our experiments

In our "dry" experiments, the capsules were dried (as described above) and immediately welded shut. However, Fourier transform infrared (FTIR) measurements of quenched glasses from near-liquidus experiments revealed a water content of these capsules of 0.52 wt%. Experiments with silver oxalate (without added water) also did not reach perfectly "dry" conditions. Moreover, these experiments resulted in even higher water contents compared to the procedure described above. We assume that absorbed water due to the hygroscopic character of the silver oxalate is responsible for increasing the water content of the system.

We consider two possible origins of the water in these capsules. First, there is always a certain amount of air in the capsule. The experiments were conducted as a "closed system" with the exception of hydrogen (which controls the oxygen fugacity). Hydrogen diffuses through the capsule wall and produces water inside the capsule. Second, the prevailing oxygen fugacity during the experiments is lower compared to the syntheses of the starting material. If so, some of the Fe^{3+} is reduced to Fe^{2+} and the released oxygen forms water with the hydrogen of the buffer.

These "nominally dry" experiments (0.52 wt% H_2O) change their water content with the degree of crystallization and can reach water-saturation depending on pressure and temperature. In accordance with Berndt et al. (2005), these experiments show a distinct

difference to the experiments which are water-saturated from beginning on. Berndt et al. (2005) explained this effect by the different amount and composition of crystals and melt. Our experiments fit well with the observation that the bulk water has a significant control. Even at low temperatures, the systematic effect of water on the phase compositions is present (see chapter "phase chemistry").

1.2.5. Analytical methods

The products of the experiments were analyzed with a "Cameca SX100" electron microprobe equipped with an operating system "Peak sight" based on Microsoft Windows. All data were obtained using 15 kV acceleration potential, a static (fixed) beam, Ka emission from all elements, and a matrix correction according to Pouchou and Pichoir (1991). The minerals were analyzed with a focused beam, 15 nA beam current and counting times of 5 s for Na and K, 30 s for Ni and Cr and 10 s for all other elements. The coexisting glass was measured with a 5μm defocused beam at 15kV, 4nA beam current and counting times of 4 s for Na and K, 30 s for Ni, Cr and P, and 8 s for all other elements. For small glass pools, a beam diameter of 2 - 5 μm was used. Potential sodium loss was checked by mass balance calculations and found to be negligible.

The water content of the experimental glasses was estimated by the "by-difference" method (e.g., Devine et al. 1995). For this, standard glasses of MORB composition with known water contents (published in Berndt et al. 2002) were also analysed during each analytical session.

"Nominally dry" near liquidus experiments were analysed with an FTIR-spectrometer to determine the minimum water content that was reached in the experiments. For the measurements, sample plates with thicknesses of 175-200 μm (each sample ± 2μm) were prepared and polished from both sides. Crystal-free glass was located with an optical microscope and analysed with a spot size of ~ 100 x 100 μm (50 scans, 2 cm^{-1} resolution).

The measurements were performed in the mid-infrared with a Bruker IFS 88 coupled with an IR-Scope II microscope. The setup of the spectrometer contains an InSb-MCT sandwich narrow range detector, a KBr beamsplitter and a "globar" light source. Spectra in the range of $500 - 5000$ cm^{-1} were recorded and the absorption bands at ~ 3570 cm^{-1} (attributed to the fundamental OH^{-} stretching vibration) was used to determine the water content (Leschik et al. 2004; Mandeville et al. 2002) with a density of 2808 g/l ($\rho = - 20.8 * c_{water} + 2819$; after Ohlhorst et al. 2001) and an absorption coefficient of 70 (Scholze 1959). We determined a minimum water content for the "nominally dry" experiments of ~ 0.52 wt%.

1.3. Results

1.3.1. Achievement of equilibrium

Previous studies under similar conditions and compositions using the same IHPV (e.g., Berndt et al. 2005) show that chemical equilibrium is reached after 2 - 5 hours at temperatures > 1000°C and 5 - 10 hours at temperatures of 950 - 1000°C and water-bearing conditions. The durations of our experiments were 20 to 91 hours (depending on temperature) The following observations suggest that equilibrium was obtained: (1) The newly formed crystals are chemically homogeneous and generally euhedral (Figs. 1.1 and 1.2). (2) Glasses are also homogeneous (within the counting statistics of the microprobe analyses), irrespective of location within the sample. (3) Glass and crystals are homogeneously distributed along the capsule. (4) Phase compositions vary systematically with intensive variables (e.g., temperature). (5) Mineral-melt and mineral-mineral element partitioning relations are generally in good agreement with published data from other studies (see below). (6) Most

mass balance calculations for individual runs result in $\Sigma R^2 < 1$ (ΣR^2 = sum of residual squares, e.g., Albarède and Provost 1977; see also Tab. 1.1).
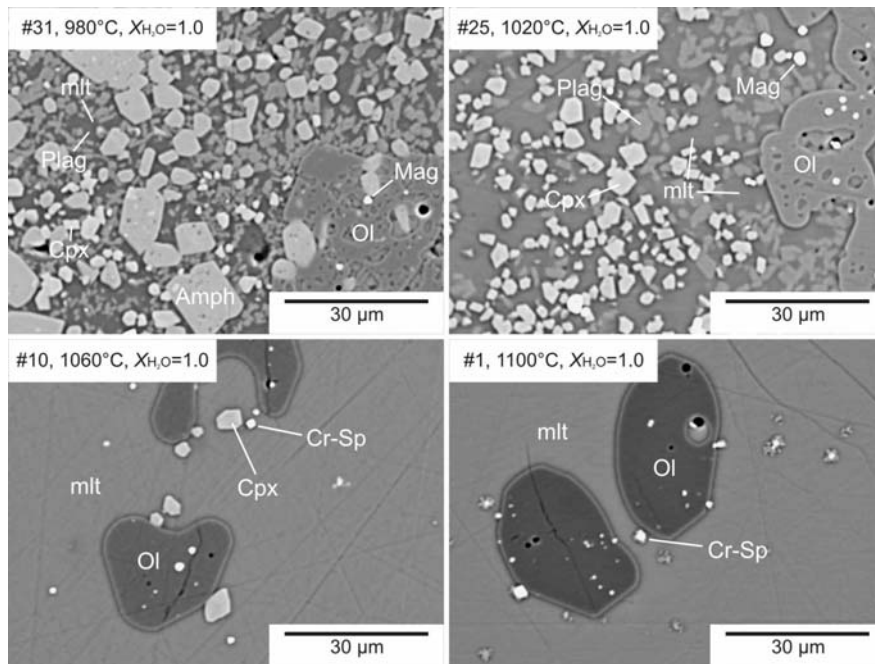
Fig. 1.1: Back-scattered electron (BSE) images of the experimental products (P = 200 MPa, log fO_2=QFM+4.2 and water-saturated conditions). Shown is the effect of temperature on the phase relations. Abbreviations: Ol - olivine; Cr-Sp - chromium-rich spinel; Cpx - clinopyroxene; Plag - plagioclase; Mag - magnetite; Amph – amphibole; mlt – melt
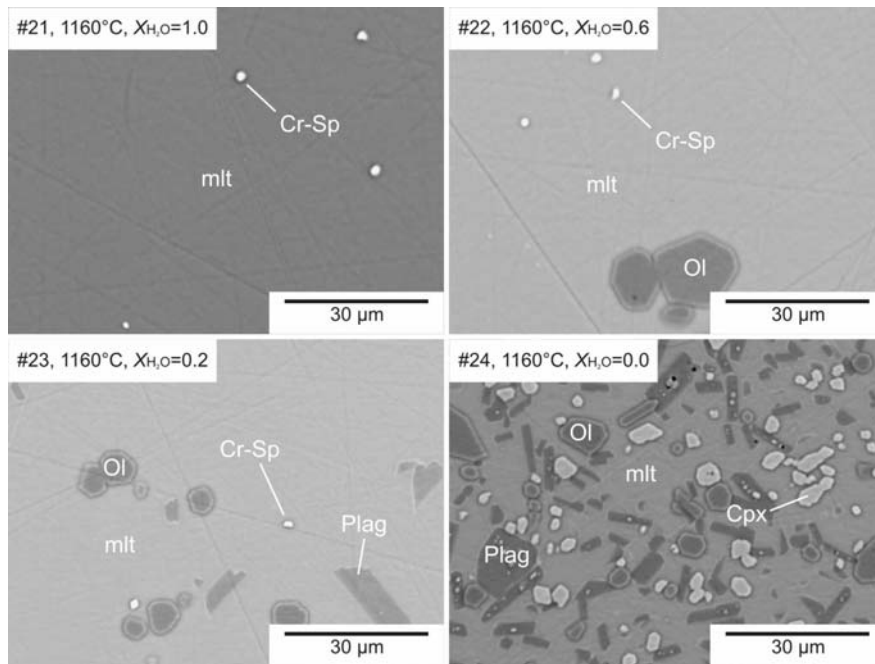
Fig. 1.2: BSE images of the experimental products (P = 200 MPa, log fO_2=QFM+1 - QFM+4.2 and a temperature of 1160°C). Shown is the effect of water content on the phase relations. Abbreviations as in Fig. 1.1.

1.3.2. Phase relations

The water content has a large effect on the stabilities of phases in a basaltic system. The addition of water to the dry system shifts the solidus about 250°C to lower temperatures, increases the amount of melt drastically (compare run #1 with #5; 12.5 % glass and 96.3 % glass respectively) and affects the order of mineral crystallization significantly. The phase relations obtained for 100, 200 and 500 MPa are shown in T-H_2O diagrams (Fig. 1.3a-c). Experimental conditions and phase proportions are listed in Table 1.1. At all pressures and water contents, a chrome-rich spinel is the primary liquidus phase, followed by olivine. At lower temperatures, plagioclase and clinopyroxene follow. Their relative order of appearance depends on both pressure and water content. At 100 MPa plagioclase crystallizes before clinopyroxene at all water contents. At pressures above 100 MPa, plagioclase crystallizes before clinopyroxene at low melt water contents (less than ~ 3 wt%), but after clinopyroxene at high water contents, which is in agreement with Gaetani et al. (1993, 1994). The clinopyroxene-saturation curve more or less parallels the olivine-saturation curve at lower temperatures at all pressures and water contents, and the changing of the crystallization order at pressures above 100 MPa is due to a drastic shift of the plagioclase-saturation curve to lower temperatures with increasing water contents (Fig. 1.3a-c).

Chrome-rich spinel disappears generally after the crystallization of clinopyroxene, suggesting that the Cr content in the melt is lowered by the incorporation of Cr into the clinopyroxene. After a gap of 30 to 100°C, magnetite becomes stable, which reflects the oxidizing conditions in our experiments. At relatively low temperatures, orthopyroxene crystallizes, showing a stability field that depends strongly on the prevailing pressure (see discussion below). Amphibole crystallizes only at temperatures < 1020°C.
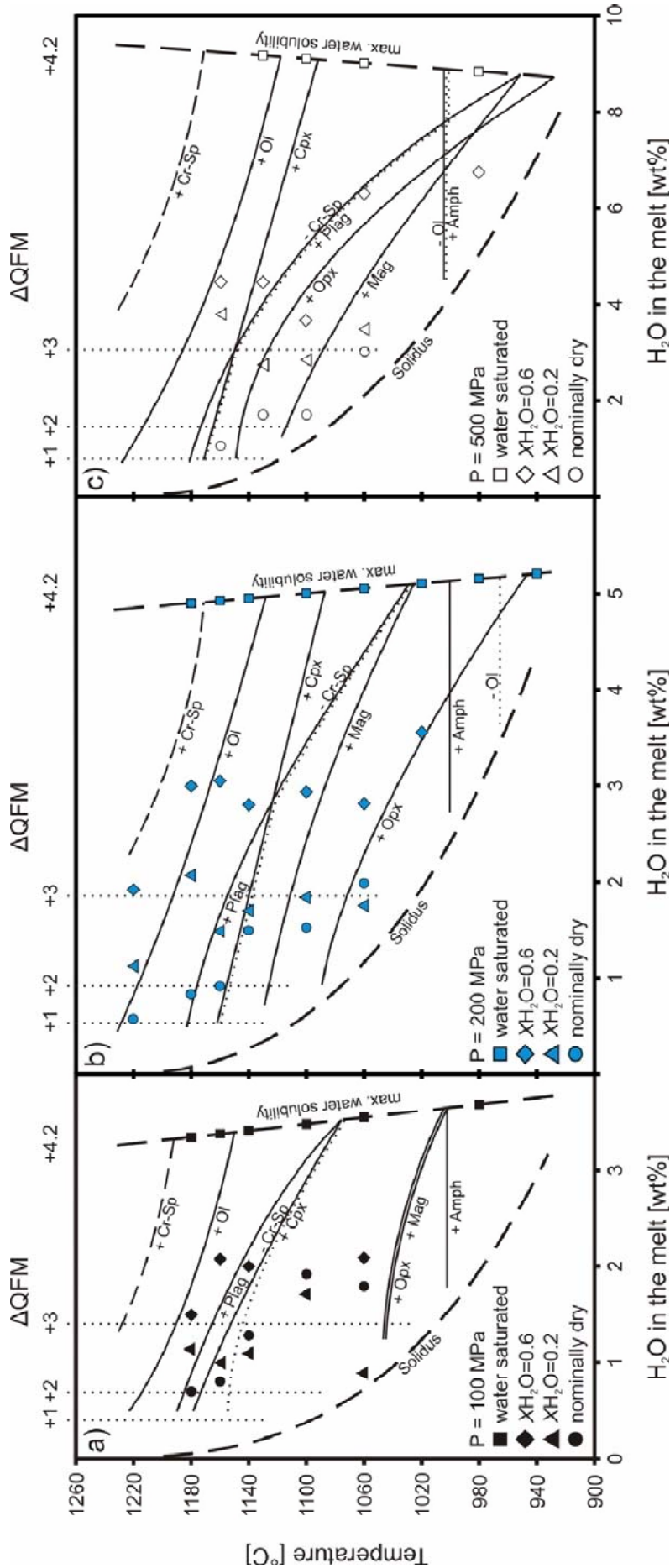
Fig. 1.3: Phase relations for a hydrous tholeiitic basalt for 100 (a), 200 (b) and 500 (c) MPa. The water-saturation curve included in the phase diagrams is obtained from the water solubility in a primitive MORB of Berndt et al. (2005) and from the temperature and pressure dependence on water solubility by Holtz et al. (1995). The amount of water was determined with the "by-difference" method. Depending on the water activity, the oxygen fugacity (dotted vertical lines) varies between QFM+1 and QFM+4.2. The symbols represent the experimentally investigated conditions. The total pressure is shown by the filling of the symbol; the water content is shown by the shape of the symbol. The phase boundaries correspond to the appearance (+) and disappearance (-, dotted) of phases. Abbreviations: Ol - olivine; Cr-sp - chromium-rich spinel; Cpx - clinopyroxene; Opx - orthopyroxene; Plag - plagioclase; Mag - magnetite; Amph - amphibole

In Figure 1.4 we present the phase relations only for the water-saturated conditions, in order to allow comparison with those experimental studies in basaltic systems which were performed exclusively under water-saturated conditions. For example, our 200 MPa water-saturated experiments are in good agreement with the results of Gaetani et al. (1994) for a basaltic andesite at the same pressure.

Figure 1.4 also illustrates the pressure effect on the liquidus temperatures of the mineral phases. A negligible pressure effect under water-saturated conditions is observed for clinopyroxene and amphibole. Olivine and chromium-rich spinel show a slight decrease in liquidus temperature with increasing pressure, whereas plagioclase, magnetite and orthopyroxene show a strong decrease in liquidus temperature with increasing pressure.
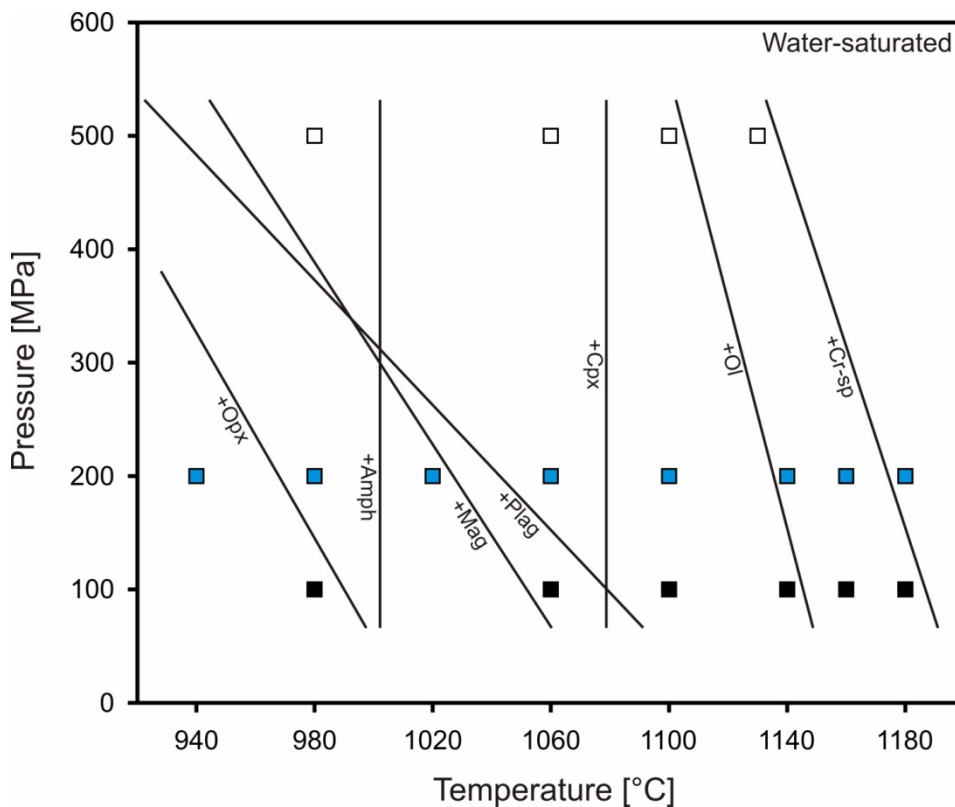
Fig. 1.4: Liquidus temperatures of the occurring mineral phases as a function of pressure under water-saturated conditions. The symbols represent the experimentally investigated conditions. Abbreviations: Ol - olivine; Cr-sp - chromium-rich spinel; Cpx - clinopyroxene; Opx - orthopyroxene; Plag - plagioclase; Mag - magnetite; Amph - amphibole.

1.3.3. Phase chemistry

1.3.3.1. Olivine

Olivine (ol) compositions are listed in Table 1.2. Figure 1.5 shows a dramatic increase of forsterite (Fo) component in olivine with increasing water in the system. For instance, at T=1100°C the increase of Fo content between "nominally dry" and water-saturated runs is ~12 mol% (at 200 MPa). This effect can partly be ascribed to the increase in melt fraction due to water, and partly to the increase of oxygen fugacity, which is a direct consequence of increasing water activities in a H_2-buffered system. The oxygen fugacity controls the Fe^{2+} content and therefore, the Fe^{2+}/Mg ratio of the melt (e.g., Berndt et al. 2005; Toplis and Carroll 1995). For the example from above, the increase in fO_2 correspond to ~ 1.4 log units (Table 1.1). In Figure 1.5 it can be observed that the Fo content tends to rise again at low temperatures, which is due to the crystallization of magnetite extracting FeO from the melt. The same effect was reported in the experiments in a primitive MORB system from Berndt et al. (2005) and is a characteristic of oxidizing conditions.
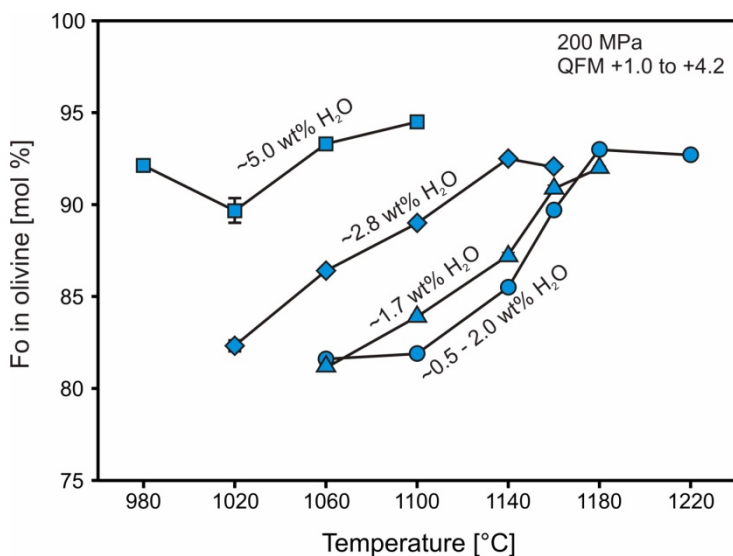
Fig. 1.5: Forsterite content of olivine as a function of temperature for different water contents at 200 MPa. The signature of the symbols is described in Fig. 1.3

The element partitioning coefficient $K_{D\,Fe-Mg}^{Ol-Melt}$ according to Roeder and Emslie (1970) was calculated using equation 1.

$$K_{D\,Fe-Mg}^{Ol-Melt} = \frac{X_{FeO}^{Ol}}{X_{FeO}^{Melt}} \frac{X_{MgO}^{Melt}}{X_{MgO}^{Ol}} \text{ in mole} \qquad (1)$$

The Fe^{2+}/Fe^{3+} ratio of the glass was calculated after Kress and Carmichael (1991). The $K_{D\,Fe-Mg}^{Ol-Melt}$ values obtained for our experiments vary between 0.3 - 0.47 (Tab. 1.1), deviating systematically from the canonical value of Roeder and Emslie (1970) of ~ 0.3 with the amount of water in the system. Toplis (2005) showed that deviations from this value can be expected, mainly due to the influence of melt composition, but also due to water. Values calculated with the model of Toplis (2005) produce $K_{D\,Fe-Mg}^{Ol-Melt}$ values of 0.3 ±0.01, independent of the prevailing water content.

1.3.3.2. Plagioclase

Plagioclase compositions are listed in Table 1.2. Figure 1.6 shows the strong influence of water on the anorthite content (An) in plagioclase. For instance, at a given temperature of 1020°C the increase of An between a run with a moderate bulk water content of 2.8 wt% and a water-saturated run is ~ 25 mol% (at 200 MPa). This dramatic increase of An contents due to a higher water content is in full agreement with previous studies (e.g., Berndt et al. 2005; Koepke et al. 2004; Martel et al. 1998; Panjasawatwong et al. 1995).
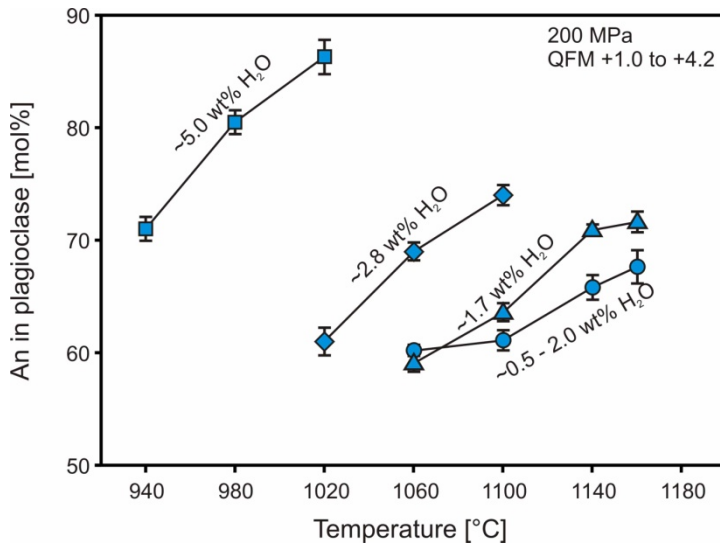
Fig. 1.6: Anorthite content of plagioclase as a function of temperature for different water contents at 200 MPa. The signature of the symbols is described in Fig. 1.3.

1.3.3.3. Clinopyroxene

The clinopyroxene (cpx) compositions are listed in Table 1.2. Water shifts the Mg# to higher values, as described above for the forsterite content of olivine, and for the same reasons. An effect of water itself on the composition of the pyroxenes cannot be distinguished from the effects mentioned before. In the pyroxene quadrilateral (Fig. 1.7) the experimental low Ca- and high Ca-pyroxene pairs plot on parallel tie-lines suggesting equilibrium conditions (Lindsley, 1983). As a consequence of the effect of water described above, the experiments show a systematic shift to lower ferrosilite component with increasing water activity.
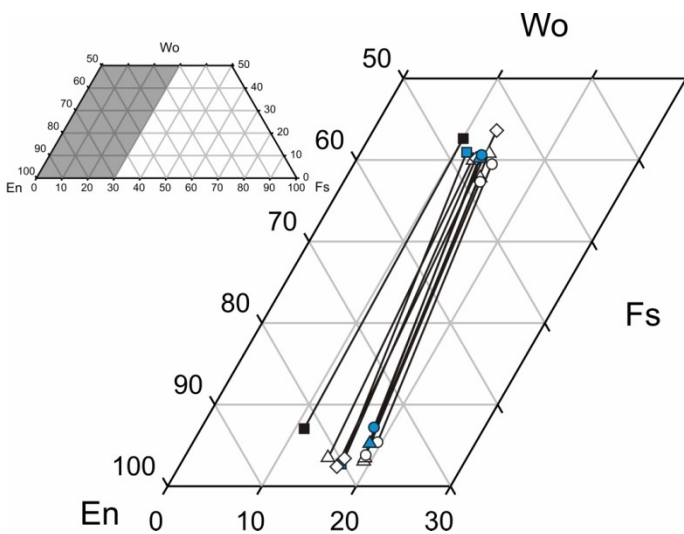
Fig. 1.7: Pyroxene quadrilateral and the experimental low Ca- and high Ca-pyroxene pairs. Coexisting pyroxenes are connected with tie-lines. The signature of the symbols is described in Fig. 1.3

30
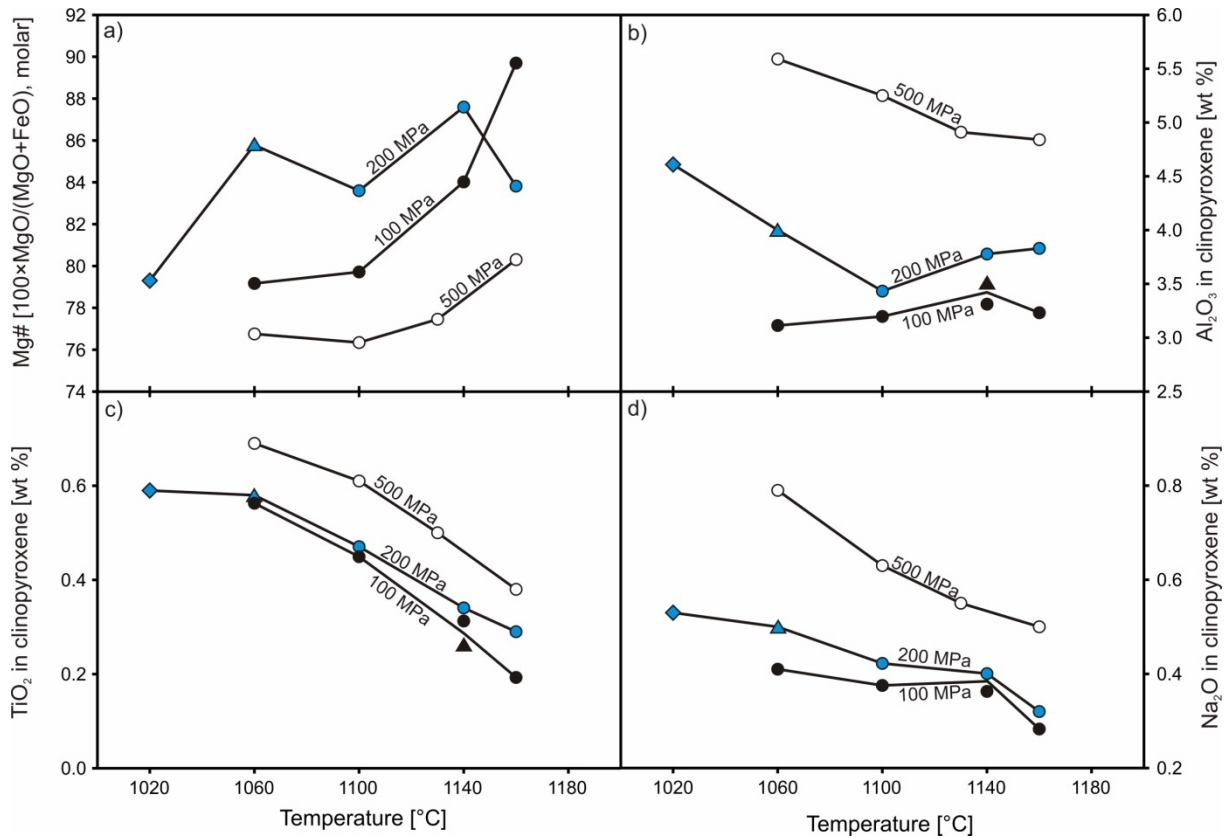
Fig. 1.8: Mg# and selected components of the clinopyroxenes of the experiments with the lowest water content for the three different pressures as a function of temperature. The signature of the symbols is shown in Fig. 1.3

In Figure 1.8 only clinopyroxenes of those runs with the lowest aH_2O for the three different pressures are plotted, displaying well-developed trends for Mg# and some minor components against temperature. It should be mentioned that the water contents of the nominally dry experiments used are not constant, causing some variations within individual trends. As expected, temperatures correlate positively with Mg#, but negatively with TiO_2 and Na_2O, apparently reflecting compositional effects due to higher activities of these components in the melt with decreasing temperature. Figure 1.8b shows the well-known pressure dependence of Al_2O_3 in clinopyroxene at more or less constant temperatures. The observed trends confirm the potential of clinopyroxene composition for thermobarometry (e.g., Putirka et al. 1996; Putirka et al. 2003) in dry systems.

The well-developed trends for low water contents displayed in Figure 1.8 are destroyed when experimental data obtained at higher water contents are included. For clarity, these data points

31

are left out of Figure 1.8. This has consequences for applying thermobarometry to clinopyroxene compositional data of hydrous systems. For instance, Putirka et al. (2003) provided a commonly used model to calculate pressures and temperatures using the melt and clinopyroxene composition. We applied their model to our experiments and were able to reproduce the experimental pressures for those runs with low aH_2O well (± 130 MPa) at least for temperatures ≥ 1100°C, but failed for those runs with high aH_2O (Fig. 1.9). The temperature dependence shows a systematic deviation from the experimental values to higher temperatures with increasing water activity (Fig. 1.10).
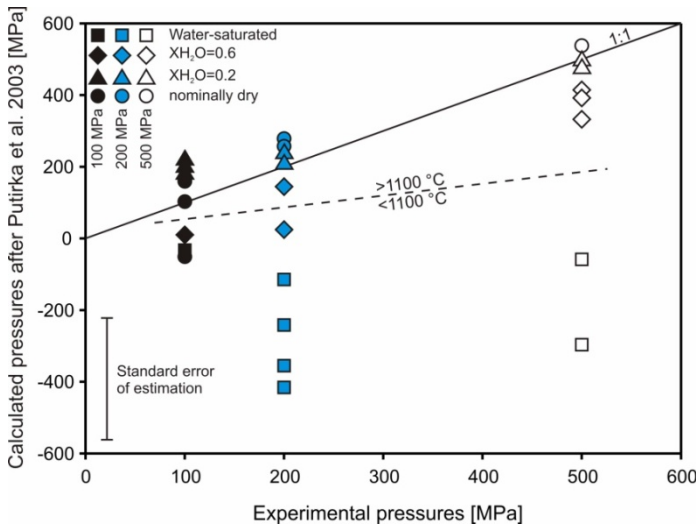
Fig. 1.9: Thermobarometer of pyroxenes from Putirka et al. (2003) was used to calculate the pressures of the experiments. At high temperatures the calculated pressures reproduce the experimental pressures within the error of the model, at temperatures <1100°C the error increases rapidly.
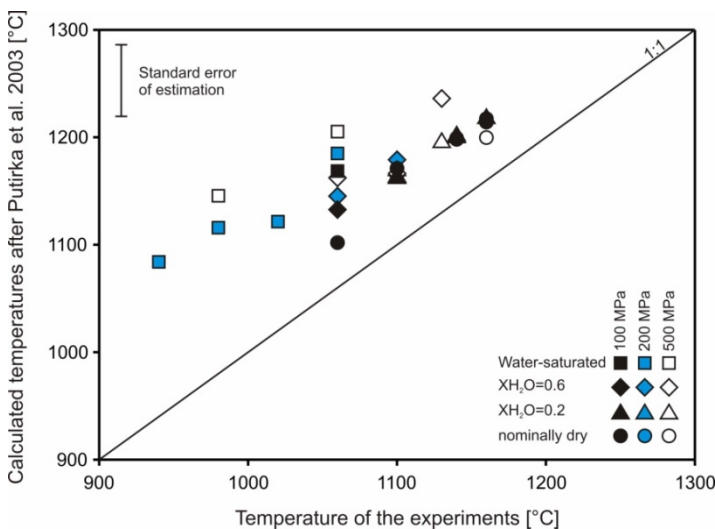
Fig. 1.10: Thermobarometer of pyroxenes from Putirka et al. (2003) was used to calculate the temperature of the experiments. All pyroxene-bearing experiments show a systematic deviation from the 1:1-line to higher temperatures with increasing water activity in the system.

1.3.3.4. Orthopyroxene

The orthopyroxene (opx) compositions are listed in Table 1.2. In contrast to clinopyroxene, orthopyroxene is very sensitive both to total pressure and aH$_2$O. From 100 to 500 MPa, its saturation curve is shifted by ~ 100°C to higher temperatures at low aH$_2$O. Due to the limited experiments containing orthopyroxene, clear systematic trends for low and high aH$_2$O cannot be obtained. Since the Mg# of orthopyroxene correlates well with the Mg# of the associated clinopyroxene (within ~ 5 mol%; see also Fig. 1.7) both for high and low aH$_2$O, we infer that increasing melt fraction and fO$_2$ caused by increasing aH$_2$O, leads to a shift of Mg# to higher values, analogous to clinopyroxene and olivine. The orthopyroxene with the highest Mg# (88.6) is derived from a run performed under water-saturation at a remarkably low temperature of 980°C (#58).

1.3.3.5. Fe-Ti-Cr-Al Oxides

We observed both chromite and magnetite as spinel phases in our experiments, forming tiny crystals often too small for reliable electron microprobe analysis (compositions are presented in the electronic supplementary material only). Chromite typically crystallized at high temperatures and magnetite is the only stable oxide phase at low temperatures. The experimental chromites show compositions typical for those in MORB´s and oceanic gabbros (e.g., Rollinson et al. 2002), ranging in composition between Cr#31-56 [Cr# = Cr / (Cr + Al)] and Mg#72-83. At 200 and 500 MPa for high aH$_2$O chromite and magnetite obviously form solid solutions. For low aH$_2$O at these pressures and at 100 MPa for all water contents both spinels show distinct stability fields separated by a temperature gap. However, due to the close relationship between water activity and oxygen fugacity in our experiments, it is not possible to trace back the observed compositional trends affected by water to either *a*H$_2$O or

fO$_2$. Ilmenite was not observed in our experiments, probably due to the low TiO$_2$ content of the system. Due to the oxidizing conditions in our experiments, the ulvöspinel component of magnetite is high, ranging between 1.3 and 15.4 mole% (calculated after Stormer 1983).

1.3.3.6. Amphibole

The amphiboles are pargasite-hastingsite solid solutions (classification after Leake et al., 1997; compositions are presented in the electronic supplementary material only) and are stable at all three pressures at temperatures below 1020°C. Due to the limited experimental products containing amphibole, systematic trends cannot be obtained. At 200 MPa amphibole crystallized at 980°C show higher tetrahedral Al and Na on the A-site as an amphibole formed at 940°C, which is in agreement with previous experimental studies (Blundy and Holland 1990; Ernst and Liu 1998; Koepke et al. 2004; Sisson and Grove 1993a). When applying the experimental amphibole compositions to the hornblende-plagioclase geothermometer of Blundy and Holland (1990), the experimental temperatures can be reproduced well (experiment #31 and #32 within 20°C; #58 and #83 within 40 °C).

1.3.3.7. Glass compositions

The effect of water on the evolution of the residual melts (compositions in Table 1.2) is complex due to the interplay of different effects. First, with increasing pressure we observe a strong depression of the plagioclase-saturation temperatures, caused by the water content affecting the plagioclase component in the melt. Second, since our experiments are performed under H$_2$-buffered conditions, water shifts the oxygen fugacity drastically to higher values, affecting mainly the MgO/FeO ratio in the melt and the stability of magnetite and mafic minerals and their compositions. This leads in general to significantly lower FeO contents in

34

water-rich melts in comparison to dry melts at a given temperature. One consequence of this is that water can change the differentiation trend from "tholeiitic" to "calc-alkaline" as shown by Berndt et al. (2005) for a primitive MORB system. Third, water not only delays the crystallization of the minerals, it affects also their compositions and consequently the composition of the coexisting liquids. The effect of water on the liquid lines of descent obtained from our experiments performed at 200 MPa is shown in Figure 1.11 where the concentration of selected elements in the melt is plotted versus melt fraction. We did this because water shifts the crystal-saturation curves to significantly lower temperatures. This increases the melt fraction considerably, which affects in turn the melt composition, preventing the adequate evaluation of the effect of water on melt compositions in temperature–related plots.
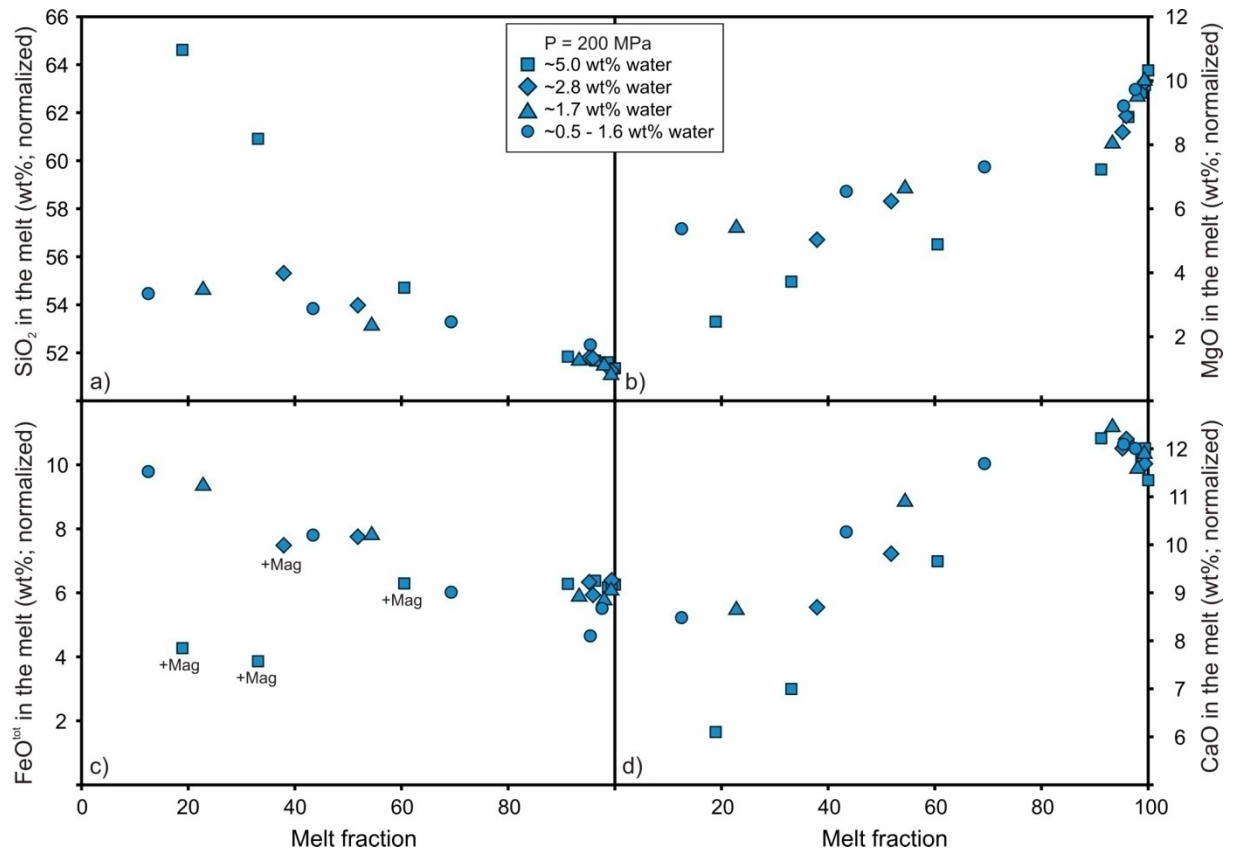
Fig. 1.11: Selected components of the experimental melts as a function of the melt fraction, calculated by mass balance, for different water contents at 200 MPa. Abbreviations: Mag - magnetite; Amph – amphibole

From Figure 1.11a it can be inferred that water forces the melt to higher silica contents. The residual melt compositions range from "primitive" basaltic to evolved melts approaching the composition of tonalites. Such silicic melts were only observed in water-saturated experimental runs. MgO contents of the residual glasses decrease rapidly with decreasing glass fraction, due to the crystallization of spinel and olivine at high temperatures (Fig. 1.11b). Because of the delayed plagioclase crystallization and the increased forsterite contents in olivine due to the higher oxygen fugacity, water shifts the MgO content of the melt to lower values. The FeO^{tot} content of the melt is shown in Figure 1.11c. In an early evolution state, the iron content remains more or less constant and is thus not significantly affected by the crystallization of spinel and olivine. FeO^{tot} content in the melt starts to increase with the crystallization of plagioclase. In the low temperature experiments at high water contents, significant amounts of magnetite crystallize resulting in a downward trend. High iron contents in the melts were only reached at reduced water activities. During early crystallization CaO increases in the residual melts (Fig. 1.11d) due to the negligible CaO contents in the liquidus minerals spinel and olivine. When plagioclase and clinopyroxene starts to crystallize, CaO in the melt decreases rapidly. Due to the strong effect of water on the plagioclase composition, the CaO content of the melt shows a characteristic shift in the trends for the different water contents to lower CaO values.

1.4. Discussion

1.4.1. The stability of orthopyroxene in oceanic gabbros

Knowledge of the stability of orthopyroxene in experimental MORB systems is important, since the genesis of oceanic plutonic rocks containing primary orthopyroxene is still under

debate (e.g. gabbronorites in the Oman ophiolite or at the Mid-Atlantic Ridge, Boudier et al. 2000; Nonnotte et al. 2005; Shipboard Scientific Party 2004). From experimental studies it is well known that the stability field of orthopyroxene is increased by (1) higher silica activities and (2) by higher pressures of crystallization.

(1) Our experiments show that the silica activity at crustal pressures of our primitive tholeiitic basalt is probably not high enough to produce near liquidus orthopyroxene under dry conditions. In the experiments, orthopyroxene always crystallizes late, at relatively low temperatures (Fig. 1.3). Even at 500 MPa, where the stability of orthopyroxene is enlarged (under nominally dry conditions), the system has to crystallize more than 66 wt%, before the first orthopyroxene is formed. This implies that the formation of typical gabbronoritic cumulates by simple crystal fractionation seems unlikely. At least one or two fractionation steps are necessary to increase the silica activity in the residual melt (see also Berndt et al., 2005). This is in accord with observations in natural gabbros from the Oman ophiolite where Boudier et al. (2000) found that in a given crustal section typical gabbronorites do not differ chemically from olivine gabbros, except a characteristic SiO_2 enrichment in the former.

(2) The experiments show that the stability of orthopyroxene is significantly affected by the crystallization pressure (Fig. 1.12). Under nominally dry conditions the orthopyroxene-saturation curve is significantly shifted to higher temperatures (~100°C for a pressure shift from 100 to 500 MPa), whereas under water-saturated conditions, the opposite trend is observed. Thus, pressure enhances the orthopyroxene stability significantly, but only under dry conditions. This is in accord with studies of gabbronorites from the Mid-Atlantic Ridge where pressures up to 800 MPa were considered necessary for the intrusion of gabbroic plutons into the mantle beneath the crust (Shipboard Scientific Party 2004).

The phase diagram in Figure 1.12 clearly shows that higher water contents in the melts destabilizes orthopyroxene which could be either the result of a change in melt composition as a function of pressure, water as a chemical component or due the rise in oxygen fugacity with

increasing water content. Since it is well-known that higher oxygen fugacities stabilize orthopyroxene (e.g., Berndt et al. 2005; Boudier et al. 2000; Grove and Baker 1984; Grove and Juster 1989) it seems clear that water itself or the change in melt composition destabilizes orthopyroxene in our experiments. The experiments do not allow to distinguish between these effects. However, the melt composition is strongly effected by the water-sensitivity of the stability of plagioclase, which is a key parameter for silica enrichment under water-saturated conditions. Increasing pressure shifts the crystallization temperature of plagioclase to lower temperatures and therefore delays the silica enrichment in the melt and the precipitation of orthopyroxene. This is in accord with the experimental findings of Gaetani et al. (1993, 1994) for a basaltic andesite. Thus, our study supports a model that orthopyroxene-rich rocks can be generated by simple hydration of a tholeiitic basaltic system (e.g. Boudier et al. 2000) only under low pressures, where the oxidizing effect of the hydrations is dominating. Under higher pressures, however, the delay in plagioclase crystallization caused by water resulting in a lower silica activity of the melt becomes more important preventing orthopyroxene crystallization.
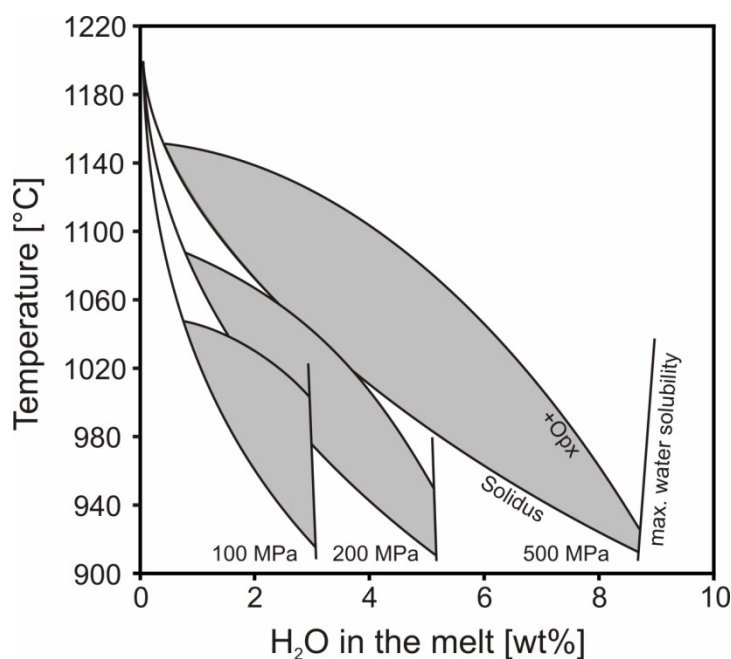
Fig. 1.12: Stability field of orthopyroxene at different pressures. At low water contents the liquidus temperature is shifted to significantly higher temperatures, whereas water-saturated conditions shift the stability of orthopyroxene to lower temperatures.

1.4.2. Effect of H$_2$O on element partitioning

1.4.2.1. Ca partitioning between olivine and melt

The amount of calcium in olivine has been the object of many studies (Jurewicz and Watson 1988; Libourel 1999; Longhi et al. 1978; Roeder 1974; Watson 1979). The melt and olivine compositions have the major control on the CaO content, whereas the effects of temperature, pressure and oxygen fugacity are negligible. Libourel (1999) developed a model to calculate the calcium partition coefficient between olivine and melt based on their compositions. The model provides good predictions for dry magmatic systems. In a water-bearing system Berndt et al. (2005) observed a deviation from the predicted values and supposed that water affects the partition coefficient. Our results correlate well with the effects described by Berndt et al. (2005). While the dry experiments, independent of pressure, correspond with the model of Libourel (1999), our water-bearing experiments show a systematic deviation from the calculated values (Fig. 1.13). This deviation is a function of water in the coexisting melt, which is controlled by the adjusted water activity and by the prevailing pressure. But besides the effect of water, temperature also influences the deviation. At lower temperatures the deviation is smaller.
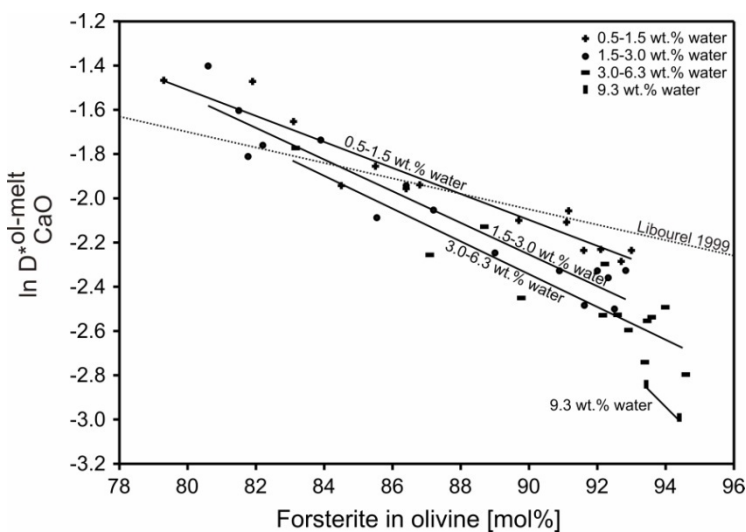
Fig. 1.13: The influence of the water content of the melt on the Ca-partitioning in olivine. The dotted line in the plot belongs to the equilibrium study of (Libourel 1999). The solid lines show the water-content of the melt of the performed experiments. It is noticeable that their is a significant influence of water on the Ca-partitioning in olivine. With increasing water-content, the lnD* ol-melt/CaO value is depressed to lower values.

To separate the effect of temperature from the water effect, we included the forsterite content of olivine into the calcium partitioning calculations. This allows the calcium partitioning to be plotted as a function of temperature (Fig. 1.14). The effect of water is expressed by a strong increase of calcium partitioning into olivine with decreasing water content. This increase mainly reflects the lower calcium content of olivine in water-bearing systems. In a water diffusion study, Behrens and Schulze (2000) observed a strong bonding of hydrous species on Ca-complexes in the melt. This effect could result in a reduced calcium activity in the melt and thus decreases the calcium content in olivine. However, further experiments at different oxygen fugacities are necessary to determine a systematic effect of the redox-conditions on the calcium partitioning. With the help of an extended database, the calcium partitioning between olivine and melt has the potential to be used as a "geohygrometer". A possible application could be the determination of the initial water content of a degassed olivine basalt.
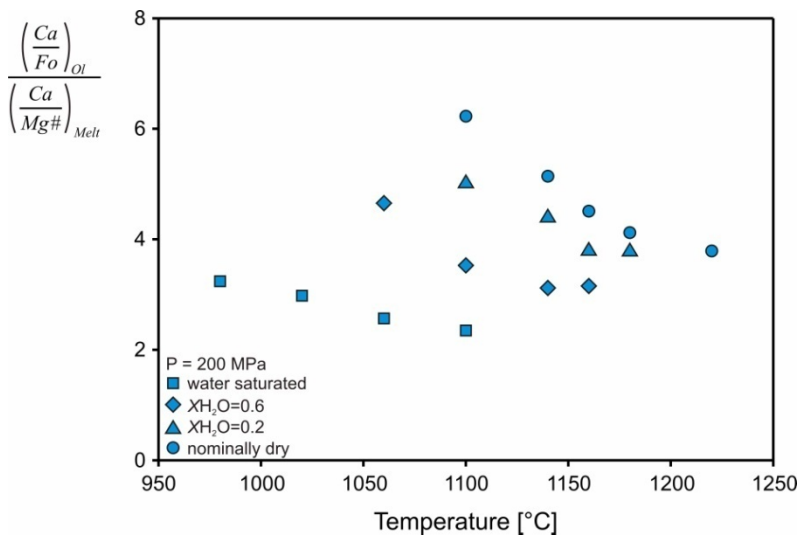
Fig. 1.14: Molar ratios of Ca/Fo in olivine and Ca/Mg# in the melt are used to illustrate the Ca-partitioning between olivine and melt as a function of temperature. The calculated Ca-partitioning varies systematically with water in the system

1.4.2.2. Ca/Na partitioning between plagioclase and melt

Sisson and Grove (1993a) showed with melting experiments on a high-alumina basalt that the $K_{D\,Ca-Na}^{Plag-Melt}$ (calculated using equation 2) is very water sensitive, with higher $K_{D\,Ca-Na}^{Plag-Melt}$ values with increasing amount of water in the melt.

$$K_{D\,Ca-Na}^{Plag-Melt} = \frac{(Ca/Na)_{plag}}{(Ca/Na)_{Melt}} \text{ in mole} \qquad (2)$$

They determined a $K_{D\,Ca-Na}^{Plag-Melt} = 5.5$ at 200 MPa (~6 wt% H_2O in the melt) and a $K_{D\,Ca-Na}^{Plag-Melt} = 3.4$ at 100 MPa (~4 wt% H_2O in the melt). Further experiments under dry conditions and pressures between 800 and 1200 MPa produced $K_{D\,Ca-Na}^{Plag-Melt}$ values below 2.0, which infers that the increase in $K_{D\,Ca-Na}^{Plag-Melt}$ in their water-bearing experiments is related to water.

To better understand the effect of bulk composition on the element partitioning, we collected plagioclase-glass pairs from a number of experimental studies showing a wide range in mafic compositions. All were water-saturated (except for 1 atm experiments), and as the pressure mainly controls the water content, an effect of the composition on the water solubility is negligible compared to the scattering of the experiments. At the same pressure (same water content) all compositions have similar $K_{D\,Ca-Na}^{Plag-Melt}$ values (Fig. 1.15).
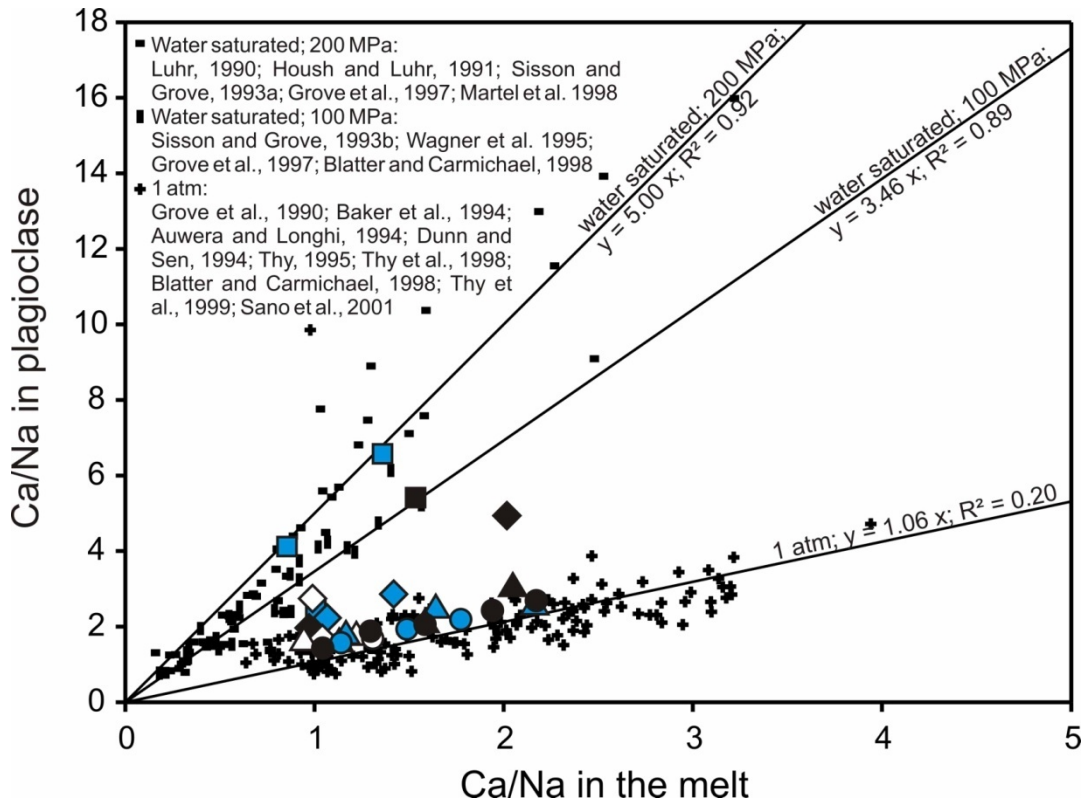
Fig. 1.15: Effect of water on Ca/Na pairs of plagioclase and the coexisting melt. The different pressures marked in the diagram control the water solubility in the melt. In this diagram they are used to compare the effect of different water contents on the K_D value. The effect of pressure itself is negligible. The big symbols correspond to our experimental study (see Fig. 3 for the signature). The small symbols correspond to a number of experimental studies with a huge variety of different compositions (basalts, andesitic basalts, andesites, high alumina basalts, komatites, alkaline basalts). The different compositions deviate only slightly in water solubility and thus plot on the same line. Water shifts the K_D value from ~1 (dry conditions) to ~3.5 under water-saturated conditions at 100 MPa (~3.2 wt% water) and to ~5 under water-saturated conditions at 200 MPa (~5 wt% water), respectively.

In agreement with the study of Berndt et al. (2005), we conclude that the effect of total pressure is negligible. Our "nominally dry" experiments should confirm this, as they were prepared with the same procedure and should have the same water content. In these experiments, the determined $K_{D\,Ca-Na}^{Plag-Melt}$ values for the three different pressures are indistinguishable from each other (Fig. 1.15). To determine the pressure effect it is necessary to perform experiments in a system that is really dry. But as discussed above, iron-bearing systems always contain a certain amount of water.

However, the $K_{D\,Ca-Na}^{Plag-Melt}$ determined from our experiments fit well with the values from others (Fig. 1.15) indicating that equilibrium was approached in our experiments.

1.4.3. Comparison of the experimental results with thermodynamic models

The experimental results that we provide about the detailed effect of water in the phase proportions and compositions of mafic systems could be incorporated in thermodynamic models. Below we discuss how our results differ from those calculated with currently available thermodynamic calibrations and highlight the problems that one might encounter when applying them to water-rich systems.

Thermodynamic models are often used to calculate phase relations and compositions of magmatic systems. They are used to describe the magmatic evolution including the differentiation paths. Two of the most commonly used models are "MELTS" (Ghiorso and Sack 1995) and "Comagmat" (Ariskin 1999). "MELTS" is a thermodynamic model which performs Gibbs free energy minimization with the use of regular solutions models for both minerals and melt. "Comagmat" is a semi-empirical model where the task of equilibrium is solved iteratively for the system of non-linear equilibrium equations and the mass action law using dependencies of equilibrium constants for each mineral–melt reaction on temperature and composition (Ariskin 1999). The lack of a sufficient number of experiments in hydrous mafic systems introduces a large uncertainty in the phase equilibria results of both models (Fig. 1.16). To compare the calculations of the models with our experimental results, we used the same conditions as in the experiments (fO$_2$, P, H$_2$O and equilibrium mode).

"MELTS" for example slightly overestimates the liquidus temperature for olivine independent of the prevailing water content. In the calculations, the stability of olivine at low temperatures is strongly related to the stability of orthopyroxene. With the strong increase of orthopyroxene

43

stability with pressure the "olivine-out" boundary is shifted to much higher temperatures than we have observed.
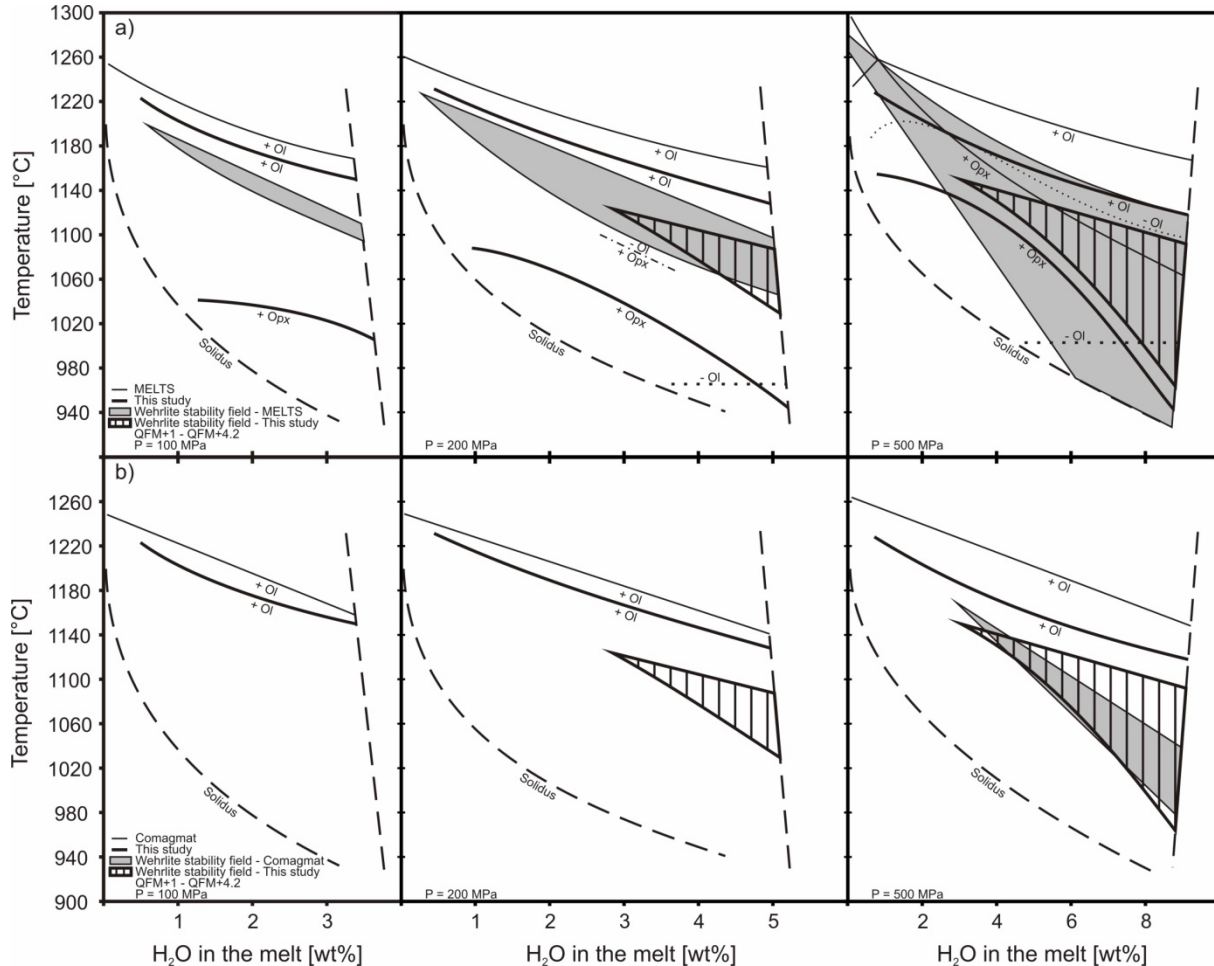
Fig. 1.16: Phase relations of our system compared with two of the most commonly used models - MELTS (a) and Comagmat (b). The thin lines are calculated phase boundaries, the thick lines correspond to our observations. It should be noted that MELTS is only able to predict phase equilibria for redox conditions ≤ QFM+3. Since those experiments with very high water-activity were conducted at higher oxygen fugacities, the corresponding phase equilibria calculated by MELTS was extrapolated.

The phase boundaries of clinopyroxene and plagioclase form the stability field for wehrlites (cumulate rocks consisting of olivine, clinopyroxene ± spinel without plagioclase) shown in Figure 1.16. This field is produced by a shift of the stability of plagioclase to lower temperatures due to water. In the experiments, the wehrlitic paragenesis was only observed at pressures >100 MPa and high water contents. "MELTS" overestimates the stability of

wehrlites in our system and produces wehrlites even at pressures of 100 MPa and at nearly dry conditions (Fig. 1.16a).

 "Comagmat" calculates the stability field of olivine well. Even at high water contents, the calculated liquidus depression is in agreement with the experiments. Due to the limitation of the numerical model to ~80% crystal fraction, no orthopyroxene was observed. Compared to the experiments and in contrast to "MELTS", "Comagmat" underestimates the stability field of wehrlites and produces wehrlites only at pressures > 200 MPa (Fig. 1.16b).

1.4.4. Evolution trends for different bulk water contents

Since our experiments show that water may significantly influence the phase relations, it is of interest to know how water would affect potential differentiation trends in a primitive tholeiitic basaltic system. Figure 1.17 shows the estimated evolution trends for a melt with different bulk water contents at a pressure of 200 MPa based on the phase equilibria obtained from our experiments in combination with mass balance calculations. The evolution lines terminate at those conditions where the residual melt fraction is expected to be less than ~ 10 wt%.

At the lowest bulk water content of 0.2 wt%, the estimated evolution trend is practically indistinguishable from the case of completely dry crystallization. Thus, the fractionation/accumulation of crystallized minerals would produce typical troctolitic or gabbroic cumulate rocks as a function of temperature. However, due to the increased water content, both plagioclase and olivine/clinopyroxene would show increased An contents and Mg#, respectively, compared to the dry system.
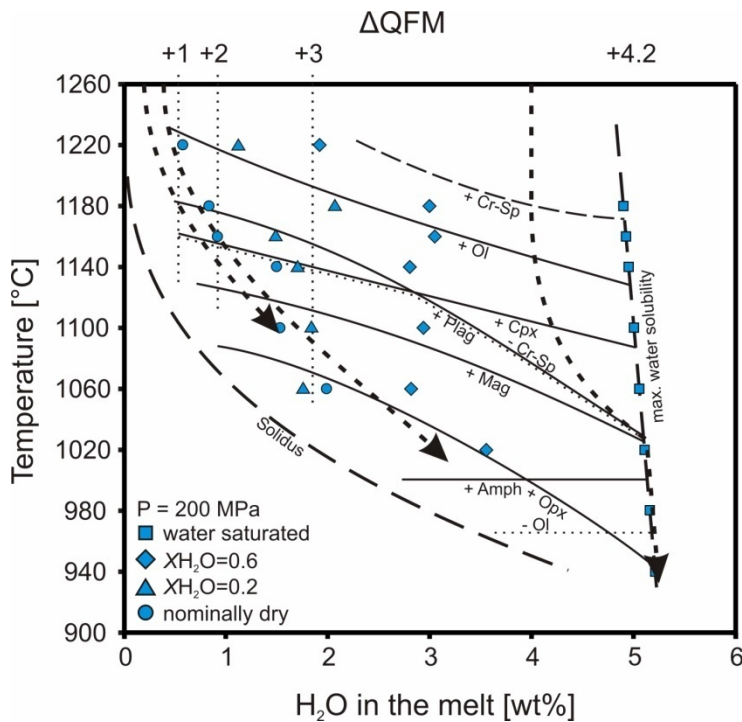
Fig. 1.17: Determined phase relations at 200 MPa (similar to Fig. 1.3b), with estimated evolution trends of the system for different water contents of the starting material (0.2 wt %, 0.4 wt % and 4 wt %; represented by arrows). The shape of the evolution lines is estimated from the mass balance calculations of the performed experiments (Tab. 1.1).

With a water content of 0.4 wt%, the evolution line is more or less parallel to the above trend, at slightly higher water contents. Fractionation/accumulation of crystallized minerals at temperatures > 1100°C would produce similar cumulate rocks as before, but with slightly higher An and Mg# in plagioclase and olivine/clinopyroxene, respectively. At temperatures below 1060°C orthopyroxene crystallizes. At lower temperatures the residual melt has the potential for significant water enrichment reaching the stability field of amphibole at temperatures below ~ 1000°C. Thus the probability for forming gabbroic cumulates including interstitial orthopyroxene and/or amphibole is increased.

Starting with a high bulk water content of 4 wt% results in a completely different evolution trend, as illustrated in Figure 1.17. The main effect is that the plagioclase-saturation curve is significantly depressed, resulting in a change in the crystallization order and in the co-precipitation of olivine and clinopyroxene without plagioclase. Thus, a potential cumulate rock formed by crystal accumulation at temperatures of ~ 1100°C would result in typical wehrlite. This aspect is discussed in detail in the next section.

1.4.5. Implications for the origin of wehrlites within the lower oceanic crust

Many ophiolites contain wehrlitic rocks, characteristically intruding the deeper parts of the magmatic section (for details see Nicolas (1989) and references therein). For instance, in the Oman ophiolite, wehrlite bodies were found at different crustal levels from the sheeted dikes down to the Moho transition zone (e.g., Adachi and Miyashita 2001; Juteau et al. 1988). The Mg# of the olivines and clinopyroxene of these rocks are characteristically quite high, often > 90 (Juteau et al. 1988; Koepke et al. 2005a). However, such rocks are rare in drilled or dredged samples of mid-ocean ridges.

In the ophiolite of Macquarie Island, crustal wehrlites are observed as intrusions up to the sheeted dyke level (Jeff Karson, personal communication). This would seem to indicate a water-rich magma in the crustal section, based on our results. The mantle section at Macquarie also shows geochemical characteristics typical of ophiolitic mantle sections, and atypical of mid-oceanic ridge mantle sections (Wertz et al. 2004) and caused by hydrous re-melting and metasomatism of the mantle. Thus, although Macquarie Island appears to be a nearly in-situ slice of mid-ocean ridge, it appears to have had a more hydrous origin than is typical of MORB. This may be related to the highly oblique nature of the plate boundary at that time, though this point is by no means settled.

The origin of wehrlite intrusions within the oceanic crust is not clear. Current models explain the wehrlite bodies as impregnated mantle peridotites (Benn et al. 1988), as cumulates from subduction zone-related tholeiitic basaltic melts (Kelemen et al. 1997), or from picritic melts (Juteau et al. 1988). Studies of Koga et al. (2001) and Koepke et al. (2005a) showed that the clinopyroxenes of the crustal wehrlites from the Oman ophiolite could be in chemical equilibrium with typical MORB and suggest that models involving mantle impregnation or picritic melts are probably not important here.

Since these crustal wehrlites show typical cumulate structures, it is likely that these rocks "intruded" as mushes of accumulated crystals in a MORB-type system. To form the critical wehrlite paragenesis of olivine + clinopyroxene ± spinel (without plagioclase) by crystal accumulation in a dry MORB at shallow pressures is nearly impossible, since in "dry" MORB melts, plagioclase crystallizes together with olivine, distinctly before the precipitation of clinopyroxene (see previous section). Our experiments show that at pressures > 100 MPa, water changes the crystallization order and forms a field where the wehrlite paragenesis is stable (as shown in Fig. 1.3). The corresponding olivines and clinopyroxenes typically show high Mg# (up to ~ 93 mole % Fo in olivine). This agrees with the phase compositions of natural wehrlites from the Oman ophiolite (Koepke et al. 2005a; Koga et al. 2001). Thus, the experiments suggest that typical crustal wehrlites present in many ophiolites could be interpreted as cumulates of very water-rich tholeiitic melts, formed at pressures > 100 MPa, temperature ~ 1060°C and water contents of more than 3 wt%.

For this model, special requirements are necessary, since it is well-known that typical MORB is more or less dry with water contents significantly below the 3 wt% mentioned above. There are two possible origins for the water-enrichment in MORB melts under the ridges. First, high water-contents can be achieved in MORB melts generated above subduction zones, which in principle can be related to spreading systems from fore-arc or marginal basin settings (e.g., Ishikawa et al. 2002; Lachize et al. 1996; Miyashiro 1974; Nicolas 1989; Pearce et al. 1984). Second, there is more and more evidence supporting a model that aqueous fluids derived from seawater may penetrate into magma chambers beneath ridges (Benoit et al. 1999; Bosch et al. 2004; Boudier et al. 2005; Koepke et al. 2005c; Koepke et al. 2005b; Koga et al. 2001; Nicolas and Mainprice 2005; Nicolas et al. 2003; Nonnotte et al. 2005). For these reasons, further investigation of water-bearing MORB systems, particularly at lower fO_2, is likely to prove fruitful for understanding the magmatic evolution of mid-ocean ridges.

1.5. Conclusions

Water dramatically influences the phase equilibria of a tholeiitic basaltic system, and therefore magmatic processes at mid-ocean ridges and marginal basins in general. The results of this study support many of the well-known effects with water, like depression of liquidus and solidus, increasing melt fraction at a given temperature, depressing the saturation of plagioclase, changing of the liquid lines of descent, and influencing the element partitioning between crystals and melt.

This study defines clearly the shifting of phase boundaries and mineral compositions as a systematic function of water content between "dry" conditions and water saturation. These conditions correspond somewhat indirectly to the conditions of actual MORB formation, as the oxygen fugacity studied here was higher than those thought to be characteristic of MORB. However these results delineate the general trends of petrogenesis in hydrous basaltic systems.

One interesting result of our investigation is a re-investigation of the term "dry". We realized that the melt compositions of even nominally dry runs still contained up to half a percent of water. In many previous experiments conducted under "dry" conditions, the content of water was never actually measured, but simply assumed to be zero. For example, nominally anhydrous high pressure experiments performed in Piston Cylinder apparatus are often not absolutely water-free (Hirschmann et al. 1998; Holtz et al. 2001; Kagi et al. 2005). This may result in a considerable amount of water-induced fluctuation in the current experimental literature that should be investigated more fully.

The genesis of wehrlites in the ocean crust is more than just academic in nature. Wehrlites are a component of most ophiolites, but are extremely rare to nonexistent in samples dredged and drilled from modern ocean crust *in situ*. This has led many researchers to assert that wehrlites

are present even in dry mid-ocean ridge systems, but are simply not dredgeable or drillable because of their location in the mid-segment lower crust. Our results suggest that this difference between ophiolites and ocean crust is a critical one, since a high water content is truly required for the generation of wehrlites. This is not to suggest that wehrlite formation at mid-ocean ridges is impossible, but it seems unlikely that large volumes of it are hiding somewhere beneath most mid-ocean ridges. Macquarie Island seems to be an exception to this (Wertz et al. 2004).

Another result of this work is the effect of water on Ca partitioning into olivine. In principle, with further work, it should be possible to calibrate a "geohygrometer" based on this effect that should be of great use in determining the water content of subaerial basalts and those oceanic basalts which reach water saturation during eruption and degas. A surprising number of MORB samples, even form relatively deep water show large scale vesicle formation. If the water content of erupted basalts could be measured post hoc, then the vesicularity and residual water content of ocean floor basalts might well be useful in determining the eruption history.

The results from this study show significant departures of the temperatures of crystallization and the compositions of phases crystallized to those predicted by hybrid thermodynamic/empirical and purely empirical models such as "MELTS" and "Comagmat". This is to be expected, since the lack of observations in this region of pressure-temerature-composition space were one of the motivating factors of this study. One benefit of this study is that these data represent an internally consistent data set for a primitive tholeiitic basaltic system in terms of temperature, water content, and pressure. Thus, these data should serve to improve future models. The next critical step in the exploration of tholeiitic systems will be a parallel set of water-bearing experiments in the same system at lower fO_2 under otherwise similar conditions. This study covering a redox range from QFM-3 to QFM+2 is in progress.

2. Effect of oxygen fugacity on phase equilibria of a hydrous tholeiitic basalt

2.1. Introduction

The prevailing oxygen fugacity (fO_2) of a magmatic system strongly affects the magma evolution from partial melting to volcanic eruption. Most striking is the effect of different redox conditions on the crystallization processes within a magma chamber. Generally, the oxygen fugacity controls the Fe^{2+}/Fe^{3+} ratio in the melt and therefore affects the relative phase stabilities of iron-bearing mineral phases and oxides, their compositions and their proportions in a crystallizing magmatic system (e.g., Berndt et al., 2005; Toplis and Carroll, 1995). Consequently, the prevailing oxygen fugacity also has a significant effect on melt differentiation trends (e.g., Berndt et al., 2005; Koepke et al., 2007; Osborn, 1959; Snyder et al., 1993; Toplis and Carroll, 1995). Whereas the calc-alkaline differentiation trend is characterized by a significant increase of silica content under relatively constant Fe/Mg ratios, the tholeiitic differentiation trend is characterized by a continuous iron enrichment of the melt (e.g., Grove and Kinzler, 1986; Sisson and Grove, 1993a; Toplis and Carroll, 1995; Wager and Deer, 1939). All these observations make the oxygen fugacity an important parameter for the understanding and the characterization of magmatic processes and of natural magmatic systems in general.

Fundamental for the application of the parameter "oxygen fugacity" on magmatic systems is a accurate measurement of the Fe^{2+}/Fe^{3+} ratio in the melt (e.g., Fialin et al., 2004; Mysen et al., 1985; Wilke, 2005). Based on experimental studies (see next chapter), the prevailing oxygen fugacity was correlated with the Fe^{2+}/Fe^{3+} ratio of the melt, and empiric and thermodynamic models were calibrated to predict prevailing redox conditions (e.g., Kilinc et al., 1983; Kress and Carmichael, 1991; Moretti, 2005; Sack et al., 1980). However, the effect of redox

conditions and especially the interplay between water activity and prevailing oxygen fugacity of natural tholeiitic basaltic systems is poorly understood. This study is aimed to get a better understanding of details of these complex relationships and is strongly linked with chapter 1 (Feig et al., 2006). The chemical system, the investigated temperature interval and the used equipment of both studies is identical. While chapter 1 focused on the effect of water and pressure on the phase equilibria, this study aims on the effect of variable oxygen fugacities in a hydrous, primitive tholeiitic basaltic system. We present here new crystallization experiments (about 44 runs) in which oxygen fugacity and water content was varied (from "nominally dry" to water-saturation) to investigate the interplay between redox conditions and an aqueous phase. The whole investigated experimental range in oxygen fugacity covers about 7 log units including those typical redox conditions known for basaltic magmatism (Bezos and Humler, 2005; Christie et al., 1986; Johnson et al., 1994). Together with the study of results of chapter 1 (Feig et al., 2006), we present here a consistent experimental data base in a primitive tholeiitic system which is well-constrained in terms of temperature (940-1220°C), pressure (100 to 500 MPa), water content (nominal dry to water-saturation), and oxygen fugacity (7 log units).

2.1.1. Previous experimental work

The effect of redox conditions on the phase equilibria and differentiations trends in basaltic systems has been the object of many experimental studies. Most of recent experimental studies were related to the stability of iron-titanium oxides (e.g. Snyder et al., 1993; Thy and Lofgren, 1994; Toplis and Carroll, 1995), or were aimed on the composition of mafic phases as a function of oxygen fugacity (e.g. McCanta et al., 2004; Mysen, 2006; Snyder and Carmichael, 1992). All of these experimental studies were conducted in gas mixing furnaces at 1 atm with accurate control on the prevailing oxygen fugacity. The disadvantage of 1 atm

experiments is that they are limited to dry conditions and do not allow predictions about the interplay between fluids and redox conditions in the system.

Investigating the effect of oxygen fugacity under elevated pressures is more complicated. Generally, experiments at a given pressure were performed in noble metal capsules representing a closed system with the exception of hydrogen. The hydrogen in turn controls the prevailing oxygen fugacity in the capsule. There are two different approaches to controlling the hydrogen in the system, the double capsule technique (Eugster, 1957) and the hydrogen membrane (Berndt et al., 2002; Scaillet et al., 1992; Schmidt et al., 1995; Shaw, 1963). In double capsule experiments, the capsule containing the charge is surrounded by a second capsule filled with a solid buffer (e.g. Ni-NiO) + H_2O, which fixes the hydrogen pressure. This approach is mainly used in piston cylinder setups (e.g. Gaetani and Grove, 1998; Kagi et al., 2005; Muntener et al., 2001). The second approach (which was used in this study) is restricted to gas pressure vessels and is based on different argon-hydrogen mixtures of the pressure medium. The hydrogen membrane allows determining the oxygen fugacity by measuring the hydrogen pressure within the membrane (e.g. Berndt et al., 2005; Botcharnikov et al., 2005; Martel et al., 1999).

Double capsule experiments and the hydrogen membrane technique were used to investigate the effect of oxygen fugacity on the phase relations, phase chemistry, element partitioning and differentiation trends of basic systems at elevated pressures. However, their are only a few experimental studies under controlled water activity and oxygen fugacity under crustal pressures and their influence on the phase equilibria of basaltic systems cannot be estimated accurately. Sisson and Grove (1993a) performed experiments under water-saturated conditions using a high-alumina basalt. They showed that beside oxygen fugacity also water could change the differentiation trend from tholeiitic to calc-alkaline. Berndt et al. (2005) conducted crystallization experiments at two different oxygen fugacities in a MORB system at 200 MPa. Under both oxygen fugacities, four different bulk water contents were applied to

investigate the effect fO_2 and H_2O on the phase equilibria. Close to the QFM-buffer the obtained liquid lines of descent shows a tholeiitic differentiation trend, while at oxidizing conditions close to QFM+4 a calc-alkaline differentiation trend was observed. Botcharnikov et al. (2005) investigated the effect of water activity on the oxidation state of iron in a ferrobasaltic system. The experiments show that the oxygen fugacity of the system is directly related to the applied water activity.

2.2. Experimental and analytical methods

2.2.1. Experimental strategy

Two sets of experiments with different nominal fO_2 were performed at a pressure of 200 MPa, corresponding at water-saturation ($aH_2O = 1$; aH_2O: water activity) to ~QFM (quartz-magnetite-fayalite buffer) and ~QFM+2, respectively. As a third experimental data set for highly oxidizing conditions we used the experimental results presented in chapter 1 (Feig et al., 2006) performed at a nominal fO_2 corresponding to QFM+4.2 (at water-saturation) in the same chemical system at the same pressure of 200 MPa. For convenience we name these three sets of different redox conditions in the following "reducing" (QFM), "intermediate" (QFM+2), and "oxidizing" (QFM+4.2). Since the redox conditions in our experiments are controlled by hydrogen buffering, each experimental set is characterized by a distinct hydrogen partial pressures, which is high at reducing and low at oxidizing conditions.

For each experimental set we applied 4 different water activities resulting in experimental runs ranging from nominally dry to water-saturation. Decreasing aH_2O decreases the fO_2 for individual runs, since the prevailing oxygen fugacity is strongly affected by the water activity (e.g. Berndt et al., 2005; Botcharnikov et al., 2005; Feig et al., 2006; Scaillet et al., 1995).

Thus, the nominal fO_2 was only reached in those experiments under water saturation, while all experiments performed under $aH_2O < 1$ showed fO_2 below the nominal value. Since aH_2O in each experimental series varies from a very small value to 1, the corresponding fO_2 range covers about three orders of magnitude for each of the three experimental sets. Thus, the variations in water activity for all three experimental series resulted in redox conditions corresponding to a range of fO_2 from QFM-3 up to QFM+4.2. On the one hand, this feature opens interesting possibilities to investigate phase equilibria for a very broad range of redox conditions with fO_2 covering more than 7 orders of magnitude. On the other hand, the phase equilibria are always the function of the combined effects of fO_2 and aH_2O, and it is very difficult to evaluate the individual effects of either aH_2O or fO_2 from this type of experiment.

2.2.2. Experimental technique

Most of the experimental techniques, including capsule preparation, starting material, analytical methods and the calculation of water activity and oxygen fugacity are identical to those described in chapter 1 and by Feig et al. (2006) and are therefore presented here only briefly. As capsule materials, gold (at temperatures $\leq 1020°C$) and $Au_{80}Pd_{20}$ (at higher temperatures) were used. To minimize iron loss, all $Au_{80}Pd_{20}$ capsules were pre-saturated with iron. For the pre-saturation process, a glass was synthesized with the same composition as the starting material of the experiments. The glass was crushed and filled into corundum containers together with the $Au_{80}Pd_{20}$ tubes. The containers were held for three days in a gas mixing furnace (H_2-H_2O) at 1300°C above the liquidus of the system, at an oxygen fugacity corresponding to that of the experimental runs. Only tubes that were completely surrounded by glass were used for the experiments. In the final step of the pre-saturation procedure, the glass surrounding the tubes was dissolved with hydrofluoric acid.

In each experimental run, four different XH_2O (molar $H_2O/(H_2O+CO_2)$) were applied: 0.0 (nominally dry), 0.2, 0.6, and 1.0 (water-saturated). All experiments except the nominally dry ones were fluid-saturated. XH_2O of 0.2 and 0.6 are fixed via mixtures of water and silver oxalate ($Ag_2C_2O_4$). For each run 10 to 40 mg of starting glass powder (pre-dried), and the desired amounts of water (using a micro syringe) and silver oxalate were transferred into the capsule. For the "nominally dry" runs, only glass powder was inserted into the capsule and dried at 500°C for ten minutes.

The experiments were performed in an internally heated pressure vessel (IHPV), equipped with a rapid quench system to prevent the formation of quench-crystals (Berndt et al., 2002; Holloway et al., 1992; Roux and Lefevre, 1992) and with a hydrogen membrane to measure the prevailing hydrogen pressure during the experiment (Shaw, 1963). Methodical details on the used IHPV can be found in Berndt et al. (2002). To apply different oxygen fugacities, the vessel was filled with different mixtures of argon and hydrogen. The desired amounts of hydrogen for the experimental conditions (temperature and pressure under water-saturation) were calculated according to the procedure outlined by Scaillet et al. (1995), using data of Shaw and Wones (1964) for the prevailing hydrogen fugacity, Pitzer and Sterner (1994) for the water fugacity, a K_W of Robie et al. (1978) and the equation of Chou (1987) for the oxygen fugacity using values of Schwab and Küstner (1981) and Huebner and Sato (1970). All experiments were performed at a pressure of 200 MPa in the temperature range 940 - 1220 °C. The temperature was measured with four S-type thermocouples, showing a gradient of ≤4°C along the sample and an uncertainty less than ±10°C.

After a certain run duration, the capsules were quenched by melting a platinum wire fixing the capsule in the hot zone of the furnace during the experiment. In order to reach osmotic equilibrium between hydrogen membrane and the gas volume of the vessel, pressure and temperature conditions prevailing in the vessel were maintained after quenching the capsules until pressure increase in the membrane has stopped (for details see Berndt et al., 2002). The

measured hydrogen pressure in the membrane was used to calculate the prevailing oxygen fugacity of the experiment (see Table 2.1).

2.2.3. Starting material

A micrograbbro from the Southwest Indian Ridge (SWIR) drilled by ODP (Ocean Drilling Program; ODP designation: 176-735B-178R-6:132-138; Snow, 2002) was used as starting material for the crystallization experiments. A detailed description of the sample is given in chapter 1. The chemical composition of the sample is close to a primitive tholeiitic basalt, but it contains also a certain cumulate character.

For the crystallization experiments, the sample was crushed and ground in a rotary mortar. The rock powder was fused at 1600°C in an iron pre-saturated platinum crucible and quenched with water. The homogeneity of the glass was confirmed by electron microprobe analyses. In contrast to the procedure described in chapter 1 and by Feig et al. (2006), the sample was crushed again and refused in a corundum crucible at 1300°C for 3 h in a gas mixing furnace at an oxygen fugacity corresponding to the QFM-buffer. After quenching with water, a cylinder was drilled from the glass of the centre of the crucible to avoid alumina contamination of the charge. The composition of the starting material was confirmed again by electron microprobe analyses. Finally, the glass was crushed and ground to a powder with a grain size of <150μm.

Table 2.1: Conditions and phases of the performed experiments

Run	Pressure [bar]	Temperature [°C]	Duration [h]	H_2O in the melt [wt%][1]	aH_2O[2]	fH_2 [bar]	$\log fO_2$ [bar]	ΔQFM	Phases[3]	ΣR^2	K_D Ol-melt/Fe-Mg	Fe-loss [wt%]
#142	2000	1020±4	48	5.12	1.00	25.75	-10.5	-0.02	Ol(9.5) Plag(12.2) Cpx(18.1) glass(60.1)	0.4	0.30	0.2
#143	2000	1020±4	48	n.a.	---	25.75	---	---	Ol Plag Cpx glass	4)		
#145	2007	940±4	115	5.25	1.00	22.82	-11.76	-0.02	Ol Plag Cpx Amph glass	4)		
#146	2046	980±2	90	5.18	1.00	24.44	-11.09	-0.01	Ol(12.5) Plag(26.8) Cpx(22.7) glass(38.0)	0.48	0.29	0.2
#147	2046	980±2	90	n.a.	---	24.44	---	---	Ol Plag Cpx Opx glass	4)		
#148	2034	1060±3	5	5.05	1.00	25.88	-9.86	+0.03	Ol(7.1) Cpx(6.8) glass(86.1)	0.41	0.30	0.3
#149	2034	1060±3	5	n.a.	---	25.88	---	---	Ol Plag Cpx glass	4)		
#150	2034	1060±3	5	n.a.	---	25.88	---	---	Ol Plag Cpx glass	4)		
#151	2034	1060±3	5	n.a.	---	25.88	---	---	Ol Plag Cpx glass	4)		
#152	1989	1100±3	5	4.99	1.00	27.26	-9.34	+0.01	Ol Cr-Sp glass	5)	0.31	
#153	1989	1100±3	5	2.67	0.43	27.26	-10.06	-0.71	Ol(8.9) Plag(15.1) Cpx(12.2) glass(63.8)	0.57	0.30	0.0
#154	1989	1100±3	5	2.25	0.34	27.26	-10.28	-0.92	Ol(13.2) Plag(37.1) Cpx(18.5) glass(31.3)	0.74	0.30	0.0
#155	1989	1100±3	5	n.a.	---	27.26	---	---	Ol Plag Cpx glass	4)		
#156	2017	1140±3	3	4.93	1.00	28.08	-8.80	+0.04	Ol(0.5) Cr-Sp(0.1) glass(99.4)	0.66	0.31	0.0
#157	2017	1140±3	3	1.99	0.26	28.08	-9.97	-1.13	Ol(5.3) Cr-Sp(0.2) glass(94.4)	0.84	0.30	0.2
#158	2017	1140±3	3	1.28	0.14	28.08	-10.50	-1.66	Ol(8.5) Plag(14.8) Cpx(7.0) glass(69.7)	0.49	0.30	0.0
#159	2017	1140±3	3	0.98	0.09	28.08	-10.92	-2.08	Ol(7.8) Plag(16.0) Cpx(9.9) glass(66.2)	1.66	0.29	0.8
#160	2001	1180±3	2	4.86	1.00	29.07	-8.32	+0.04	glass(100.0)			0.2
#161	2001	1180±3	2	2.07	0.31	29.07	-9.32	-0.96	Ol(1.4) glass(98.6)	0.77		0.4
#162	2001	1180±3	2	1.04	0.10	29.07	-10.31	-1.96	Ol(4.4) glass(95.6)	0.99	0.30	0.6
#163	2001	1180±3	2	0.63	0.04	29.07	-11.07	-2.72	Ol Plag Cr-Sp glass	5)	0.30	0.1
#164	2019	1220±1	2	2.28	0.36	32.84	-8.81	-0.91	glass(100.0)			1.6
#165	2019	1220±1	2	1.00	0.09	32.84	-9.98	-2.08	glass(100.0)			2.0
#166	2019	1220±1	2	0.54	0.03	32.84	-10.94	-3.04	Ol(1.4) glass(98.6)	1.76	0.30	1.0
#170	2036	1020±1	42	5.12	1.00	3.45	-8.73	+1.75	Ol(9.9) Plag(12.4) Cpx(15.7) glass(62.0)	0.29	0.30	0.0
#171	2036	1020±1	42	n.a.	---	3.45	---	---	Ol Plag Cpx glass	4)		
#173	2036	1020±1	42	n.a.	---	3.45	---	---	Ol Plag Cpx glass	4)		
#174	1989	1060±2	5	5.05	1.00	2.56	-7.86	+2.04	Ol(7.1) Cpx(8.1) Cr-sp(0.2) glass(84.6)	0.29	0.30	0.0
#175	1989	1060±2	5	n.a.	---	2.56	---	---	Ol Plag Cpx glass	4)		
#178	2042	1100±2	5	4.99	1.00	3.18	-7.44	+1.91	Ol(5.1) Cr-sp(0.8) glass(94.1)	0.73	0.31	0.0

Table 2.1: Continued

Run	Pressure [bar]	Temperature [°C]	Duration [h]	H$_2$O in the melt [wt%][1]	fH$_2$ [bar]	aH$_2$O[2]	log fO$_2$ [bar]	ΔQFM	Phases[3]					ΣR^2	K$_D$ Ol-melt/Fe-Mg	Fe-loss [wt%]
#179	2042	1100±2	5	2.79	3.18	0.47	-8.10	+1.25	Ol(10.4)	Plag(22.6)	Cpx(12.8)	glass(54.3)		0.52	0.30	0.0
#180	2042	1100±2	5	2.24	3.18	0.34	-8.38	+0.97	Ol(13.0)	Plag(40.3)	Cpx(20.4)	glass(26.3)		0.23	0.30	0.0
#182	2060	1220±1	2	4.80	3.31	1.00	-5.91	+1.99	glass(100.0)							
#183	2060	1220±1	2	2.27	3.31	0.37	-6.78	+1.12	glass(100.0)							
#184	2060	1220±1	2	1.09	3.31	0.11	-7.81	+0.09	Ol(0.7)	glass(99.3)				0.49	0.30	0.0
#185	2060	1220±1	2	0.37	3.31	0.02	-9.53	-1.63	Ol	Cr-sp	glass			[4]	0.30	
#186	2056	1180±1	2	4.86	3.25	1.00	-6.38	+1.97	Cr-sp	glass				[4]		
#187	2056	1180±1	2	2.74	3.25	0.47	-7.04	+1.32	Ol(1.9)	Cr-sp(0.3)	glass(97.8)			0.53	0.31	0.0
#188	2056	1180±1	2	1.16	3.25	0.12	-8.21	+0.15	Ol(6.0)	Plag(5.9)	Cr-sp(0.4)	glass(87.7)		0.40	0.30	0.0
#189	2056	1180±1	2	0.84	3.25	0.07	-8.70	-0.35	Ol(7.7)	Plag(16.4)	Cpx(5.2)	glass(70.8)		0.34	0.30	0.0
#190	2038	940±2	68	5.25	2.47	1.00	-9.81	+1.93	Plag(30.9)	Cpx(11.2)	Opx(4.6)	Amph(38.8)	glass(14.5)	0.36		0.0
#191	2047	980±4	50	5.18	2.55	1.00	-9.12	+1.96	Ol(6.0)	Plag(22.6)	Cpx(16.5)	Amph(21.7)	glass(33.3)	0.20	0.30	0.0
#192	2047	980±4	50	n.a.	2.55	---	---	---	Ol	Plag	Cpx	Opx	glass	[4]		0.0
#193	2049	1140±2	2.5	4.93	2.60	1.00	-6.71	+2.13	Ol(1.3)	Cr-sp(1.0)	glass(97.7)			0.84	0.31	0.0
#195	2049	1140±2	2.5	2.18	2.60	0.34	-7.66	+1.18	Ol(11.6)	Plag(34.7)	Cpx(14.2)	glass(39.6)		0.52	0.31	0.0
#196	2049	1140±2	2.5	n.a.	2.60	---	---	---	Ol	Plag	Cpx	glass		[4]		0.0

Abbreviations: ol - olivine; plag - plagioclase; cpx - clinopyroxene; opx - orthopyroxene; cr-sp - Cr-rich spinel; mag - magnetite; amph - amphibole

[1] water content determined with "by-difference" method (e.g., Devine et al. 1995)

[2] aH$_2$O calculated after Burnham (1979)

[3] Phase proportions calculated by mass balance

[4] At least one phase to tiny for reliable microprobe analyses

[5] a negative value is calculated for at least one phase

2.2.4. Iron loss

To minimize iron loss to the sample container Au was used as capsule material at temperatures $\leq$ 1020°C. In these runs, mass balance calculations and element partitioning coefficients infer that iron loss is negligible (Table 2.1). At temperatures >1020°C $Au_{80}Pd_{20}$ was used as capsule material. With decreasing oxygen fugacity, an increase of iron diffusion into the $Au_{80}Pd_{20}$ capsule was observed. To minimize iron loss, we used iron pre-saturated $Au_{80}Pd_{20}$ capsules for the experiments. Additionally, we applied short run durations, maximized the sample powder within a each capsule, and focused the analyses of the phases to the center of the capsule. Mass balance calculations of the run products confirmed that no significant iron loss occurred (Table 2.1). This assumption is supported by the compositions of the iron-bearing phases, which show typical trends as a function of temperature, water content and oxygen fugacity.

2.2.5. Analytical methods

The run products were analyzed with a "Cameca SX100" electron microprobe equipped with the operating system "Peak sight" based on Microsoft Windows. The analytical conditions were identical to those listed in chapter 1.2.5. The water content of the experimental glasses was estimated using the "by-difference" method (e.g., Devine et al., 1995). For this approach, standard glasses of MORB composition with known water contents (published in Berndt et al., 2002) were analysed during each analytical session to calibrate the method.

2.2.6. Calculation of aH$_2$O and fO$_2$

The calculations of the water activity and oxygen fugacity were done in the same way as described in chapter 1.2.3. and by Feig et al. (2006) and is only discussed briefly. Based on the determined water contents of each experiment, the individual water activities were calculated using the model of Burnham (1979) and are presented in Table 2.1. The prevailing oxygen fugacity of the water-saturated experiments were calculated according the procedure outlined by Scaillet et al. (1995), using values of Shaw and Wones (1964) for the prevailing hydrogen fugacity, Pitzer and Sterner (1994) for the water fugacity, a K_W of Robie et al. (1978) and the equation of Chou (1987), using values of Schwab and Küstner (1981) and Huebner and Sato (1970), for the oxygen fugacity. To determine the prevailing oxygen fugacity of the experiments with reduced aH$_2$O, the water fugacities were multiplied with the calculated water activity. An overview of the prevailing oxygen fugacities of the experimental runs is given in Table 2.1. Figure 2.1 shows the effect of water addition on the fO$_2$ of the system. In all the water-saturated experiments, the measured oxygen fugacity tracks the intended buffer perfectly, while with decreasing water content, the effective oxygen fugacity is lowered.
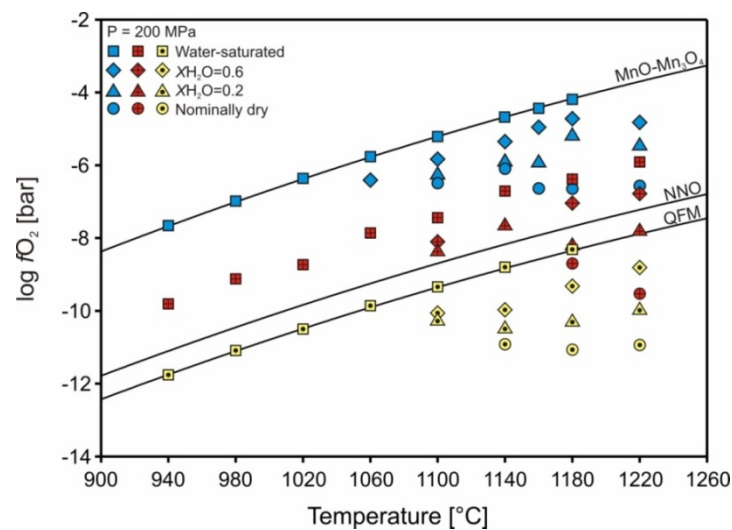
Fig. 2.1: Oxygen fugacity of the performed experiments as a function of temperature. The oxygen buffer curves are calculated after Chou (1987) with values of Schwab and Küstner (1981; QFM and NNO) and Huebner and Sato (1970; MnO-Mn$_3$O$_4$). The calculated values are shown in Table 2.1.

2.3. Results

2.3.1. Achievement of equilibrium

Experimental studies performed in the same IHPV in similar, tholeiitic systems, under similar conditions (e.g., Almeev et al., 2007; Berndt et al., 2005; Freise et al., 2007) reached chemical equilibrium after 5–10 hours at temperatures <1000°C, and after 2-5 hours at temperatures >1000°C, respectively. According to these observations, we applied short run durations (2-5 hours) to our high temperature experiments (>1020°C) to minimize iron loss to the sample container and longer run durations to our low temperature experiments (≤1020°C) to reach larger grain sizes. The following observations suggest that equilibrium was obtained: (1) Glass and crystals are homogeneously distributed along the capsule. (2) The newly formed crystals are chemically homogeneous (Tab. 2.1) and generally euhedral. (3) Measured glasses vary within the counting statistics of the microprobe analyses (Tab. 2.1). (4) The determined phase compositions vary systematically with intensive variables (e.g., water content, temperature). (5) Mineral-melt and mineral-mineral element partitioning relations are generally in good agreement with published data from other studies (e.g., $K_{D\,Fe-Mg}^{Ol-Melt}$ calculated after Toplis, 2005). (6) Most mass balance calculations for individual runs result in $\Sigma R^2 < 1$ (ΣR^2 = sum of residual squares, e.g., Albarède and Provost, 1977; see also Tab. 2.1).

2.3.2. Phase relations

The phase relations were obtained from the presence/absence of mineral phases in the experimental runs. Based on these observations, saturation temperatures for the individual phases were plotted into T-H_2O diagrams. To simplify the discussion of the effect of oxygen

fugacity, we have subdivided the experiments into "oxidizing", "intermediate" and "reducing" (Fig. 2.2a-c), based on the three experimental series performed at nominal QFM+4.2 ("intrinsic" redox conditions; data from Feig et al., 2006), QFM+2 and QFM under water-saturated conditions. Most striking is the effect of oxygen fugacity on the stabilities of mafic minerals, whereas iron-free minerals show only minor changes.

A chrome-rich spinel is the first mineral phase precipitating under oxidizing conditions and at high water-contents under an intermediate oxygen fugacity, followed by olivine. Under intermediate conditions and low water-contents and under reducing conditions respectively, chrome-rich spinel crystallizes after olivine. At lower temperatures clinopyroxene (Cpx) and plagioclase start to crystallize. Independent of the prevailing oxygen fugacity, clinopyroxene crystallizes before plagioclase at high water-contents ($>$ ~3 wt%), but after plagioclase at low water contents. Generally, the chrome-rich spinel disappears with the crystallization of clinopyroxene. Under oxidizing conditions the crystallization of plagioclase and clinopyroxene is followed by magnetite, while under intermediate and reducing conditions magnetite was not observed. A further decrease of temperature results in the precipitation of orthopyroxene (Opx) and amphibole near to the solidus of the system. Under oxidizing conditions, we observe a shift of the saturation temperature of orthopyroxene to slightly higher temperatures compared to more reducing conditions.

It is a characteristic feature of hydrogen-buffered experiments used in this study that water activity directly affects fO$_2$. This effect is expressed in Fig. 2.2 by presenting values for ΔQFM directly correlated with the melt water content in each phase diagram. Therefore, the phase relations presented in Fig. 2.2 are always controlled by the combined effect of water as a chemical component and of fO$_2$ controlled by aH$_2$O. A typical effect of water as a chemical component is the well-known enhanced shift of the plagioclase saturation curve to lower temperatures compared to other mineral phases (e.g., clinopyroxene). On the other hand, a
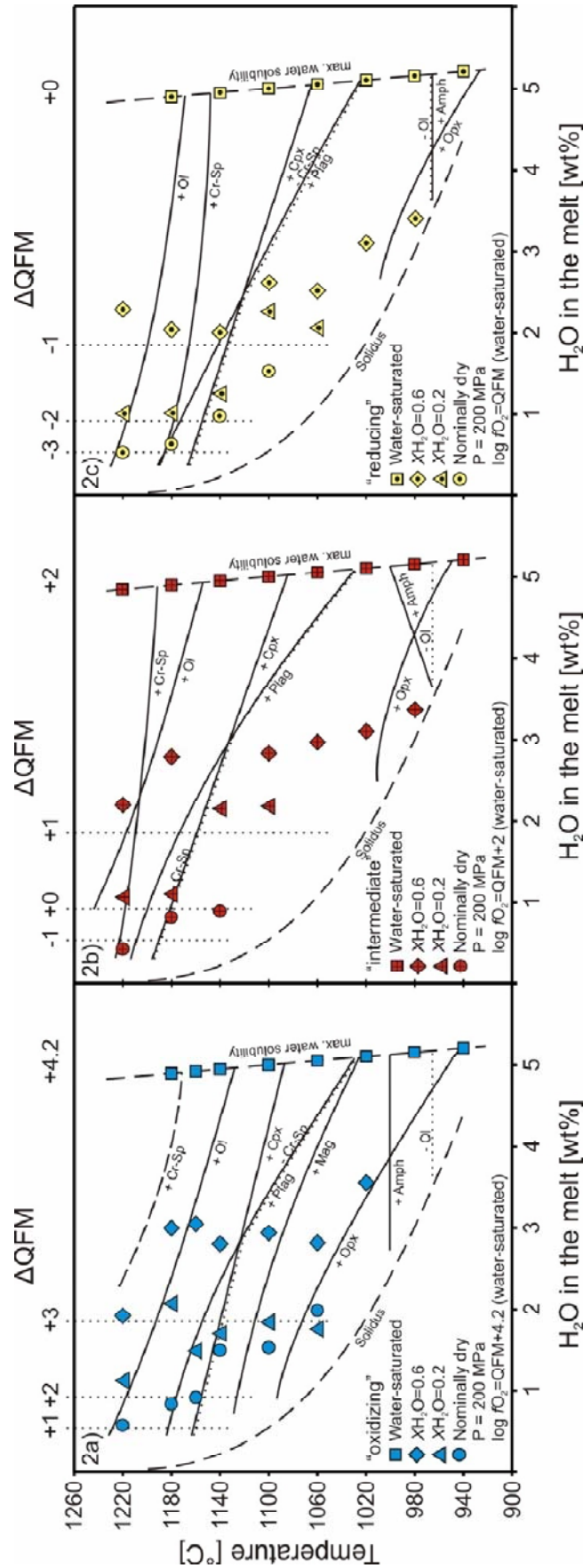
Fig. 2.2: Phase relations for a hydrous tholeiitic basalt for different nominal fO_2: (a) oxidizing (QFM+4.2; according to Feig et al., 2006), (b) intermediate (QFM+2), (c) reducing (QFM). Depending on the water activity, the oxygen fugacity (dotted vertical lines) varies by ~3 log units. The water-saturation curve included in the phase diagrams is obtained from the water solubility in a primitive MORB of Berndt et al. (2005) and from the temperature and pressure dependence on water solubility by Holtz et al. (1995). Abbreviations: Ol - olivine; Cr-sp - chromium-rich spinel; Cpx - clinopyroxene; Opx - orthopyroxene; Plag - plagioclase; Mag - magnetite; Amph – amphibole

typical effect related to the increase in fO_2 due to increasing water contents is the stabilization of magnetite.

Fig. 2.3 shows the pure effect of water on the phase relations at two constant fO_2 conditions excluding the oxidizing effect of water. For these diagrams, only selected experiments from Fig. 2.2 were used. In Fig. 2.3a for a redox condition corresponding to QFM+2, the saturation curves for the individual phases were constructed using the water-saturated experiments at intermediate redox conditions (obtained from Fig. 2.2b) and those experiments from oxidizing conditions with melt water content of ~1 wt% corresponding also to an fO_2 of ~ QFM+2 (obtained from Fig. 2.2a). In a similar manner the phase diagram for QFM conditions (Fig. 2.3b) was constructed. Most striking in these diagrams is that the change in the crystallization sequence of olivine and chrome-rich spinel with water observed under "intermediate" oxygen fugacities (Fig. 2.2b), has disappeared, showing that the relative increase of saturation temperature of chrome-rich spinel in Fig. 2.2b is due to an increase of fO_2 with water. Furthermore, magnetite is also present at a constant fO_2 corresponding to QFM+2 at low water-contents, while it is absent in Fig. 2.2b. Increasing water-content seems to destabilize magnetite in our basaltic tholeiitic system.
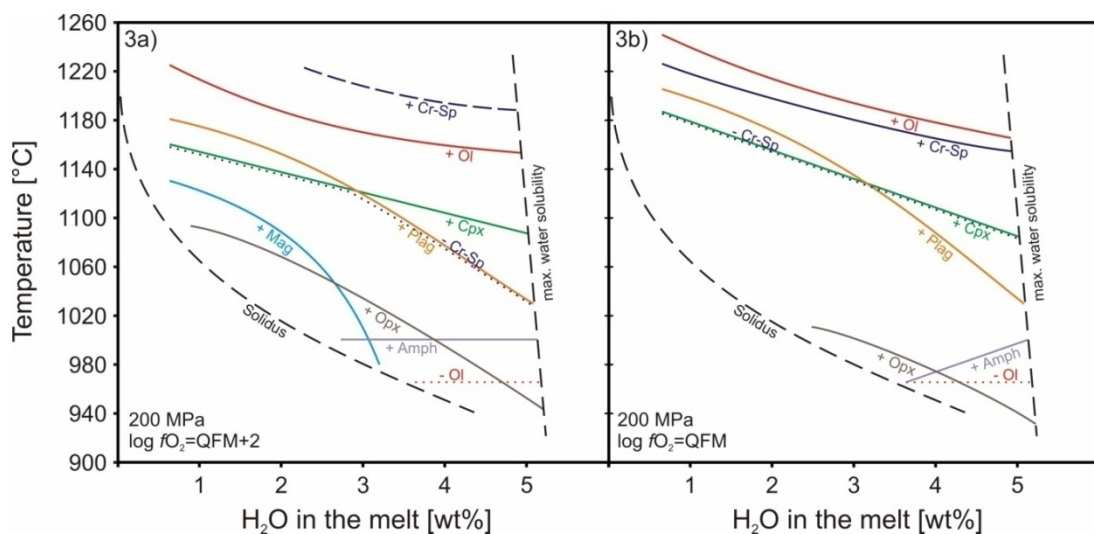

Fig. 2.3: Phase relations as a function of water in the melt for two constant fO_2 conditions (QFM+2 and QFM) excluding the oxidizing effect of water. For details see text. Abbreviations as in Fig. 2.2

Another possibility to decouple the effects of fO_2 and aH_2O is to consider only water-saturated experiments since here the prevailing fO_2 of the run corresponds to the nominal one. Fig. 2.4 shows the saturation temperatures of the solid phases as a function of pure oxygen fugacity. Interestingly, for the chrome-rich spinel the highest crystallization temperature was observed under "intermediate" redox-conditions. This observation coincides also with the shape of the saturations curves of Fig. 2.2. The stability of olivine slightly decreases with increasing oxygen fugacity. Magnetite is present only under oxidizing conditions. Finally, a slight increase of the saturation temperature of amphibole and orthopyroxene was recorded with increasing oxygen fugacity. For clinopyroxene and plagioclase, no significant changes in the saturation temperature as a function of oxygen fugacity were observed.
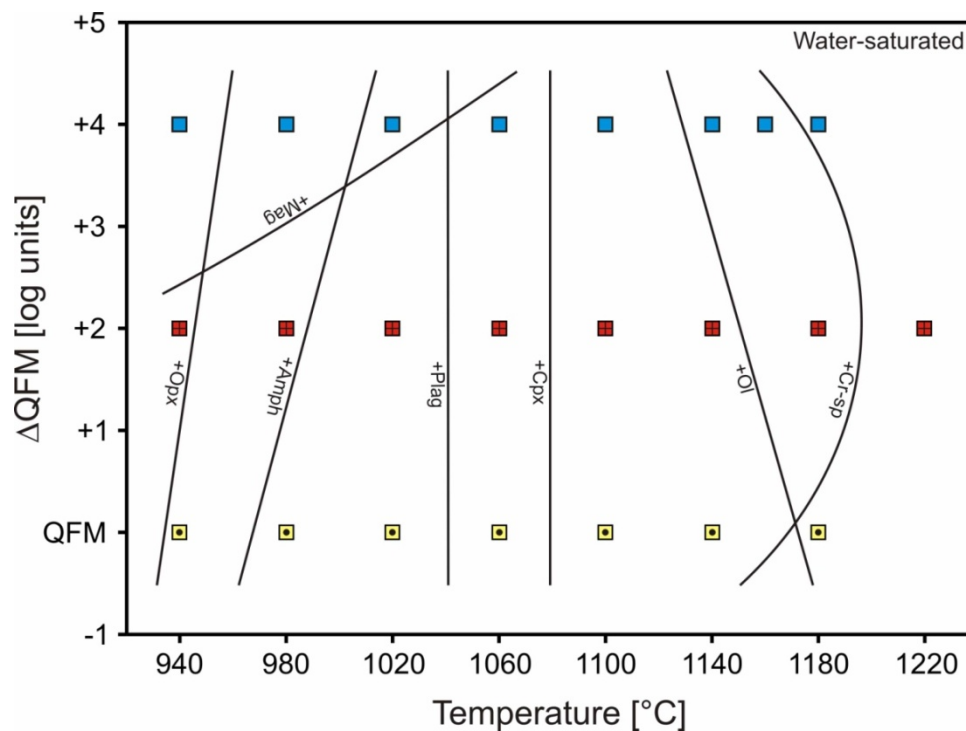

Fig. 2.4: Saturation temperatures of the mineral phases as a function of pure oxygen fugacity. The oxidizing effect of water is excluded by considering only experiments under water-saturated conditions. Abbreviations as in Fig. 2.2

Table 2.2: Compositions of the experimental phases in wt%, starting material: R6a

Run	Temp. (°C)	Phase	n[1]	SiO$_2$	TiO$_2$	Al$_2$O$_3$	FeO[tot]	MnO	MgO	CaO	Na$_2$O	K$_2$O	NiO	Cr$_2$O$_3$	P$_2$O$_5$	Total	X[2]
starting composition: R6a			97	50.95 (.43)	0.35 (.04)	17.24 (.23)	6.39 (.27)	0.14 (.09)	10.06 (.19)	11.73 (.28)	2.98 (.20)	0.03 (.02)	0.02 (.05)	0.06 (.04)	0.01 (.08)	100.00	
starting material: R6a (QFM at water-saturation)																	
#142	1020	ol	7	40.05 (.11)		0.07 (.02)	15.29 (.17)	0.26 (.05)	45.40 (.28)	0.32 (.02)						101.39 (.33)	84.3 (.13)
		plag	9	46.39 (.35)		33.43 (.71)	0.56 (.18)		0.25 (.19)	17.40 (.40)	1.59 (.15)					99.63 (.45)	85.4 (1.33)
		cpx	7	51.08 (.40)	0.33 (.03)	4.89 (.51)	5.71 (.36)	0.17 (.02)	16.90 (.54)	20.47 (.65)	0.32 (.05)			0.25 (.03)		100.11 (.34)	84.2 (.89)
		glass	11	50.97 (.33)	0.49 (.04)	19.35 (.22)	5.33 (.43)		4.51 (.21)	9.16 (.27)	4.21 (.21)					94.02 (.61)	64.6
#143	1020	ol	7	39.06 (.14)		0.12 (.05)	20.03 (.28)	0.30 (.06)	41.16 (.14)	0.37 (.04)						101.05 (.33)	78.8 (.26)
		plag	8	51.41 (.63)	0.11 (.03)	29.26 (.35)	1.03 (.26)		0.58 (.08)	13.41 (.16)	3.67 (.15)					99.47 (.54)	66.2 (1.13)
		cpx	9	51.64 (.45)	0.50 (.05)	3.80 (.81)	6.24 (.28)	0.16 (.05)	16.00 (.42)	20.81 (.49)	0.36 (.06)			0.27 (.07)		99.79 (.46)	82.2 (.84)
		glass	n.a.[4]														
#145	940	ol	2	38.55 (.05)		0.06 (.04)	23.65 (.17)	0.41 (.11)	37.74 (.34)	0.38 (.07)						100.80 (.26)	74.0 (.31)
		plag	8	52.76 (.24)		29.56 (.35)	0.63 (.12)		0.18 (.07)	12.61 (.27)	4.37 (.10)					100.11 (.36)	61.4 (.89)
		cpx	11	53.16 (.42)	0.34 (.07)	2.11 (.48)	7.96 (.33)	0.27 (.03)	16.97 (.48)	19.34 (.63)	0.28 (.06)			0.14 (.03)		100.58 (.37)	79.2 (.46)
		Amph	4	46.87 (1.08)	1.56 (.41)	11.97 (.83)	8.77 (.47)		15.38 (.77)	11.34 (.48)	2.63 (.14)			0.18 (.02)		98.69 (.49)	75.8 (.21)
		glass	n.a.[4]														
#146	980	ol	8	39.04 (.22)			19.18 (.27)	0.33 (.04)	41.62 (.18)	0.28 (.02)						100.45 (.22)	79.5 (.27)
		plag	9	47.75 (.26)		32.35 (.32)	0.63 (.14)		0.22 (.09)	15.77 (.20)	2.43 (.08)					99.15 (.53)	78.2 (.45)
		cpx	10	51.58 (.63)	0.36 (.07)	3.60 (.62)	6.39 (.66)	0.17 (.05)	16.40 (.73)	20.39 (1.05)	0.33 (.06)			0.19 (.06)		99.41 (.47)	82.1 (1.39)
		glass	7	53.64 (.33)	0.62 (.03)	19.32 (.24)	4.88 (.21)		3.26 (.16)	6.82 (.17)	5.06 (.09)				0.22 (.07)	93.83 (.46)	59.1
#147	980	ol	6	38.11 (.21)		0.19 (.14)	23.18 (.31)	0.37 (.04)	37.23 (.29)	0.44 (.08)						99.52 (.37)	74.1 (.27)
		plag	6	52.98 (.29)	0.09 (.02)	29.00 (.31)	0.60 (.06)		0.28 (.11)	11.79 (.12)	4.80 (.06)					99.54 (.47)	57.6 (.47)
		cpx	7	51.86 (.47)	0.88 (.06)	3.48 (.51)	7.37 (.36)	0.27 (.08)	16.00 (.38)	19.10 (.43)	0.48 (.13)			0.20 (.03)		99.64 (.77)	79.5 (.78)
		opx	3	53.85 (.15)	0.43 (.06)	2.11 (.35)	13.56 (.58)	0.33 (.02)	26.66 (.59)	2.64 (1.09)	0.16 (.04)			0.13 (.03)		99.87 (1.00)	77.8 (.42)
		glass	n.a.[4]														
#148	1060	ol	7	40.73 (.20)			11.91 (.37)	0.19 (.06)	47.77 (.23)	0.35 (.03)			0.10 (.05)			101.04 (.31)	87.9 (.36)
		cpx	7	51.57 (.59)	0.26 (.03)	4.76 (.92)	4.23 (.51)		16.97 (.56)	21.06 (.79)	0.32 (.11)			0.53 (.21)		99.69 (.46)	87.9 (1.07)
		glass	8	49.63 (.48)	0.37 (.03)	19.10 (.24)	5.30 (.30)		6.40 (.17)	11.62 (.21)	3.28 (.23)					95.70 (.57)	72.3
#149	1060	ol	2	39.11 (.13)		0.28 (.04)	21.94 (.12)	0.28 (.05)	39.48 (.28)	0.51 (.03)	0.08 (.01)		0.14 (.03)			101.83 (.00)	75.9 (.22)
		plag	3	52.43 (.67)	0.15 (.03)	28.85 (.38)	1.00 (.18)		0.44 (.05)	12.43 (.39)	4.32 (.13)					99.63 (.34)	61.1 (1.10)
		cpx	4	51.85 (.40)	0.58 (.08)	4.00 (.54)	7.21 (.19)	0.20 (.03)	16.40 (.59)	19.21 (.70)	0.50 (.14)			0.24 (.01)		100.20 (.09)	79.9 (.34)
		glass	n.a.[4]														
#150	1060	ol	1	39.13		0.86	22.55	0.30	37.79	0.76	0.06		0.10			101.55	74.6
		plag	4	52.57 (.70)	0.10 (.02)	28.98 (.29)	0.86 (.14)		0.60 (.20)	12.55 (.29)	4.38 (.20)					100.03 (.26)	61.0 (1.57)
		cpx	5	52.35 (.44)	0.58 (.01)	3.65 (.49)	7.14 (.13)	0.25 (.06)	16.17 (.26)	19.56 (.43)	0.41 (.09)			0.22 (.01)		100.34 (.49)	79.8 (.43)
		glass	n.a.[4]														

Table 2.2: Continued

Run	Temp. (°C)	Phase	$n^{1)}$	SiO_2	TiO_2	Al_2O_3	FeO^{tot}	MnO	MgO	CaO	Na_2O	K_2O	NiO	Cr_2O_3	P_2O_5	Total	$X^{2)}$
#151	1060	ol	3	39.58 (.35)		0.36 (.10)	18.62 (.17)	0.29 (.07)	41.81 (.71)	0.45 (.01)	0.06 (.02)		0.11 (.04)			101.30 (1.06)	79.7 (.37)
		plag	5	52.63 (.35)	0.13 (.04)	28.42 (.22)	1.11 (.15)		1.00 (.27)	12.79 (.18)	4.09 (.20)					100.17 (.45)	63.1 (1.34)
		cpx	1	51.33	0.62	4.60	7.55	0.26	16.20	19.15	0.54			0.21		100.45	79.0
		glass	n.a.$^{4)}$														
#152	1100	ol	15	40.68 (.23)	0.12 (.13)		10.16 (.25)	0.18 (.03)	48.56 (.39)	0.34 (.02)			0.12 (.05)			100.03 (.52)	89.5 (.27)
		cr-sp	4	0.28 (.09)		29.94 (.09)	16.48 (.50)		16.48 (.19)	0.32 (.00)				34.24 (.58)		97.87 (.71)	0.43
		glass	10	48.61 (.50)	0.35 (.05)	17.77 (.28)	5.74 (.15)		7.80 (.20)	11.87 (.20)	2.92 (.12)					95.06 (.72)	74.5
#153	1100	ol	6	40.27 (.12)		0.06 (.01)	12.75 (.42)	0.23 (.03)	45.18 (.18)	0.42 (.02)			0.12 (.04)			99.03 (.40)	86.3 (.40)
		plag	4	49.05 (.25)		30.79 (.30)	0.66 (.03)		0.65 (.14)	14.87 (.16)	2.89 (.10)					98.91 (.30)	74.0 (.70)
		cpx	6	52.08 (.17)	0.33 (.03)	3.92 (.24)	5.29 (.21)	0.17 (.05)	16.60 (.18)	20.36 (.36)	0.32 (.05)			0.38 (.06)		99.45 (.33)	84.9 (.42)
		glass	7	51.62 (.44)	0.44 (.05)	18.45 (.23)	6.30 (.22)		6.13 (.17)	10.37 (.27)	3.69 (.26)					97.01 (.47)	66.5
#154	1100	ol	7	39.43 (.22)		0.27 (.10)	17.92 (.36)	0.28 (.04)	41.59 (.44)	0.53 (.06)	0.05 (.03)		0.14 (.03)			100.20 (.56)	80.2 (.34)
		plag	8	51.45 (.36)	0.08 (.01)	29.30 (.54)	0.81 (.18)		0.60 (.17)	13.16 (.22)	3.82 (.16)					99.22 (.55)	65.5 (.84)
		cpx	4	52.33 (.11)	0.41 (.04)	3.97 (.48)	6.04 (.43)	0.17 (.03)	16.30 (.43)	19.78 (.49)	0.39 (.06)			0.29 (.05)		99.68 (.98)	82.5 (.93)
		glass	7	53.98 (.45)	0.82 (.04)	17.45 (.32)	6.74 (.39)		5.15 (.13)	9.03 (.21)	4.18 (.45)					97.36 (.77)	60.6
#155	1100	ol	7	40.73 (.15)		0.17 (.04)	11.59 (.74)	0.27 (.05)	47.42 (.71)	0.41 (.01)						100.59 (.46)	87.9 (.81)
		plag	n.a.$^{3)}$														
		cpx	6	52.87 (.19)	0.34 (.04)	3.09 (.44)	5.71 (.27)	0.17 (.03)	17.58 (.51)	19.72 (.38)	0.35 (.07)			0.30 (.02)		100.11 (.41)	84.6 (.71)
		glass	n.a.$^{4)}$														
#156	1140	ol	5	40.90 (.13)		0.08 (.03)	8.83 (.19)	0.16 (.06)	49.00 (.30)	0.40 (.02)			0.17 (.03)			99.60 (.10)	90.8 (.23)
		cr-sp	1	1.52	0.20	29.11	14.03		17.20	0.56	0.16			36.52		99.28	0.46
		glass	27	49.20 (.33)	0.35 (.04)	17.00 (.23)	5.78 (.22)		9.60 (.21)	11.02 (.26)	2.84 (.23)					95.78 (.56)	78.0
#157	1140	ol	8	40.82 (.09)	0.20 (.01)	0.09 (.01)	9.54 (.21)	0.17 (.03)	48.47 (.31)	0.43 (.02)			0.12 (.05)			99.64 (.31)	90.1 (.23)
		cr-sp	5	0.21 (.13)		33.52 (.26)	12.87 (.14)		17.26 (.29)	0.36 (.02)				34.53 (.38)		98.95 (.26)	0.41
		glass	16	50.96 (.45)	0.35 (.04)	18.30 (.19)	5.45 (.28)		7.97 (.18)	11.98 (.34)	2.99 (.16)					98.00 (.60)	74.5
#158	1140	ol	5	40.14 (.12)		0.18 (.08)	12.54 (.12)	0.20 (.05)	45.96 (.24)	0.50 (.02)			0.15 (.04)			99.66 (.35)	86.7 (.15)
		plag	7	51.15 (.38)	0.08 (.02)	28.78 (.46)	0.91 (.16)		1.15 (.27)	13.77 (.20)	3.44 (.17)					99.28 (.23)	68.8 (1.36)
		cpx	5	52.21 (.18)	0.32 (.05)	4.87 (.37)	4.84 (.38)	0.14 (.04)	16.20 (.38)	19.96 (.04)	0.49 (.03)			0.55 (.06)		99.59 (.60)	85.7 (.87)
		glass	5	51.71 (.65)	0.48 (.03)	17.75 (.17)	6.47 (.18)		6.95 (.28)	11.39 (.19)	3.44 (.12)					98.20 (.62)	67.7
#159	1140	ol	8	40.94 (.16)		0.19 (.04)	9.93 (.38)	0.19 (.04)	48.52 (.38)	0.48 (.04)			0.11 (.02)			100.35 (.30)	89.7 (.41)
		plag	4	50.72 (.11)	0.06 (.02)	29.66 (.26)	0.61 (.12)		1.03 (.21)	14.20 (.30)	3.27 (.15)					99.55 (.09)	70.6 (1.38)
		cpx	6	52.50 (.10)	0.30 (.02)	3.52 (.22)	5.90 (.40)	0.18 (.01)	17.87 (.14)	19.34 (.30)	0.32 (.02)			0.38 (.05)		100.31 (.21)	84.4 (.89)
		glass	5	53.43 (.40)	0.50 (.05)	18.53 (.33)	4.57 (.18)		7.39 (.52)	11.28 (.39)	3.67 (.09)					99.38 (.58)	75.7
#160	1180	glass	23	48.88 (.33)	0.33 (.04)	16.94 (.19)	5.94 (.38)		9.76 (.17)	11.45 (.18)	2.82 (.20)					96.13 (.46)	77.8
#161	1180	ol	6	41.34 (.09)		0.07 (.02)	8.20 (.41)	0.15 (.03)	49.38 (.32)	0.38 (.01)			0.10 (.07)	0.06 (.01)		99.64 (.48)	91.5 (.41)
		glass	25	50.51 (.32)	0.34 (.04)	17.73 (.17)	5.43 (.27)		9.64 (.21)	11.63 (.32)	2.95 (.23)					98.29 (.57)	78.1

Table 2.2: Continued

Run	Temp. (°C)	Phase	n[1]	SiO_2	TiO_2	Al_2O_3	FeO^{tot}	MnO	MgO	CaO	Na_2O	K_2O	NiO	Cr_2O_3	P_2O_5	Total	X[2]
#162	1180	ol	6	41.28 (.22)		0.10 (.03)	8.91 (.23)	0.14 (.04)	48.93 (.12)	0.43 (.02)			0.13 (.02)			99.92 (.24)	90.7 (.23)
		glass	12	51.27 (.32)	0.35 (.03)	18.50 (.20)	4.98 (.28)		8.61 (.20)	12.13 (.27)	3.03 (.22)			0.06 (.02)		98.92 (.55)	76.9
#163	1180	ol	7	41.14 (.07)		0.11 (.03)	8.73 (.25)	0.17 (.06)	48.51 (.30)	0.45 (.01)			0.14 (.02)	0.06 (.01)		99.31 (.37)	90.8 (.26)
		plag	6	51.02 (.30)	0.06 (.02)	28.91 (.53)	0.95 (.17)		1.26 (.31)	14.18 (.27)	3.27 (.06)					99.66 (.26)	70.6 (.73)
		cr-sp	3	0.91 (.66)	0.22 (.01)	27.95 (.45)	15.12 (.24)	0.19 (.02)	16.21 (.21)	0.52 (.13)	0.12 (.07)		0.10 (.02)	37.55 (.70)		98.81 (.09)	0.47
		glass	8	52.10 (.45)	0.37 (.05)	17.73 (.18)	5.75 (.26)		8.50 (.26)	12.11 (.35)	3.03 (.17)			0.06 (.01)		99.65 (.69)	73.6
#164	1220	glass	26	51.32 (.40)	0.34 (.03)	17.68 (.26)	4.67 (.33)		10.09 (.13)	11.70 (.27)	3.01 (.20)			0.06 (.01)		98.86 (.61)	81.3
#165	1220	glass	15	52.12 (.44)	0.35 (.03)	17.98 (.22)	4.37 (.21)		10.18 (.17)	11.82 (.29)	2.94 (.22)			0.06 (.01)		99.82 (.44)	81.7
#166	1220	ol	3	41.66 (.12)		0.11 (.03)	5.89 (.15)	0.14 (.04)	50.99 (.24)	0.37 (.02)				0.07 (.01)		99.23 (.47)	93.9 (.13)
		glass	13	52.52 (.36)	0.36 (.05)	18.03 (.24)	4.25 (.26)		10.09 (.17)	11.98 (.30)	3.05 (.14)			0.07 (.02)		100.35 (.63)	81.6
starting material: R6a (QFM-2 at water-saturation)																	
#170	1020	Ol	8	39.93 (.23)		0.06 (.02)	13.97 (.24)	0.23 (.05)	45.50 (.23)	0.29 (.04)			0.11 (.04)			100.08 (.24)	85.3 (.25)
		Plag	9	45.44 (.25)		33.55 (.30)	0.83 (.07)		0.19 (.08)	17.90 (.30)	1.27 (.06)					99.19 (.44)	88.6 (.55)
		Cpx	9	50.88 (.44)	0.26 (.03)	4.05 (.53)	5.75 (.44)		16.33 (.23)	21.82 (.63)	0.30 (.04)			0.26 (.05)		99.64 (.34)	83.5 (1.06)
		glass	9	50.75 (.48)	0.42 (.04)	18.94 (.23)	6.06 (.24)		4.61 (.19)	9.20 (.22)	4.00 (.19)					93.97 (.48)	66.4
#171	1020	Ol	8	38.53 (.13)		0.14 (.04)	20.19 (.17)	0.36 (.04)	40.15 (.16)	0.38 (.04)						99.75 (.35)	78.0 (.10)
		Plag	6	51.50 (.47)	0.10 (.01)	28.95 (.48)	1.16 (.14)		0.38 (.09)	13.03 (.22)	4.01 (.10)					99.13 (.16)	64.2 (.80)
		Cpx	6	50.51 (.34)	0.60 (.05)	4.17 (.21)	7.27 (.24)	0.18 (.04)	15.28 (.20)	20.62 (.15)	0.45 (.03)			0.25 (.03)		99.34 (.54)	78.9 (.55)
		glass	n.a.[4]														
#173	1020	Ol	5	38.46 (.23)		0.13 (.04)	21.94 (.40)	0.38 (.05)	38.87 (.37)	0.43 (.07)						100.22 (.49)	76.0 (.38)
		Plag	8	52.51 (.39)	0.10 (.03)	28.18 (.21)	1.05 (.08)		0.64 (.12)	12.22 (.20)	4.54 (.19)					99.23 (.45)	59.8 (1.34)
		Cpx	7	50.70 (.11)	0.78 (.09)	3.53 (.26)	8.07 (.43)	0.24 (.06)	15.95 (.34)	19.58 (.48)	0.46 (.04)			0.21 (.08)		99.51 (.34)	77.9 (.78)
		glass	n.a.[4]														
#174	1060	Ol	8	40.71 (.18)		0.06 (.02)	10.52 (.16)	0.20 (.04)	48.34 (.29)	0.32 (.02)			0.18 (.05)			100.33 (.37)	89.1 (.17)
		Cpx	6	49.84 (.42)	0.28 (.04)	5.62 (.42)	5.16 (.18)		15.77 (.24)	21.70 (.35)	0.30 (.03)			0.63 (.12)		99.30 (.32)	84.5 (.41)
		Cr-sp	1	0.70	0.34	27.33	30.55	0.22	14.37	0.32	0.09		0.14	22.91		96.97	0.36
		glass	7	49.73 (.41)	0.34 (.03)	18.77 (.35)	6.00 (.18)	0.11 (.08)	5.96 (.17)	11.13 (.20)	3.15 (.26)	0.07 (.01)	0.01 (.02)	0.02 (.01)	0.07 (.04)	95.36 (.39)	72.9
#175	1060	Ol	7	39.35 (.19)		0.22 (.12)	17.73 (.16)	0.33 (.06)	42.09 (.21)	0.46 (.07)			0.13 (.02)			100.30 (.33)	80.9 (.15)
		Plag	3	50.83 (.24)	0.09 (.04)	29.04 (.90)	1.42 (.25)		0.56 (.26)	13.60 (.28)	3.68 (.16)					99.23 (.61)	67.1 (1.00)
		Cpx	5	50.62 (.33)	0.40 (.02)	4.96 (.30)	7.21 (.22)	0.15 (.06)	15.96 (.35)	19.78 (.47)	0.47 (.05)			0.27 (.04)		99.82 (.20)	79.8 (.46)
		glass	n.a.[4]														
#178	1100	Ol	6	41.30 (.21)		0.06 (.01)	8.72 (.16)	0.14 (.07)	50.27 (.22)	0.31 (.01)			0.22 (.04)	0.06 (.01)		100.94 (.34)	91.1 (.15)
		Cr-sp	3	0.49 (.15)	0.22 (.01)	27.59 (.64)	25.21 (1.40)		15.85 (.30)	0.38 (.07)	0.05 (.05)		0.19 (.04)	27.09 (.58)		97.22 (.18)	0.40
		glass	10	50.03 (.32)	0.34 (.04)	17.57 (.23)	5.90 (.21)		7.55 (.23)	11.34 (.34)	3.02 (.21)					95.76 (.49)	77.1

Table 2.2: Continued

Run	Temp. (°C)	Phase	$n^{1)}$	SiO_2	TiO_2	Al_2O_3	FeO^{tot}	MnO	MgO	CaO	Na_2O	K_2O	NiO	Cr_2O_3	P_2O_5	Total	$X^{2)}$
#179	1100	Ol	8	40.09 (.13)		0.06 (.02)	13.44 (.14)	0.22 (.04)	45.94 (.13)	0.40 (.02)			0.14 (.03)			100.30 (.30)	85.9 (.12)
		Plag	5	50.01 (.17)		30.14 (.58)	0.85 (.13)		0.59 (.27)	14.70 (.24)	3.10 (.10)					99.40 (.33)	72.4 (.54)
		Cpx	5	51.62 (.75)	0.27 (.04)	4.23 (.31)	5.63 (.26)		16.57 (.15)	20.69 (.21)	0.37 (.06)			0.40 (.06)		99.77 (.50)	84.0 (.61)
		glass	6	52.19 (.39)	0.46 (.04)	17.76 (.17)	7.00 (.33)	0.17 (.05)	5.73 (.25)	10.08 (.12)	3.52 (.20)	0.12 (.04)				97.01 (.61)	66.2
#180	1100	Ol	6	39.40 (.11)		0.30 (.10)	18.62 (.31)	0.31 (.04)	41.28 (.16)	0.53 (.06)			0.12 (.02)			100.56 (.27)	79.8 (.29)
		Plag	5	51.83 (.25)	0.05 (.02)	29.32 (.25)	0.78 (.04)		0.30 (.06)	13.24 (.20)	4.00 (.13)					99.53 (.49)	64.6 (1.04)
		Cpx	6	52.06 (.34)	0.39 (.04)	3.92 (.33)	6.68 (.34)	0.19 (.05)	16.34 (.28)	19.68 (.20)	0.42 (.10)			0.28 (.03)		99.95 (.56)	81.4 (.74)
		glass	6	53.06 (.27)	0.88 (.02)	16.99 (.20)	8.69 (.28)		4.79 (.15)	8.53 (.14)	4.09 (.19)	0.14 (.03)				97.18 (.63)	55.9
#182	1220	glass	26	49.31 (.39)	0.33 (.03)	17.00 (.28)	6.19 (.29)		9.47 (.16)	11.02 (.25)	2.89 (.21)			0.06 (.02)		96.27 (.51)	79.9
#183	1220	glass	33	50.29 (.38)	0.34 (.03)	17.33 (.24)	6.31 (.28)		9.79 (.19)	11.49 (.22)	2.94 (.17)			0.06 (.02)		98.56 (.50)	78.4
#184	1220	Ol	5	41.18 (.13)		0.11 (.03)	8.56 (.21)	0.16 (.03)	50.43 (.26)	0.43 (.03)			0.14 (.03)	0.06 (.00)		101.06 (.33)	91.3 (.19)
		glass	33	51.23 (.41)	0.34 (.04)	17.50 (.22)	6.10 (.40)		9.90 (.17)	11.66 (.25)	3.02 (.19)			0.06 (.01)		99.82 (.75)	77.6
#185	1220	Ol	8	41.26 (.13)		0.18 (.06)	7.90 (.16)		50.77 (.22)	0.44 (.04)			0.13 (.05)	0.07 (.03)		100.74 (.23)	92.0 (.16)
		Cr-sp	n.a.$^{3)}$														
		glass	10	51.41 (.35)	0.34 (.03)	18.02 (.21)	5.63 (.19)		9.68 (.18)	11.96 (.24)	3.03 (.29)			0.06 (.01)		100.14 (.37)	77.0
#186	1180	Cr-sp	n.a.$^{3)}$														
		glass	11	48.78 (.34)	0.32 (.04)	16.61 (.15)	6.30 (.22)		9.42 (.23)	11.10 (.25)	2.78 (.21)					95.30 (.42)	79.6
#187	1180	Ol	7	41.26 (.19)		0.09 (.02)	8.95 (.27)	0.15 (.04)	50.21 (.27)	0.37 (.02)			0.17 (.02)			101.19 (.50)	91.0 (.26)
		Cr-sp	1	3.27	0.16	28.97	15.68	0.24	17.49	0.80	0.27		0.12	33.66		100.66	0.44
		glass	15	50.51 (.46)	0.35 (.04)	17.48 (.27)	6.19 (.24)		9.17 (.16)	11.41 (.25)	2.95 (.20)					98.07 (.45)	78.0
#188	1180	Ol	7	41.06 (.12)		0.09 (.02)	10.45 (.15)	0.17 (.03)	48.98 (.15)	0.45 (.02)			0.18 (.04)			101.38 (.28)	89.4 (.13)
		Plag	6	49.29 (.22)		31.26 (.31)	0.55 (.07)		0.51 (.12)	15.47 (.25)	2.78 (.11)					99.86 (.33)	75.1 (.92)
		Cr-sp	2	0.51 (.17)	0.21 (.01)	28.66 (.82)	15.85 (.32)	0.16 (.05)	16.54 (.48)	0.38 (.01)	0.05 (.04)			37.42 (.61)		99.77 (.51)	0.47
		glass	8	52.07 (.21)	0.37 (.02)	17.55 (.26)	6.60 (.22)		8.09 (.14)	12.04 (.24)	3.05 (.20)					99.76 (.43)	72.5
#189	1180	Ol	7	40.36 (.18)		0.16 (.06)	11.73 (.37)	0.22 (.03)	47.65 (.25)	0.49 (.03)			0.12 (.02)			100.72 (.50)	87.9 (.34)
		Plag	7	50.98 (.62)	0.07 (.03)	28.84 (.60)	0.80 (.13)		1.16 (.32)	13.98 (.26)	3.55 (.13)					99.37 (.48)	68.3 (1.29)
		Cpx	6	51.38 (.60)	0.28 (.05)	4.52 (.48)	6.01 (.38)	0.18 (.03)	17.63 (.35)	18.76 (.42)	0.42 (.08)			0.48 (.04)		99.66 (.50)	84.0 (.73)
		glass	5	52.30 (.48)	0.50 (.03)	17.28 (.67)	6.93 (.30)		7.63 (.34)	11.77 (.12)	3.37 (.33)	0.09 (.01)				99.86 (.42)	69.6
#190	940	Plag	8	50.80 (.35)	0.19 (.02)	29.65 (.57)	0.88 (.11)		0.23 (.11)	13.47 (.43)	3.56 (.17)					98.58 (.49)	67.6 (1.51)
		Cpx	8	51.55 (.31)	0.08 (.02)	3.35 (.15)	8.26 (.17)	0.30 (.04)	16.17 (.30)	19.13 (.37)	0.34 (.04)			0.10 (.01)		99.41 (.31)	77.7 (.29)
		Opx	6	53.81 (.25)		2.51 (.14)	13.81 (.15)	0.42 (.07)	27.68 (.29)	1.64 (.14)				0.08 (.02)		100.03 (.33)	78.1 (.18)
		Amph	10	44.50 (.22)	0.76 (.05)	11.32 (.14)	10.20 (.29)	0.16 (.04)	16.28 (.17)	11.01 (.16)	2.49 (.10)	0.04 (.01)		0.11 (.02)		96.87 (.44)	74.0 (.54)
		glass	9	57.36 (.48)	0.17 (.03)	19.11 (.79)	4.44 (.29)		2.10 (.25)	5.82 (.51)	3.65 (.28)	0.23 (.03)				92.90 (.96)	55.5

Table 2.2: Continued

Run	Temp. (°C)	Phase	n[1]	SiO_2	TiO_2	Al_2O_3	FeO^{tot}	MnO	MgO	CaO	Na_2O	K_2O	NiO	Cr_2O_3	P_2O_5	Total	$X^{[2]}$
#191	980	Ol	5	39.17 (.12)		0.08 (.03)	18.28 (.25)	0.30 (.05)	42.19 (.30)	0.29 (.02)						100.30 (.33)	80.5 (.28)
		Plag	4	48.54 (.20)	0.03 (.01)	31.66 (.17)	0.85 (.09)	0.03 (.04)	0.15 (.05)	15.63 (.08)	2.59 (.03)	0.01 (.01)				99.49 (.39)	77.0 (.26)
		Cpx	6	51.01 (.43)	0.34 (.05)	3.99 (.43)	7.31 (.22)	0.18 (.06)	16.06 (.39)	20.10 (.53)	0.38 (.07)	0.05 (.01)		0.15 (.02)		99.53 (.34)	79.7 (.37)
		Amph	10	43.43 (.21)	0.97 (.13)	12.69 (.16)	9.12 (.26)		16.54 (.22)	11.20 (.20)	2.78 (.10)	0.16 (.03)		0.12 (.03)		96.90 (.35)	76.4 (.63)
		glass	7	54.81 (.34)	0.44 (.03)	18.51 (.20)	5.51 (.29)		3.21 (.10)	6.62 (.29)	4.53 (.13)					93.79 (.81)	61.0
#192	980	Ol	1	37.71	0.15	0.44	23.20	0.33	37.28	0.46	0.08					99.64	74.1
		Plag	6	53.16 (.42)	0.08 (.03)	28.11 (.53)	0.90 (.17)		0.44 (.31)	11.90 (.33)	4.64 (.19)	0.08 (.02)				99.31 (.80)	58.7 (1.44)
		Cpx	9	50.69 (.26)	0.78 (.17)	3.57 (.30)	8.78 (.30)	0.21 (.04)	15.73 (.51)	19.13 (.60)	0.45 (.03)			0.14 (.04)		99.49 (.28)	76.2 (.51)
		Opx	2	54.12 (.50)	0.30 (.05)	5.50 (.01)	13.65 (.11)	0.36 (.04)	24.00 (.14)	3.14 (.19)	0.50 (.12)			0.08 (.01)		101.65 (.32)	75.8 (.05)
		glass	n.a.[4]														
#193	1140	Ol	6	41.54 (.26)			7.65 (.35)	0.16 (.04)	50.84 (.31)	0.30 (.02)			0.25 (.02)			100.73 (.31)	92.2 (.36)
		Cr-sp	3	3.59 (.25)	0.24 (.02)	23.32 (.35)	21.77 (.34)	0.15 (.04)	16.52 (.49)	0.91 (.09)	0.30 (.05)		0.16 (.03)	31.58 (.17)		98.54 (.79)	0.48
		glass	42	50.03 (.32)	0.33 (.04)	16.85 (.21)	6.15 (.27)		9.08 (.21)	10.91 (.27)	2.86 (.19)	0.06 (.02)				96.26 (.57)	79.9
#195	1140	Ol	5	39.92 (.22)		0.37 (.20)	15.12 (.13)	0.26 (.05)	43.96 (.47)	0.53 (.09)			0.13 (.04)			100.29 (.42)	83.8 (.15)
		Plag	8	51.41 (.73)	0.08 (.02)	28.51 (.60)	0.95 (.14)		0.66 (.19)	13.23 (.49)	3.90 (.27)					98.75 (1.01)	65.2 (2.23)
		Cpx	7	52.26 (.43)	0.30 (.06)	4.20 (.61)	5.94 (.43)	0.21 (.03)	16.87 (.55)	19.16 (.25)	0.46 (.12)			0.37 (.03)		99.75 (.40)	83.5 (.93)
		glass	6	52.96 (.52)	0.60 (.05)	16.53 (.27)	8.18 (.19)		6.24 (.19)	10.34 (.22)	3.46 (.21)	0.11 (.04)				98.41 (.70)	64.3
#196	1140	Ol	5	39.88 (.21)		0.80 (.13)	18.21 (.24)	0.25 (.09)	40.60 (.23)	0.86 (.10)	0.10 (.04)		0.10 (.02)			100.81 (.35)	79.9 (.28)
		Plag	2	52.55 (.48)	0.10 (.00)	27.42 (.18)	1.22 (.01)		1.12 (.45)	12.57 (.28)	4.29 (.13)	0.05 (.00)				99.33 (.07)	61.8 (1.24)
		Cpx	3	51.67 (.30)	0.45 (.02)	4.97 (.15)	8.32 (.35)	0.25 (.06)	16.73 (.32)	17.23 (.19)	0.54 (.06)			0.24 (.04)		100.40 (.19)	78.2 (1.04)
		glass	n.a.[4]														

71

Abbreviations: ol - olivine; plag - plagioclase; cpx - clinopyroxene; opx - orthopyroxene; cr-sp - Cr-rich spinel; amph - amphibole
Missing values: below detection limit of the microprobe.
[1] Number of analyses; numbers in paratheses are standard deviations.
[2] Compositional parameter in mol%: olivine – forsterite content; plagioclase – anorthite content; pyroxene and amphibole $100 \cdot Mg/(Mg + Fe^{2+})$ with Fe_{tot} as FeO;
$\gamma/(Mg + Fe^{2+})$ with Fe^{2+} calculated after Kress and Carmicheal (1991)
[3] The crystal phase in these runs are too tiny for reliable microprobe analyses.
[4] The melt pools in these runs are too tiny for reliable microprobe analyses.

2.3.3. Phase chemistry

2.3.3.1. Olivine

The olivine compositions of the performed experiments are listed in Table 2.2. The element partitioning coefficient $K_{D\,Fe-Mg}^{Ol-Melt}$ according to Toplis (2005) was calculated to confirm equilibrium conditions between olivine and coexisting melt. The $K_{D\,Fe-Mg}^{Ol-Melt}$ values obtained for our experiments have an average of 0.3 ± 0.005 (Tab. 2.1), which is in accord with previous studies (e.g., Roeder and Emslie, 1970). At a given temperature, the olivines show an increase in forsterite content (Fo) as a function of water activity, which is in agreement with other studies (e.g., Berndt et al., 2005; Feig et al., 2006). In principle, this can be the result of the water as a chemical component, of the increase in melt fraction as a function of water-activity or of the increase in oxygen fugacity due to water. In Figure 2.5, only olivines from experiments performed under water-saturated conditions are considered. This diagram shows the pure effect of fO_2 on the forsterite content, since water as a chemical component is cancelled out, and the melt fractions in the experiments at fixed temperatures are similar. The highest forsterite contents were observed for the experiments under "oxidizing" conditions. With decreasing oxygen fugacity, the forsterite content decreases, but not linear. Between QFM+4 and QFM+2, the shift to lower forsterite contents is much more pronounced (~4 mol%) than between QFM+2 and QFM (~1 mol%). This is a direct consequence of the change in the Fe^{2+}/Fe^{3+} ratio in the melt as a function of fO_2, which is more pronounced at high oxygen fugacities. The high Fe^{3+} content under oxidizing conditions is also expressed by the crystallization of magnetite at low temperatures. The resulting decrease of the Fe^{2+} and Fe^{3+} content of the melt produces olivines with elevated forsterite contents at low temperatures (Fig. 2.5).
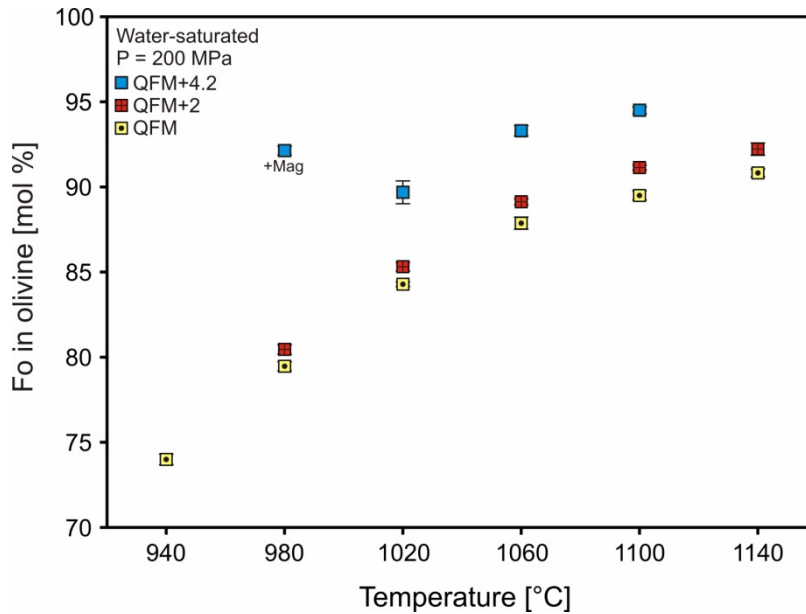
Fig. 2.5: Pure effect of oxygen fugacity on the forsterite content of olivine at 200 MPa and water-saturated conditions. Symbols as in Fig. 2.2.

2.3.3.2. Plagioclase

The Plagioclase compositions are listed in Table 2.2. In accord with previous studies (e.g. Berndt et al., 2005; Feig et al., 2006; Koepke et al., 2004; Panjasawatwong et al., 1995), the anorthite content of plagioclase (An) increases gradually as a function of water in the coexisting melt. In contrast to Fo in olivine, this increase is exclusively controlled by the water content and the increases in melt fraction due to water. It is independent of the prevailing oxygen fugacity, since none of the major plagioclase components are affected by changes in the redox state of the system. Therefore, also the saturation temperature of plagioclase is insensitive to the prevailing oxygen fugacity (Fig. 2.2 and 2.4), which is in agreement with other experimental studies (e.g., Toplis and Carroll, 1995).

Plagioclase shows a systematic increase in iron content with increasing oxygen fugacity (Fig. 2.6). This reflects a higher Fe^{3+} solubility in plagioclase compared to Fe^{2+}, which is in accord with previous experimental studies (e.g. Lundgaard and Tegner, 2004; Sugawara, 2001; Tegner, 1997; Wilke and Behrens, 1999).
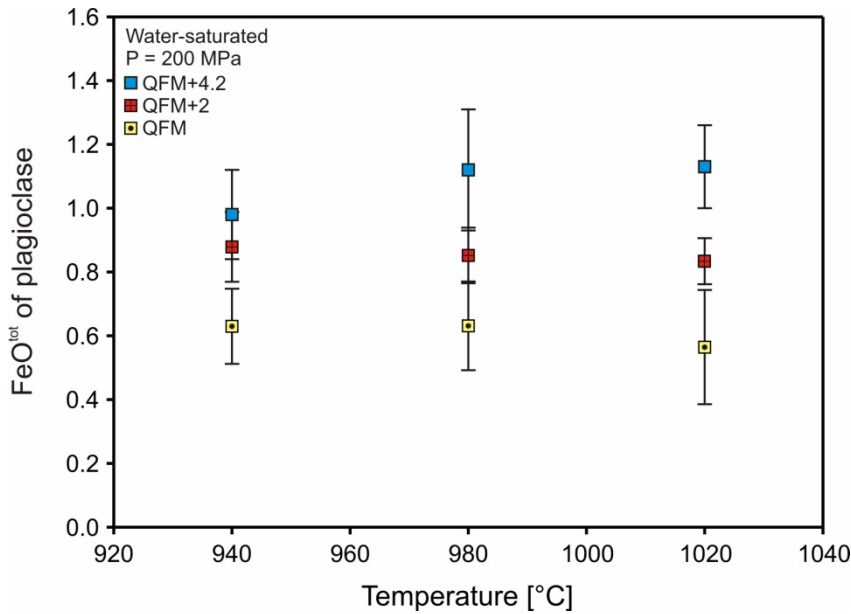
Fig. 2.6: Effect of oxygen fugacity on FeO^{tot}-content of plagioclase at 200 MPa and water-saturated conditions. Symbols as in Fig. 2.2

2.3.3.3. Pyroxenes

The compositions of the experimental high and low Ca-pyroxenes (cpx and opx, respectively) are listed in Table 2.2. To determine the pure effect of oxygen fugacity on the Mg# of clinopyroxene ($100 \times MgO/(MgO+FeO^{tot})$, molar), we considered only clinopyroxenes of water-saturated experiments performed at different oxygen fugacities. In contrast to the observed increase in forsterite content of olivine (Fig. 2.5) with fO_2, the corresponding clinopyroxene Mg# versus temperature plots for different fO_2 do not show distinct trends, when treating total iron as FeO. However, when considering only the Fe^{2+} values obtained stoichiometrically by formula calculation, then, well-defined trends for the Mg# of clinopyroxene are observed (Fig. 2.7). Similar to the increase in forsterite content of olivine, the increase of Mg# of clinopyroxene is more pronounced at high fO_2, which is a direct consequence of the nonlinear change in the Fe^{2+}/Fe^{3+} ratio in the melt as a function of oxygen fugacity. Due to the limited amount of experiments containing orthopyroxene, clear systematic trends controlled by the oxygen fugacity could not be determined.
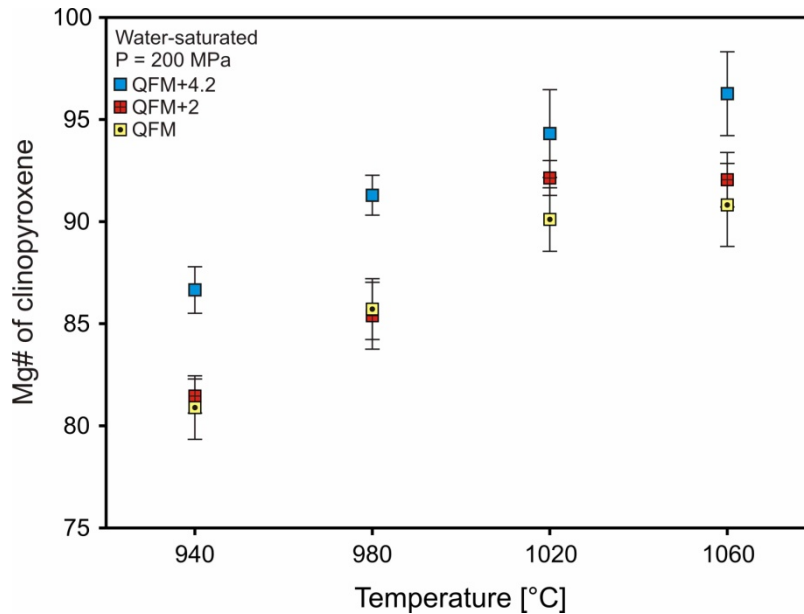
Fig. 2.7: Effect of oxygen fugacity on the Mg# of clinopyroxene at 200 MPa and water-saturated conditions. The Fe^{2+}-content of the clinopyroxenes were obtained stoichiometrically by formula calculation. Symbols as in Fig. 2.2.

2.3.3.4. Spinel

Cr-rich spinel was observed only in high temperature runs, crystallizing before or immediately after olivine as a function of fO_2. To lower temperature Cr-spinel disappears, when clinopyroxene joins the crystallizing assemblage, implying that the clinopyroxene incorporates significant amounts of Cr which destabilizes the Cr-spinel (Fig. 2.2). Since the spinel structure allows the incorporation of both Fe^{2+} and Fe^{3+}, the stability of Cr-spinel is strongly affected by the prevailing oxygen fugacity. It can be clearly obtained from Fig. 2.2 that under reducing condtions, increasing fO_2 stabilizes Cr-spinel, whereas under oxidizing conditions decreasing fO_2 stabilizes the Cr-spinel. This observation infers that the crystallization temperature of Cr-spinel does not continuously increase with fO_2, but show a maximum at ~QFM+2 (Fig. 2.4).

The ratio of Fe^{2+}# (molar $100 \times Fe^{2+}/(Fe^{2+}+Mg)$) and Cr# (molar $100 \times Cr/(Cr+Al)$) of Cr-spinels is an often used parameter for the petrogenesis of primitive basaltic magmas (e.g., Barnes and Roeder, 2001). When plotting the experimental Cr-spinels into the Fe^{2+}# versus

Cr# diagram, no apparent trends are visible (Fig. 2.8a). Compared to Cr-spinels from typical MORB, all Cr-spinels crystallized under reducing and intermediate redox conditions plot into the MORB field in Fig. 2.8a, while those crystallized under oxidizing conditions tend to plot also outside the MORB filed, due to too low Fe^{2+} values (Fe^{2+}/Fe^{3+} content of spinels were calculated stoichiometrically).
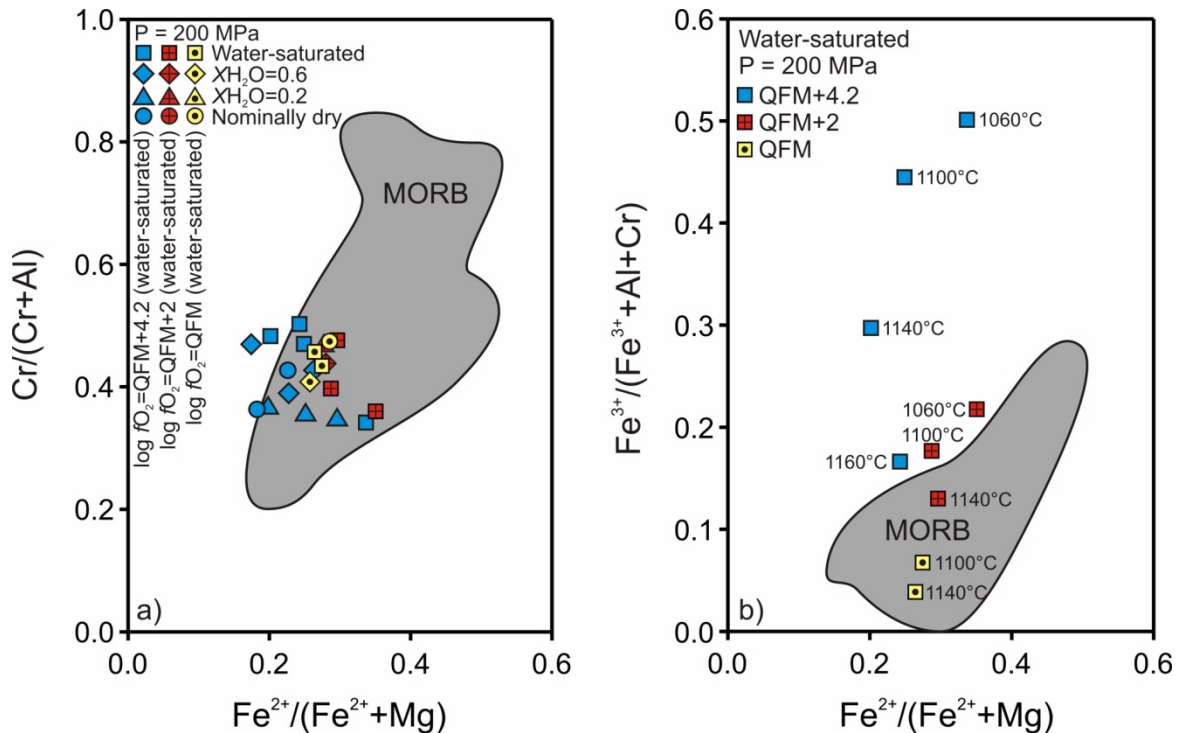
Fig. 2.8: Effect of oxygen fugacity and temperature on Cr# vs Fe^{2+}# and Fe^{3+}# vs Fe^{2+}# of the experimental chrome-rich spinels. The cation values were obtained by stoichiometric formula calculation. Included are compositions of natural chrome-rich spinels of mid-ocean ridge basalts after Barnes and Roeder (2001).

The effect of oxygen fugacity on Cr-spinel composition is more apperent in a plot considering explicitely the Fe^{3+} component which was calculated stoichiometrically. As expected, in a Fe^{3+}# (molar $100 \times Fe^{3+}/(Fe^{3+}+Al+Cr)$) versus Fe^{2+}# plot, the Cr-spinels show a distinct trend to higher Fe^{3+}# with increasing fO_2 at a given temperature (Fig. 2.8b). Moreover, Cr-spinels from experiments performed at the same oxygen fugacity show also a systematic trend to higher Fe^{3+}# with decreasing temperature. This trend is most pronounced under oxidizing

conditions - the only oxygen fugacity where solid solution with magnetite is observed. Compared to MORB, only Cr-spinels crystallized under reducing and intermediate conditions plot into the MORB field, while those from oxidizing conditions fall outside the field to higher Fe^{3+} values.

2.3.3.5. Glass compositions

The melt compositions of the performed experiments are listed in Table 2.2. It is shown above that the prevailing oxygen fugacity affects the composition and stability of the minerals precipitating from the melt which in turn controls the melt composition and the liquid line of descent of the system. In Figure 2.9, the effect of oxygen fugacity on selected components as a function of melt fraction is shown. We used the melt fraction instead of temperature in this diagram, mainly for comparison with the results of chapter 1. In order to rule out the oxidizing effect of water, we only used experiments under water-saturated conditions. Fig. 2.9a shows that silica enrichment with decreasing melt fraction occurs for all three redox conditions. The effect is most pronounced under oxidizing conditions where magnetite is among the crystallizing phases. That magnetite crystallization enhances the silica enrichment in the residual melt is well-known from other experimental studies (e.g., Berndt et al., 2005; Toplis, 2005). A less pronounced, but still strong silica enrichment is also observed under intermediate and reducing redox condition where magnetite is absent.

The Mg# (with Fe^{2+} content calculated according to Kress and Carmichael, 1991) of the melt versus melt fraction is shown in Fig. 2.9b. It correlates well with the corresponding trends observed for the forsterite content in olivine and for the Mg# of clinopyroxene. An increase in oxygen fugacity reduces the Fe^{2+} content of the melt and produces a higher Mg# both in the melt and in the mafic phases (Fig. 2.5, 2.7). Moreover, the spacing between individual experiments is much larger between QFM+4.2 and QFM+2 compared to the lower fO_2 pair

(QFM+2 and QFM) at a given temperature. This again demonstrates the non-linear change in the Fe^{2+}/Fe^{3+} ratio as a function of fO_2 which is more pronounced at high oxygen fugacity (Botcharnikov et al., 2005). An effect of the redox-conditions on melt evolution is also observed for sodium, although this element is not sensitive to the prevailing oxygen fugacity (Fig. 2.9c). Here, the sodium content of the melt content is controlled by the saturation temperatures of plagioclase and amphibole and their modal proportions. The precipitation of fO_2-sensitive mineral phases affects these parameters and therefore the Na_2O component of the melt. Only few elements in the residual melt seem not to be affected by changing redox-conditions of the system, like calcium (Fig. 2.9d).
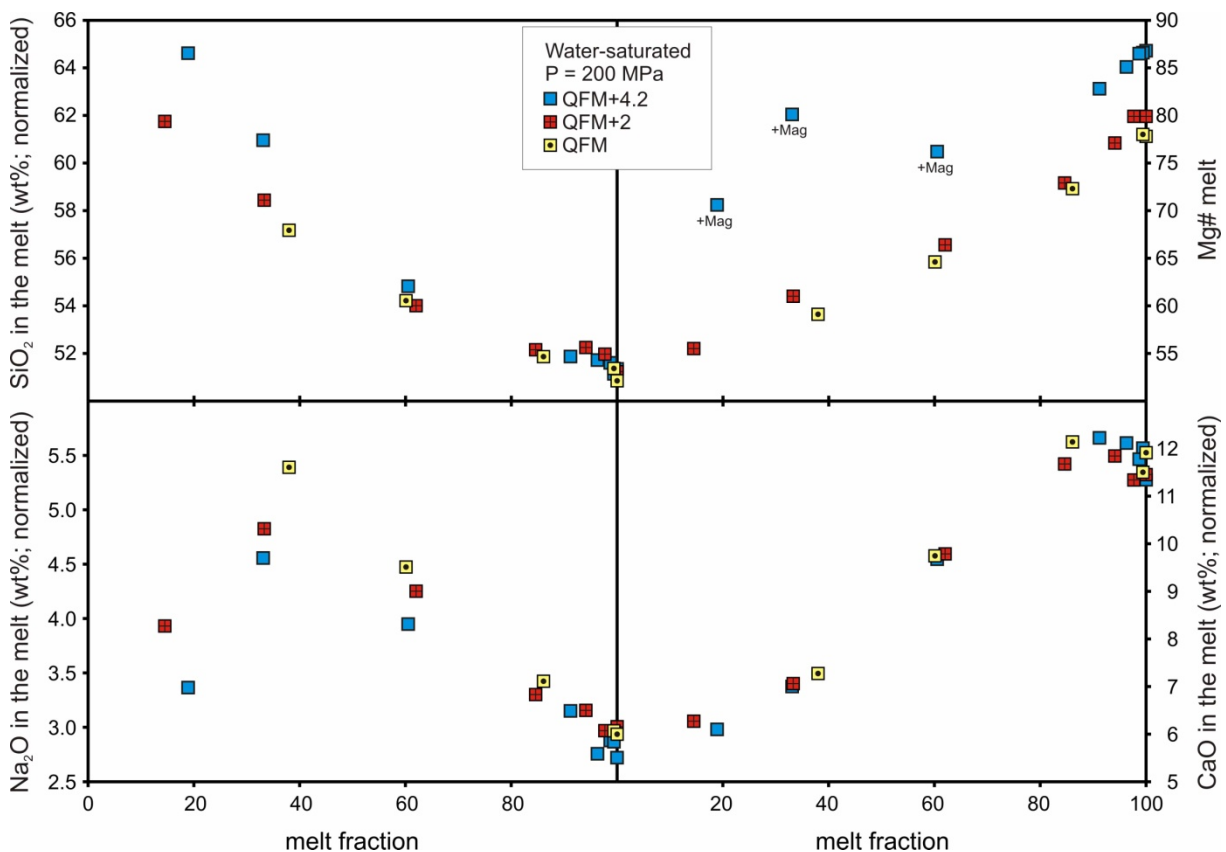
Fig. 2.9: Selected components of the experimental melts as a function of the melt fraction for different oxygen fugacities at 200 MPa. Abbreviations: Mag – magnetite

2.4. Discussion

2.4.1. Melt differentiation trend

Observations on natural rocks revealed that basaltic suites follow characteristic evolution trends, i.e. the tholeiitic and calc-alkaline differentiation trend (e.g., Irvine and Baragar, 1971; Miyashiro, 1974; Wager and Deer, 1939). The calc-alkaline differentiation trend is characterized by a significant enrichment in silica and alkalis during differentiation at rather constant FeO^{tot}/MgO ratios. Such a trend is the result of the crystallization of small amounts of calcic plagioclase and comparatively large amounts of ferromagnesian silicates at an early stage of crystallization followed by magnetite (e.g., Grove and Kinzler, 1986; Sisson and Grove, 1993a). The tholeiitic differentiation trend is characterized by considerable iron enrichment due to the lack of iron oxides in the crystallization sequence and the crystallization of high proportions of plagioclase. The evolution of a primitive basaltic system with progressive crystallization depends on the crystallization sequence and on the composition of the crystallizing mineral phases. For instance, Grove and Kinzler (1986) identified effects of pressure, oxygen fugacity and water content on the differentiation trend. Sisson and Grove (1993a) showed that water could cause an evolution following a calc-alkaline trend using a high-alumina basalt. Berndt et al. (2005) showed in a primitive and evolved hydrous MORB system that increasing fO_2 may change a differentiation trend from tholeiitic to calc-alkaline.

Our experiments are well-suited to study the early stage of basalt differentiation, since our starting system is quite primitive and most residual melts are not saturated with magnetite, except a few equilibrated at highly oxidizing conditions ($\geq$ QFM+2). We applied our

experimental results to the AFM diagram (classification after Irvine and Baragar, 1971) to evaluate the role of oxygen fugacity and water-content during early differentiation (Fig. 2.10).
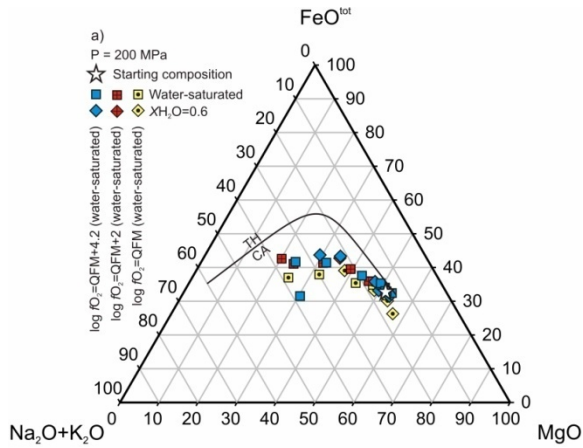
Fig. 2.10: Experimental melts obtained at 3 different oxygen fugacities projected in the AFM plot according to Irvine and Baragar (1971). The line separates calc-alkaline (CA) from tholeiitic (TH) trend. Melts containing high (a) and low (b) water contents show different crystallization trends
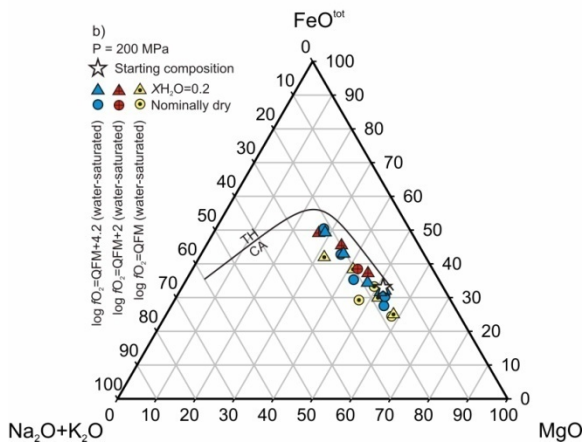
Generally, all experiments plot into the field for calc-alkaline rocks, independently of fO_2 and water content. However, distinct trends can be observed for high and low water contents: Experiments with high water contents show only slight iron enrichment followed by a significant increase in the alkaline content, which is typical for the calc-alkaline differentiation trend (Fig. 2.10a). On the other hand, experiments performed with low water contents show a gradual increase in iron content without significant enrichment in alkalis, which is characteristic for the tholeiitic differentiation trend (Fig. 2.10b). No significant effect of oxygen fugacity on the melt evolution was observed in this diagram. Therefore, Figure 2.10 implies that water may change the differentiation trend from tholeiitic to calc-alkaline in

a primitive MORB-type system. This is in agreement with experimental results of Sisson and Grove (1993a) for a hydrous high-alumina basalt.

The main effect of water in a basaltic system (besides the oxidizing effect under H_2-buffered conditions) is the change in the crystallization sequence compared to dry conditions (Fig. 2.2), favouring the crystallization of ferromagnesian silicates compared to plagioclase (Fig. 2.11). This, in turn, influences the composition of the residual melt which results in characteristic differentiation trends as shown in Fig. 2.10. The oxygen fugacity seems to have only minor effects on the differentiation trend, at least at that low FeO^{tot}/MgO ratio of our chemical system, which does not allow the crystallization of significant amounts of iron oxides.
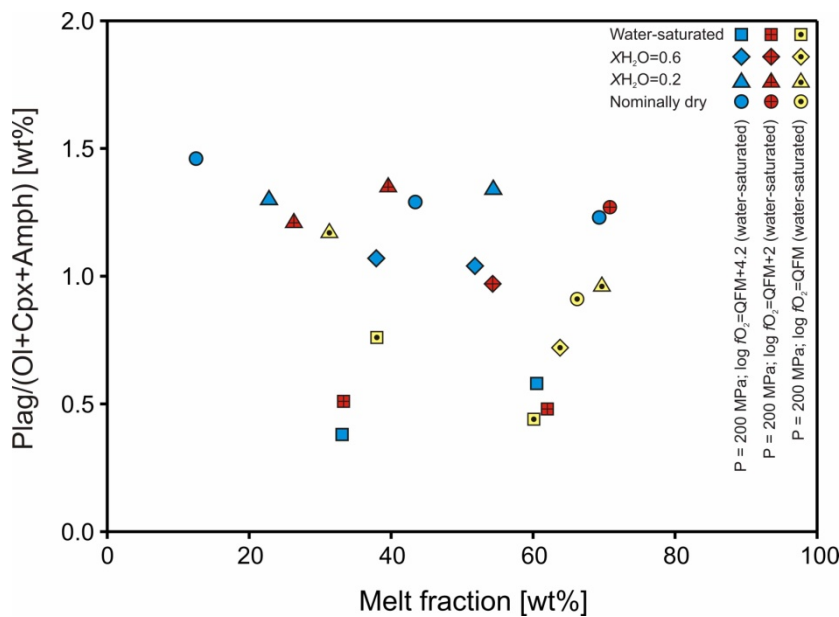
Fig. 2.11: Plagioclase/Mg-Fe-phase ratio as a function of melt fraction for different water contents.

2.4.2. Comparison with gabbroic rocks from the Southwest Indian Ridge

Gabbroic rocks of ODP Hole 735B (Legs 118 and 176) from the ultra-slow-spreading Southwest Indian Ridge represent the longest continuous section of in-situ lower oceanic crust ever drilled (total length of the profile ~ 1500m; Dick et al., 2000). Detailed petrological and

geochemical investigations performed by members of the scientific parties (Natland et al., 2002; Von Herzen et al., 1991) provides an excellent data base for an application of our experimental results (e.g., about 20,000 phase analyses presented in Dick et al., 2002). These studies show that most gabbros are of cumulate origin with very low residual melt porosities. Thus, these gabbros consist of MORB-derived pure mixtures of fractionated minerals which can principally be compared with the mineral phases of our crystallization experiments performed in a primitive MORB-type tholeiitic system.

By including the results of pressure-dependent experiments performed in the same experimental system presented in chapter 1 and published by Feig et al. (2006), the whole experimental data set allows to determine "reference" differentiation trends based on selected parameters (dry vs. hydrous, low-pressure vs. high-pressure, oxidizing vs. reducing conditions), as illustrated in mineral-mineral trends shown in Figs. 2.12-2.14. While our experiments cover only a relatively small range in the corresponding diagrams (Fig. 2.12-2.14), the natural gabbros show a broad compositional spectrum and a marked trend towards lower Mg# and An, respectively, which is clearly the effect of compositional evolution due to fractionated crystallization.

In the Fo content of olivine versus An content of plagioclase plot, the experiments correlate well with the more primitive natural samples of ODP Hole 735B (Fig. 2.12a). Most pronounced is the effect of water. Increasing water content shifts the compositions to higher anorthite and lower forsterite contents (Fig. 2.12b). Increasing oxygen fugacity affects only the olivines shifting the composition to higher forsterite contents. Since the anorthite content of plagioclase is not affected by the prevailing oxygen fugacity, the shift is a direct consequence of decreasing Fe^{2+} content in the system. Finally, a slight pressure effect can also be observed, expressed by slightly higher forsterite contents and lower anorthite contents in olivine and plagioclase, respectively.
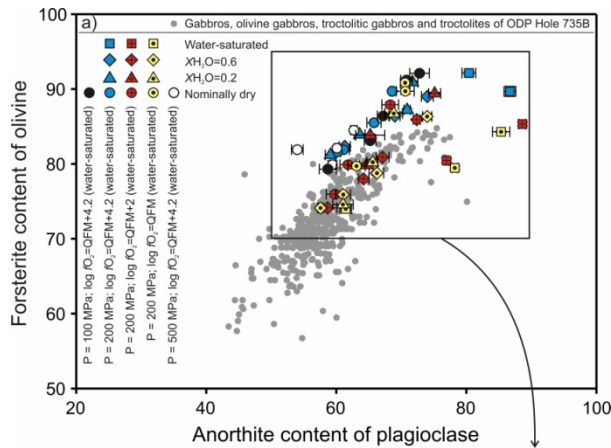
Fig. 2.12: Effect of oxygen fugacity, water content and pressure (data from chapter 1 published in Feig et al., 2006) in a forsterite content of olivine vs anorthite content of plagioclase plot. (a) Experimental runs and natural samples from SWIR (gabbros, olivine gabbros, troctolitic gabbros and troctolites; Dick et al., 2002). (b) Shown are effects of the individual parameters determined by the experimental results.
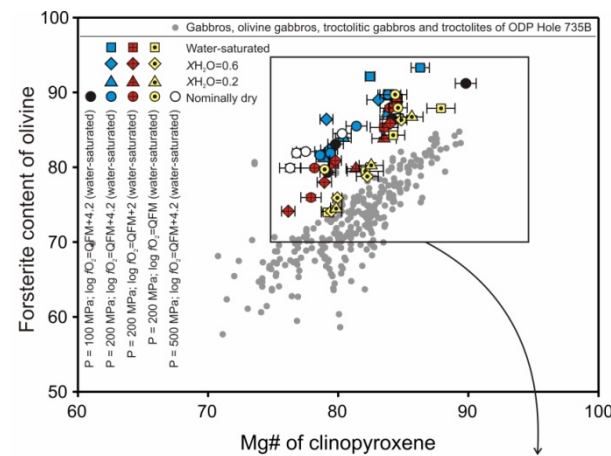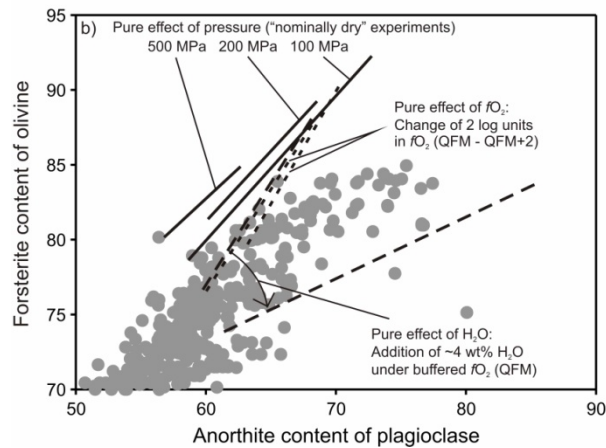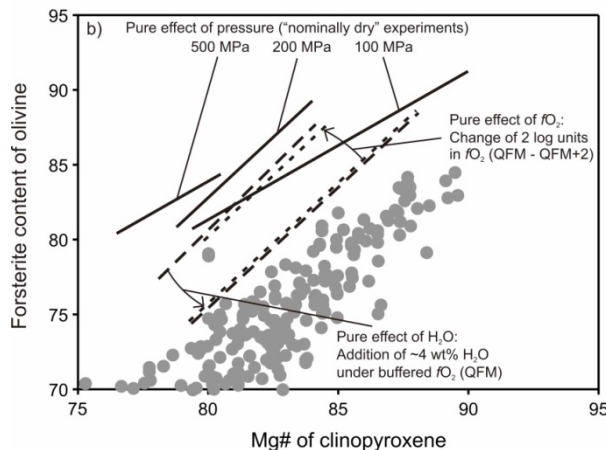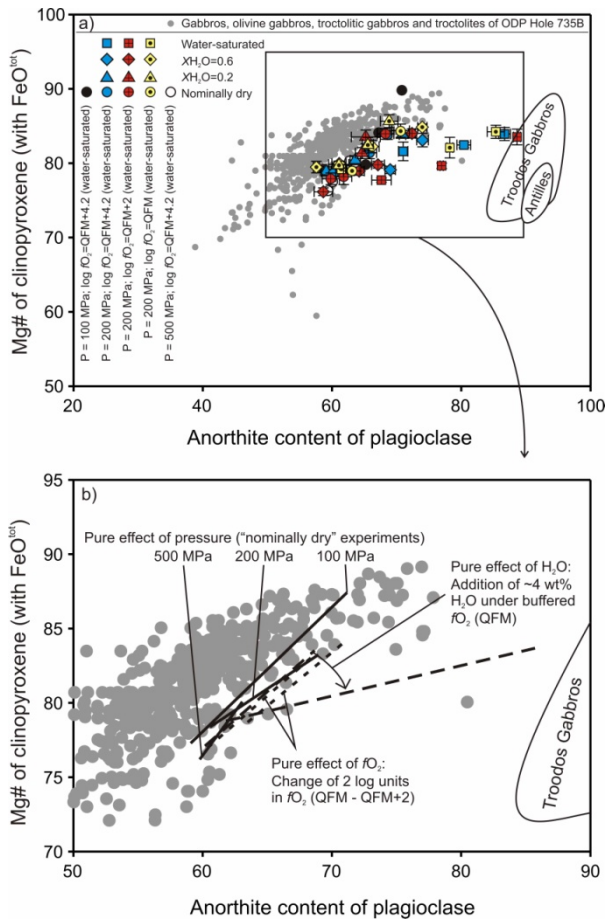

Fig. 2.13: Effect of oxygen fugacity, water content and pressure (data from chapter 1 published in Feig et al., 2006) in a forsterite content of olivine vs Mg# of clinopyroxene plot. (a) Experimental runs and natural samples from SWIR (for details see Fig. 2.12). (b) Shown are effects of the individual parameters determined by the experimental results.

Fig. 2.14: Effect of oxygen fugacity, water content and pressure (data from chapter 1 published in Feig et al., 2006) in a Mg# of clinopyroxene vs anorthite content of plagioclase plot. (a) Experimental runs and natural samples from SWIR (for details see Fig. 2.12). (b) Shown are effects of the individual parameters determined by the experimental results. Evolution trends of gabbros from the Troodos ophiolite and the Lesser Antilles are from Kvassnes et al. (2004).

In the forsterite content of olivine versus Mg# of clinopyroxene plot, a systematic deviation of the experimental from the natural trends can be observed (Fig. 2.13). Only experiments performed under low oxygen fugacities (<QFM) plot into the natural range. The diagram shows opposite effects for increasing fO_2 and increasing water (Fig. 2.13b). An increase in the prevailing oxygen fugacity affects the Fe^{2+}/Fe^{3+} ratio of the melt shifting the Mg# of olivine and clinopyroxene to higher values (Fig. 2.5 and 2.7). Thus, it is to expect that olivine and clinopyroxene should be strongly correlated in this diagram, which is not the case. The Mg# of the clinopyroxenes in Fig. 2.13 were calculated based on FeO as FeOtot, in order to compare with the natural clinopyroxenes taken from the data base of Dick et al. (2002) where the Mg# was calculated with FeO = FeOtot. We assume that the expected correlation is blurred due to the fact that the incorporation of Fe^{3+} into the experimental clinopyroxene structure is not considered, but which cannot be neglected at high fO_2. Finally a distinct

pressure effect can be observed, expressed by a shift to lower Mg# of clinopyroxene and higher Fo contents of olivine, respectively, with increasing pressure (Fig. 2.13).

In Fig. 2.14, the Mg# of clinopyroxene versus An content in plagioclase is plotted. As noted above, the Mg# of experimental clinopyroxene under oxidizing conditions are only minimum values, since the incorporation of Fe^{3+} into the structure is not considered. Most pronounced in this diagram is the effect of water, while effects of fO_2 and pressure are comparatively small. This is mainly due to the well-known fact that the Ca/Na partitioning between plagioclase and melt is strongly affected by water. The pressure dependence of the trends is negligible, at least under dry conditions as demonstrated in Fig. 2.14. In hydrous systems, however, strong effects of pressure on the An content of plagioclase are expected, since the water solubility in a basaltic melt dramatically changes in the observed pressure interval which in turn affects significantly the Ca/Na partitioning (see discussion in chapter 1.4.2.2.).

Included in Fig. 2.14 are the evolution trends for those gabbros assumed to be generated by "wet" differentiation in spreading centres above a subduction zone, e.g., Troodos ophiolite, Lesser Antilles (for details see Kvassnes et al., 2004). These evolution trends plot far away from those "wet" trends obtained by our experiments in a primitive tholeiite system. The results of our study imply, that the simple addition of water to a primitive tholeiitic basalt is by far not sufficient to produce such trends as observed from Troodos or Lesser Antilles. This implies that special compositional constraints are necessary for the evolution of such trends, e.g., the presence of boninitic parental melts.

In summary, the relations between An content of plagioclase, Fo content of olivine and Mg# of clinopyroxene show that from the parameters varied in our experiments, pressure, water content, and fO_2, the effect of water is most pronounced with the potential to change

differentiation trends. The comparison with gabbroic rocks from SWIR confirms that these were formed under low water contents and under reducing conditions, which is in accord with latest models of oceanic crust formation at mid-ocean ridges away from subduction zones (e.g., Bezos and Humler, 2005; Kovalenko et al., 2000). It is obvious that our experimental determined "reference" trends are completely overlapped by the natural samples, which is in a first order due to compositional effects. Thus, our results do not allow evaluating specific parameters of gabbroic evolution at SWIR, e.g., the role of small amounts of water, or small changing in redox conditions.

2.5. Conclusions

When including the experimental results of chapter 1 published in Feig et al. (2006) we present here an extensive experimental phase equilibria data base containing more than 100 single experiments for constraining the effect of fO_2, water content and shallow pressure in primitive MORB-type system. These experiments allow predicting both the compositional effect of these parameters on individual phases of the system as well as evolution trends based on fractional crystallization during a very early stage of MORB magma evolution.

In comparison to fO_2 and pressure, water has the strongest effect on phase stabilities and phase compositions with the potential to change differentiation trends from tholeiitic to calc-alkaline in a very early stage where iron oxides are not present. Our experiments allow determining "reference" differentiation trends as a function of pressure, water content and fO_2 of the system. But these trends also reveal that natural tholeiitic basaltic systems are highly diverse in composition, e.g. the compositional scattering of gabbros from SWIR (Fig. 2.12-2.14), or differentiation trends observed from Troodos ophiolite or Lesser Antilles (Fig. 2.14),

which are clearly related to compositional effects rather than to the external parameters controlling the conditions of crystallization.

The present study (together with the study of Feig et al., 2006) in a hydrous primitive tholeiitic basaltic system, and the phase equilibria studies performed in hydrous MORB (Berndt et al., 2005) and in a hydrous ferrobasaltic tholeiitic system (Botcharnikov et al., 2007), are strongly related to each other. First, all studies were performed in the same IHPV of the experimental lab of Hannover equipped with H_2-membrane, thus well-constrained in terms of fO_2 and water content, cancelling out problems due to the use of different experimental labs or techniques. Second, the chemical systems of all studies are tholeiitic basalts covering different compositional evolution stages from primitive to evolved. Thus, all these data provide an internally consistent database (containing now about 300 experimental runs), well-suited to evaluate especially the role of water and fO_2 during magma evolution in typical tholeiite systems at shallow pressures, like the MOR-basalts at oceanic spreading centres. Finally, these data may help to improve thermodynamic or empiric models like MELTS (Ghiorso and Sack, 1995) and COMAGMAT (Ariskin, 1999) which are up to now not able to predict accurately phase equilibria or liquid lines of descent in tholeiite systems, when water is included as shown in chapter 1.

3.   References

Adachi Y, Miyashita S (2001) Magmatic processes of layered gabbro in the northern Oman ophiolite inferred from the zoning of plagioclase. International Conference Geology of Oman Abstract Volume:6

Albarède F, Provost A (1977) Petrological and geochemical mass-balance equations: an algorithm for least-square fitting and general error analysis. Comput Geosci 3:309-326

Almeev RR, Holtz F, Koepke J, Parat F, Botcharnikov RE (2007 in press) The effect of H_2O on olivine crystallization in MORB: Experimental calibration at 200 MPa. Am Mineral

Ariskin AA (1999) Phase equilibria modeling in igneous petrology: use of COMAGMAT model for simulating fractionation of ferro-basaltic magmas and the genesis of high-alumina basalt. J Volcanol Geotherm Res 90:115-162

Asimow PD, Langmuir CH (2003) The importance of water to oceanic mantle melting regimes. Nature 421:815-820

Auwera JV, Longhi J (1994) Experimental study of a jotunite (hypersthene monzodiorite): constraints on the parent magma composition and crystallization conditions (P, T, fO_2) of the Bjerkreim-Sokndal layered intrusion (Norway). Contrib Mineral Petrol 118:60-78

Baker MB, Grove TL, Price R (1994) Primitive basalts and andesites from the Mt. Shasta region, N California - products of varying melt fraction and water content. Contrib Mineral Petrol 118:111-129

Barnes SJ, Roeder PL (2001) The range of spinel compositions in terrestrial mafic and ultramafic rocks. J Petrol 42:2279-2302

Behrens H, Schulze F (2000) Compositional dependence of water diffusivity in aluminosilicate glasses and melts. In: D. Rammlmair JM, Th. Oberthür, R.B. Heimann und H. Pentinghaus. (ed) "Applied Mineralogy in Research, Economy, Technology and Culture", vol Proc 6th Int Conf Appl Mineral. Balkema, Rotterdam, pp 95-98

Bell DR, Rossman GR (1992) Water in earth's mantle - the role of nominally anhydrous minerals. Science 255:1391-1397

Benn K, Nicolas A, Reuber I (1988) Mantle crust transition zone and origin of wehrlitic magmas - evidence from the Oman ophiolite. Tectonophysics 151:75-85

Benoit M, Ceuleneer G, Polve M (1999) The remelting of hydrothermally altered peridotite at mid-ocean ridges by intruding mantle diapirs. Nature 402:514-518

Berndt J, Koepke J, Holtz F (2005) An experimental investigation of the influence of water and oxygen fugacity on differentiation of MORB at 200 MPa. J Petrol 46:135-167

Berndt J, Liebske C, Holtz F, Freise M, Nowak M, Ziegenbein D, Hurkuck W, Koepke J (2002) A combined rapid-quench and H2-membrane setup for internally heated pressure vessels: Description and application for water solubility in basaltic melts. Am Mineral 87:1717-1726

Bezos A, Humler E (2005) The $Fe^{3+}/\Sigma Fe$ ratios of MORB glasses and their implications for mantle melting. Geochim Cosmochim Acta 69:711-725

Blatter DL, Carmichael ISE (1998) Plagioclase-free andesites from Ziticuaro (Michoacan), Mexico: petrology and experimental constraints. Contrib Mineral Petrol 132:121-138

Blundy JD, Holland TJB (1990) Calcic amphibole equilibria and a new amphibole-plagioclase geothermomemeter. Contrib Mineral Petrol 104:208-224

Bosch D, Jamais M, Boudier F, Nicolas A, Dautria JM, Agrinier P (2004) Deep and high-temperature hydrothermal circulation in the Oman ophiolite - Petrological and isotopic evidence. J Petrol 45:1181-1208

Botcharnikov RE, Koepke J, Almeev RR, Holtz F (2007 submitted) Experimental phase relations, mineral-melt equilibria and liquid lines of descent in a hydrous ferrobasalt - Implications for the Skaergaard intrusion and other natural systems. J Petrol

Botcharnikov RE, Koepke J, Holtz F, McCammon C, Wilke M (2005) The effect of water activity on the oxidation and structural state of Fe in a ferro-basaltic melt. Geochim Cosmochim Acta 69:5071-5085

Boudier F, Godard M, Armbruster C (2000) Significance of gabbronorite occurrence in the crustal section of the Semail ophiolite. Mar Geophys Res 21:307-326

Boudier FO, Nicolas A, Mainprice D (2005) Does anisotropy of thermal contraction control hydrothermal circulation at the moho level below fast spreading oceanic ridges? Int Geol Rev 47:101-112

Burnham WC (1979) The importance of volatile constituents. In: Yoder HS (ed) The evolution of the Igneous Rocks: Fiftieth Anniversary Perspectives, Princeton University Press, Princeton, pp 439-482

Chou IM (1987) Oxygen Buffer and Hydrogen Sensor Techniques at Elevated Pressures and Temperatures. In: Ulmer GC and Barnes HL (eds) Hydrothermal Experimental Techniques, John Wiley and Sons, New York, pp 61-99

Christie DM, Carmichael ISE, Langmuir CH (1986) Oxidation states of mid-ocean ridge basalt glasses. Earth Planet Sci Lett 79:397-411

Coogan LA, Wilson RN, Gillis KM, MacLeod CJ (2001) Near-solidus evolution of oceanic gabbros: Insights from amphibole geochemistry. Geochim Cosmochim Acta 65:4339-4357

Danyushevsky LV (2001) The effect of small amounts of H_2O crystallisation of mid-ocean ridge and backarc basin magmas. J Volcanol Geotherm Res 110:265-280

Danyushevsky LV, Eggins SM, Falloon TJ, Christie DM (2000) H_2O abundance in depleted to moderately enriched mid-ocean ridge magmas; Part I: Incompatible behaviour, implications for mantle storage, and origin of regional variations. J Petrol 41:1329-1364

Devine JD, Gardner JE, Brack HP, Layne GD, Rutherford MJ (1995) Comparison of microanalytical methods for estimating H_2O contents of silicic volcanic glasses. Am Mineral 80:319-328

Dick HJB, Natland JH, Alt JC, Bach W, Bideau D, Gee JS, Haggas S, Hertogen JGH, Hirth G, Holm PM, Ildefonse B, Iturrino GJ, John BE, Kelley DS, Kikawa E, Kingdon A, LeRoux PJ, Maeda J, Meyer PS, Miller DJ, Naslund HR, Niu Y, Robinson PT, Snow J, Stephen RA, Trimby PW, Worm H-U, Yoshinobu A (2000) A long in situ section of the lower ocean crust: results of ODP Leg 176 drilling at the Southwest Indian Ridge. Earth Planet Sci Lett 179:31-51

Dick HJB, Ozawa K, Meyer PS, Niu Y, Robinson PT, Constantin M, Hebert R, Maeda J, Natland JH, Hirth JG, Mackie SM (2002) Primary silicate mineral chemistry of a 1.5-km section of very slow spreading lower ocean crust: ODP Hole 735B, Southwest Indian Ridge. In: Natland JH, Dick HJB, Miller DJ, Von Herzen RP (eds) Proc. ODP, Sci. Results, vol 176, Chapter 10. Ocean Drilling Program, College Station, Texas, pp 1–61 [Online] Available from World Wide Web: http://www-odp.tamu.edu/publications/176_SR/volume/chapters/SR176_110.pdf

Dunn T, Sen C (1994) Mineral/matrix partition-coefficients for orthopyroxene, plagioclase, and olivine in basaltic to andesitic systems - a combined analytical and experimental study. Geochim Cosmochim Acta 58:717-733

Eggler DH, Burnham CW (1973) Crystallization and fractionation trends in system andesite-H_2O-CO_2-O_2 at pressures to 10 Kb. Geol Soc Am Bull 84:2517-2532

Ernst WG, Liu J (1998) Experimental phase-equilibrium study of Al- and Ti-contents of calcic amphibole in MORB - a semiquantitative thermobarometer. Am Mineral 83:952-969

Eugster HP (1957) Heterogeneous reactions involving oxidation and reduction at high pressures and temperatures. J Chem Phys 26:1760-1761

Feig ST, Koepke J, Snow JE (2006) Effect of water on tholeiitic basalt phase equilibria: an experimental study under oxidizing conditions. Contrib Mineral Petrol 152:611-638

Fialin M, Bezos A, Wagner C, Magnien V, Humler E (2004) Quantitative electron microprobe analysis of $Fe^{3+}/\Sigma Fe$: Basic concepts and experimental protocol for glasses. Am Mineral 89:654-662

Freise M, Holtz F, Nowak M, Scoates JS (2007, accepted) Differentiation and crystallization conditions of basalts from the Kerguelen large igneous province: An experimental study. Contrib Mineral Petrol

Gaetani GA, Grove TL (1998) The influence of water on melting of mantle peridotite. Contrib Mineral Petrol 131:323-346

Gaetani GA, Grove TL, Bryan WB (1993) The influence of water on the petrogenesis of subduction-related igneous rocks. Nature 365:332-334

Gaetani GA, Grove TL, Bryan WB (1994) Experimental phase relations of basaltic andesite from Hole 839B under hydrous and anhydrous conditions. In: Hawkins J, Parson, L., Allan, J., et al. (ed) Proceedings of the Ocean Drilling Program, Scientific Results, vol 135. Ocean Drilling Program, College Station, Texas, pp 557-563

Ghiorso MS, Sack RO (1995) Chemical mass transfer in magmatic processes IV. A revised and internally consistent thermodynamic model for the interpolation and extrapolation of liquid-solid equilibria in magmatic systems at elevated temperatures and pressures. Contrib Mineral Petrol 119:197-212

Grove TL, Baker MB (1984) Phase-equilibrium controls on the tholeiitic versus calc-alkaline differentiation trends. J Geophys Res 89:3253-3274

Grove TL, Bryan WB (1983) Fractionation of pyroxene-phyric MORB at low pressure - an experimental study. Contrib Mineral Petrol 84:293-309

Grove TL, Donnelly-Nolan JM, Housh T (1997) Magmatic processes that generated the rhyolite of Glass Mountain, Medicine Lake volcano, N California. Contrib Mineral Petrol 127:205-223

Grove TL, Juster TC (1989) Experimental investigations of low-Ca pyroxene stability and olivine pyroxene liquid equilibria at 1-atm in natural basaltic and andesitic liquids. Contrib Mineral Petrol 103:287-305

Grove TL, Kinzler RJ (1986) Petrogenesis of Andesites. Annu Rev Earth Planet Sci 14:417-454

Grove TL, Kinzler RJ, Bryan WB (1990) Natural and experimental phase relations of lavas from Serocki Volcano. In: Bryan WB, Juteau T, et al. (eds) Proceeding of the Ocean Drilling Program, vol 106/109 Part B. Ocean Drilling Program, College Station, Texas, pp 9-17

Hamilton DL, Burnham CW, Osborn EF (1964) The solubility of water and effects of oxygen fugacity and water content on crystallization in mafic magmas. J Petrol 5:21-39

Helz RT (1973) Phase relations of basalt in their melting ranges at PH_2O = 5kb as a function of oxygen fugacity. J Petrol 14:249-302

Helz RT (1976) Phase relations of basalt in their melting ranges at PH_2O = 5kb. Part II: melt compositions. J Petrol 17:139-193

Hirschmann MM, Aubaud C, Withers AC (2005) Storage capacity of H_2O in nominally anhydrous minerals in the upper mantle. Earth Planet Sci Lett 236:167-181

Hirschmann MM, Baker MB, Stolper E (1998) The effect of alkalis on the silica content of mantle-derived melts. Geochim Cosmochim Acta 62:883-902

Holloway JR, Burnham CW (1972) Melting relations of basalt with equilibrium water pressure less than total pressure. J Petrol 13:1-29

Holloway JR, Dixon JE, Pawley AR (1992) An internally heated, rapid-quench, high-pressure vessel. Am Mineral 77:643-646

Holtz F, Becker A, Freise M, Johannes W (2001) The water-undersaturated and dry Qz-Ab-Or system revisited. Experimental results at very low water activities and geological implications. Contrib Mineral Petrol 141:347-357

Holtz F, Behrens H, Dingwell DB, Johannes W (1995) H_2O solubility in haplogranitic melts - compositional, pressure, and temperature dependence. Am Mineral 80:94-108

Housh TB, Luhr JF (1991) Plagioclase-melt equilibria in hydrous systems. Am Mineral 76:477-492

Huebner JS, Sato M (1970) Oxygen fugacity-temperature relationships of manganese oxide and nickel oxide buffers. Am Mineral 55:934-952

Irvine TN, Baragar WRA (1971) Guide to chemical classification of common volcanic rocks. Can J Earth Sci 8:523-548

Ishikawa T, Nagaishi K, Umino S (2002) Boninitic volcanism in the Oman ophiolite: Implications for thermal condition during transition from spreading ridge to arc. Geology 30:899-902

Johnson MC, Anderson AT, Rutherford MJ (1994) Pre-eruptive volatile contents of magmas. In: Carroll MR, Holloway JR (eds) Volatiles in magmas. Rev. Mineral., vol. 30. Mineralogical Society of America, Washington, DC, United States, pp 281-330

Jurewicz AJG, Watson EB (1988) Cations in olivine: 1. Calcium partitioning and calcium-magnesium distribution between olivines and coexisting melts, with Petrologic Applications. Contrib Mineral Petrol 99:176-185

Juster TC, Grove TL, Perfit MR (1989) Experimental constraints on the generation of Fe-Ti basalts, andesites, and rhyodacites at the Galapagos spreading centre, 85°W and 95°W. J Geophys Res 94:9251-9274

Juteau T, Ernewein M, Reuber I, Whitechurch H, Dahl R (1988) Duality of magmatism in the plutonic sequence of the Sumail Nappe, Oman. Tectonophysics 151:107-135

Kagi R, Müntener O, Ulmer P, Ottolini L (2005) Piston-cylinder experiments on H_2O undersaturated Fe-bearing systems: An experimental setup approaching fO_2 conditions of natural calc-alkaline magmas. Am Mineral 90:708-717

Kawamoto T (1996) Experimental constraints on differentiation and H_2O abundance of calc-alkaline magmas. Earth Planet Sci Lett 144:577-589

Kawamoto T, Hirose K (1994) Au-Pd sample containers for melting experiments on iron and water-bearing systems. Eur J Mineral 6:381-385

Kelemen PB, Koga K, Shimizu N (1997) Geochemistry of gabbro sills in the crust-mantle transition zone of the Oman ophiolite: Implications for the origin of the oceanic lower crust. Earth Planet Sci Lett 146:475-488

Kilinc A, Carmichael ISE, Rivers ML, Sack RO (1983) The ferric-ferrous ratio of natural silicate liquids equilibrated in air. Contrib Mineral Petrol 83:136-140

Koepke J, Berndt J, Feig ST, Holtz F (2007) The formation of SiO_2-rich melts within the deep oceanic crust by hydrous partial melting of gabbros. Contrib Mineral Petrol 153: 67–84

Koepke J, Feig ST, Boudier F, Hellebrand E (2005a) Experimental study on crustal wehrlites of the Oman ophiolite: Experimental outline and microanalytical results. Ofioliti 30:197-198

Koepke J, Feig ST, Snow J (2005b) Hydrous partial melting within the lower oceanic crust. Terra Nova 17:286-291

Koepke J, Feig ST, Snow J, Freise M (2004) Petrogenesis of oceanic plagiogranites by partial melting of gabbros: an experimental study. Contrib Mineral Petrol 146:414-432

Koepke J, Feig ST, Snow JE (2005c) Late stage magmatic evolution of oceanic gabbros as a result of hydrous partial melting: Evidence from the Ocean Drilling Program (ODP) Leg 153 drilling at the Mid-Atlantic Ridge. Geochem Geophys Geosyst 6:2004GC000805

Koga KT, Kelemen PB, Shimizu N (2001) Petrogenesis of the crust-mantle transition zone and the origin of lower crustal wehrlite in the Oman ophiolite. Geochem Geophys Geosyst 2:2000GC000132

Kovalenko VI, Naumov VB, Yarmolyuk VV, Dorofeeva VA (2000) Volatile components (H_2O, CO_2, Cl, F, and S) in basic magmas of various geodynamic settings: Data on melt inclusions and quenched glasses. Petrology 8:113-144

Kress VC, Carmichael ISE (1991) The compressibility of silicate liquids containing Fe_2O_3 and the effect of composition, temperature, oxygen fugacity and pressure on their redox states. Contrib Mineral Petrol 108:82-92

Kvassnes AJS, Strand AH, Moen-Eikeland H, Pedersen R (2004) The Lyngen Gabbro: The lower crust of an Ordovician Incipient Arc. Contrib Mineral Petrol 148:358-379

Lachize M, Lorand JP, Juteau T (1996) Calc-alkaline differentiation trend in the plutonic sequence of the Wadi Haymiliyah section, Haylayn massif, Semail ophiolite, Oman. Lithos 38:207-232

Leake BE, Woolley AR, Arps CES, Birch WD, Gilbert MC, Grice JD, Hawthorne FC, Kato A, Kisch HJ, Krivovichev VG, Linthout K, Laird J, Mandarino JA, Maresch WV, Nickel EH, Rock NMS, Schumacher JC, Smith DC, Stephenson NCN, Ungaretti L, Whittaker EJW, Guo YZ (1997) Nomenclature of amphiboles: Report of the subcommittee on amphiboles of the International Mineralogical Association, commission on new minerals and mineral names. Am Mineral 82:1019-1037

Leschik M, Heide G, Frischat GH, Behrens H, Wiedenbeck M, Wagner N, Heide K, Geissler H, Reinholz U (2004) Determination of H_2O and D_2O contents in rhyolitic glasses. Phys Chem Glasses 45:238-251

Libourel G (1999) Systematics of calcium partitioning between olivine and silicate melt: implications for melt structure and calcium content of magmatic olivines. Contrib Mineral Petrol 136:63-80

Lindsley DH (1983) Pyroxene Thermometry. Am Mineral 68:477-493

Longhi J, Walker D, Hays JF (1978) Distribution of Fe and Mg between olivine and lunar basaltic liquids. Geochim Cosmochim Acta 42:1545-1558

Luhr JF (1990) Experimental phase-relations of water-saturated and sulfur-saturated arc magmas and the 1982 eruptions of El-Chichon volcano. J Petrol 31:1071-1114

Lundgaard KL, Tegner C (2004) Partitioning of ferric and ferrous iron between plagioclase and silicate melt. Contrib Mineral Petrol 147:470-483

Mandeville CW, Webster JD, Rutherford MJ, Taylor BE, Timbal A, Faure K (2002) Determination of molar absorptivities for infrared absorption bands of H_2O in andesitic glasses. Am Mineral 87:813-821

Martel C, Pichavant M, Bourdier JL, Traineau H, Holtz F, Scaillet B (1998) Magma storage conditions and control of eruption regime in silicic volcanoes: experimental evidence from Mt. Pelee. Earth Planet Sci Lett 156:89-99

Martel C, Pichavant M, Holtz F, Scaillet B, Bourdier JL, Traineau H (1999) Effects of fO_2 and H_2O on andesite phase relations between 2 and 4 kbar. J Geophys Res-Solid Earth 104:29453-29470

McCanta MC, Dyar MD, Rutherford MJ, Delaney JS (2004) Iron partitioning between basaltic melts and clinopyroxene as a function of oxygen fugacity. Am Mineral 89:1685-1693

Miyashiro A (1974) Volcanic rock series in island arcs and active continental margins. Am J Sci 274:321-355

Moretti R (2005) Polymerisation, basicity, oxidation state and their role in ionic modelling of silicate melts. Ann Geoph 48:583-608

Muntener O, Kelemen PB, Grove TL (2001) The role of H_2O during crystallization of primitive arc magmas under uppermost mantle conditions and genesis of igneous pyroxenites: an experimental study. Contrib Mineral Petrol 141:643-658

Mysen BO (2006) Redox equilibria of iron and silicate melt structure: Implications for olivine/melt element partitioning. Geochim Cosmochim Acta 70:3121-3138

Mysen BO, Carmichael ISE, Virgo D (1985) A comparison of iron redox ratios in silicate-glasses determined by wet-chemical and Fe-57 Mossbauer resonant absorption methods. Contrib Mineral Petrol 90:101-106

Natland JH, Dick HJB (2002) Stratigraphy and composition of gabbros drilled in Ocean Drilling Program Hole 735B, Southwest Indian Ridge: a synthesis of geochemical data. In: Natland JH, Dick HJB, Miller DJ, and Von Herzen RP (ed) Proc. ODP, Sci. Results, vol 176, pp 1–69 [Online] <http://www-odp.tamu.edu/publications/176_SR/VOLUME/SYNTH/SYNTH.PDF>

Natland JH, Dick HJB, Miller DJ, Von Herzen RP (2002) Proc. ODP, Sci. Results, vol 176. College Station, TX (Ocean Drilling Program) http://www-odp.tamu.edu/publications/176_SR/176sr.htm

Natland JH, Meyer PS, Dick HJB, Bloomer SH (1991) Magmatic oxides and sulfides in gabbroic rocks from Hole 735B and the later development of the liquid line of descent. In: Von Herzen RP, Robinson PT, et al., (ed) Proc. ODP, Sci. Results, vol 118, Ocean Drilling Program, College Station, TX, pp 75–111

Nicolas A (1989) Structures of ophiolites and dynamics of oceanic lithosphere. In: Kluver Academic Publishers, Dordrecht, p 367

Nicolas A, Mainprice D (2005) Burst of high-temperature seawater injection throughout accreting oceanic crust: a case study in Oman ophiolite. Terra Nova 17:326-330

Nicolas A, Mainprice D, Boudier F (2003) High-temperature seawater circulation throughout crust of oceanic ridges: A model derived from the Oman ophiolites. J Geophys Res-Solid Earth 108:2371

Nonnotte P, Ceuleneer G, Benoit M (2005) Genesis of andesitic-boninitic magmas at mid-ocean ridges by melting of hydrated peridotites: Geochemical evidence from DSDP Site 334 gabbronorites. Earth Planet Sci Lett 236:632-653

Ohlhorst S, Behrens H, Holtz F (2001) Compositional dependence of molar absorptivities of near-infrared OH- and H_2O bands in rhyolitic to basaltic glasses. Chem Geol 174:5-20

Osborn EF (1959) Role of oxygen pressure in the crystallization and differentiation of basaltic magmas. Am J Sci 257:609-647

Panjasawatwong Y, Danyushevsky LV, Crawford AJ, Harris KL (1995) An experimental study of the effects of melt composition on plagioclase - melt equilibria at 5 kbar and 10 kbar - Implications for the origin of magmatic high-An plagioclase. Contrib Mineral Petrol 118:420-432

Pearce JA, Lippard SJ, Roberts S (1984) Characteristics and tectonic significance of supra-subduction zone ophiolites. In: Kokelaar BP and Howells MJ (eds) Marginal basin geology, Blackwell, London, pp 77-94

Pitzer KS, Sterner SM (1994) Equations of state valid continuously from zero to extreme pressures for H_2O and CO_2. J Chem Phys 101:3111-3116

Pouchou JL, Pichoir F (1991) Quantitative analysis of homogeneous or stratified microvolumes applying the model "PAP". In: Heinrich KFJ and Newbury DE (eds) Electron probe quantification, Plenum Press, New York, pp 31-75

Putirka K, Johnson M, Kinzler R, Longhi J, Walker D (1996) Thermobarometry of mafic igneous rocks based on clinopyroxene-liquid equilibria, 0-30 kbar. Contrib Mineral Petrol 123:92-108

Putirka KD, Mikaelian H, Ryerson F, Shaw H (2003) New clinopyroxene-liquid thermobarometers for maric, evolved, and volatile-bearing lava compositions, with applications to lavas from Tibet and the Snake River Plain, Idaho. Am Mineral 88:1542-1554

Robie RA, Hemingway BS, Fisher JR (1978) Thermodynamic properties of minerals and related substances at 298,15 K and 1 Bar (105 Pascals) pressure and at higher temperatures. Geological Survey Bulletin 1452

Roeder PL (1974) Activity of iron and olivine solubility in basaltic liquids. Earth Planet Sci Lett 23:397-410

Roeder PL, Emslie RF (1970) Olivine-Liquid Equilibrium. Contrib Mineral Petrol 29:275-289

Rollinson H, Appel PWU, Frei R (2002) A metamorphosed, early Archaean chromitite from west Greenland: Implications for the genesis of Archaean anorthositic chromitites. J Petrol 43:2143-2170

Roux J, Lefevre A (1992) A fast-quench device for internally heated pressure vessels. Eur J Mineral 4:279-281

Saal AE, Hauri EH, Langmuir CH, Perfit MR (2002) Vapour undersaturation in primitive mid-ocean-ridge basalt and the volatile content of Earth's upper mantle. Nature 419:451-455

Sack RO, Carmichael ISE, Rivers M, Ghiorso MS (1980) Ferric-ferrous equilibria in natural silicate liquids at 1bar. Contrib Mineral Petrol 75:369-376

Sano T, Fujii T, Deshmukh SS, Fukuoka T, Aramaki S (2001) Differentiation processes of Deccan Trap basalts: Contribution from geochemistry and experimental petrology. J Petrol 42:2175-2195

Scaillet B, Pichavant M, Roux J (1995) Experimental crystallization of leukogranite magmas. J. Petrol. 36:663-705

Scaillet B, Pichavant M, Roux J, Humbert G, Lefevre A (1992) Improvements of the Shaw membrane technique for measurement and control of fH_2 at high-temperatures and pressures. Am Mineral 77:647-655

Schmidt BC, Scaillet B, Holtz F (1995) Accurate control of fH_2 in cold-seal pressure-vessels with the Shaw membrane technique. Eur J Mineral 7:893-903

Scholze H (1959) Über die quantitative IR-Spektroskopische Wasserbestimmung in Silicaten. Angew Chem-Int Edit 71:678-678

Schwab RG, Küstner D (1981) The equilibrium fugacities of important oxygen buffers in technology and petrology. N Jb Miner Mh 140:112–142

Shaw HR (1963) Hydrogen-water vapor mixtures - control of hydrothermal atmospheres by hydrogen osmosis. Science 139:1220-1222

Shaw HR, Wones DR (1964) Fugacity coefficients for hydrogen gas between 0°C and 1000°C, for pressures to 3000 atm. Am J Sci 262:918-929

Shipboard Scientific Party (2004) Drilling mantle peridotites along the mid-atlantic ridge from 14° to 16°N. In: Kelemen PB, Kikawa E, Miller DJ, et al., (ed) Proceedings of the Ocean Drilling Program, Initial Reports, vol 209. Ocean Drilling Program, College Station, Texas, pp 1-139

Sisson TW, Grove TL (1993a) Experimental investigations of the role of H_2O in calc-alkaline differentiation and subduction zone magmatism. Contrib Mineral Petrol 113:143-166

Sisson TW, Grove TL (1993b) Temperatures and H_2O contents of low-MgO high-alumina basalts. Contrib Mineral Petrol 113:167-184

Snow JE (2002) Major and trace element evolution of Hole 735B gabbros. In: Natland JH, Dick HJB, Miller DJ, Von Herzen RP (eds) Proc. ODP, Sci. Results, vol 176, Chapter 12. Ocean Drilling Program, College Station, Texas, pp 1-18 [Online]<http://www-odp.tamu.edu/publications/176_SR/chap_112/chap_112.htm>

Snyder D, Carmichael ISE, Wiebe RA (1993) Experimental study of liquid evolution in an Fe-rich, layered mafic intrusion: constraints of Fe-Ti oxide precipitation on the T-fO_2 and T-ρ paths of tholeiitic magmas. Contrib Mineral Petrol 113:73-86

Snyder DA, Carmichael ISE (1992) Olivine-liquid equilibria and the chemical activities of FeO, NiO, Fe_2O_3, and MgO in natural basic melts. Geochim Cosmochim Acta 56:303-318

Sobolev AV, Chaussidon M (1996) H_2O concentration in primary melts from supra-subduction zones and mid-ocean ridges: Implication for H_2O storage and recycling in the mantle. Earth Planet Sci Lett 137:45-55

Spulber SD, Rutherford MJ (1983) The origin of rhyolite and plagiogranite in oceanic crust - an experimental study. J Petrol 24:1-25

Stormer JC (1983) The effects of recalculation on estimates of temperature and oxygen fugacity from analyses of multicomponent iron titanium-oxides. Am Mineral 68:586-594

Sugawara T (2001) Ferric iron partitioning between plagioclase and silicate liquid: thermodynamics and petrological applications. Contrib Mineral Petrol 141:659-686

Tegner C (1997) Iron in plagioclase as a monitor of the differentiation of the Skaergaard intrusion. Contrib Mineral Petrol 128:45-51

Thy P (1995) Low-pressure experimental constraints on the evolution of komatiites. J Petrol 36:1529-1548

Thy P, Lesher CE, Fram MS (1998) Low pressure experimental constraints on the evolution of basaltic lavas from Site 917, southeast Greenland continental margin. In: Saunders AD, Larsen HC, Wise SW, Jr. (eds) Proc. ODP, Sci. Results, vol 152. Ocean Drilling Program, College Station, Texas, pp 359-372

Thy P, Lesher CE, Mayfield JD (1999) Low-pressure melting studies of basalt and basaltic andesite from the southeast Greenland continental margin and the origin of dacites at site 917. In: Larsen HC, Duncan RA, Allan JF, Brooks K (eds) Proc. ODP, Sci. Results, vol 163. Ocean Drilling Program, College Station, Texas, pp 95-112

Thy P, Lofgren GE (1994) Experimental constraints on the low-pressure evolution of transitional and mildly alkalic basalts - the effect of Fe-Ti oxide minerals and the origin of basaltic andesites. Contrib Mineral Petrol 116:340-351

Toplis MJ (2005) The thermodynamics of iron and magnesium partitioning between olivine and liquid: criteria for assessing and predicting equilibrium in natural and experimental systems. Contrib Mineral Petrol 149:22-39

Toplis MJ, Carroll MR (1995) An experimental study of the influence of oxygen fugacity on Fe-Ti oxide stability, phase relations, and mineral-melt equilibra in ferro-basaltic systems. J Petrol 36:1137-1170

Tribuzio R, Tiepelo M, Thirlwall MF (2000) Origin of titanian pargasite in gabbroic rocks from the Northern Apennine ophiolites (Italy): Insight into the late-magmatic evolution of a MOR-type intrusive sequence. Earth Planet Sci Lett 176:281-293

Von Herzen RP, Robinson PT, et al. (1991) Proc. ODP, Sci. Results, vol 118. College Station, TX (Ocean Drilling Program) doi:10.2973/odp.proc.sr.118.1991

Wager LR, Deer WA (1939) Geological investigations in East Greenland: Part III The petrology of the Skaergaard intrusion, Kangerdlugssuaq, East Greenland. Medd Groenl 105(4):1-352

Wagner TP, Donnellynolan JM, Grove TL (1995) Evidence of hydrous differentiation and crystal accumulation in the low-MgO, high-Al_2O_3 Lake basalt from Medicine Lake volcano, California. Contrib Mineral Petrol 121:201-216

Watson EB (1979) Calcium diffusion in a simple silicate melt to 30 Kbar. Geochim Cosmochim Acta 43:313-322

Wilke M (2005) Fe in magma - An overview. Ann Geoph 48:609-617

Wilke M, Behrens H (1999) The dependence of the partitioning of iron and europium between plagioclase and hydrous tonalitic melt on oxygen fugacity. Contrib Mineral Petrol 137:102-114

LEBENSLAUF

SANDRIN TILMAN FEIG

PERSÖNLICHE ANGABEN

- Anschrift: Bennostr. 1, 30451 Hannover
- Telefon: 0511 – 132 89 38 (privat)

    0511 – 762 52 80 (dienstlich)
- E-Mail: s.feig@mineralogie.uni-hannover.de
- Geburtsort: Freiburg im Breisgau
- Geburtstag: 25. Mai 1976
- Staatsangehörigkeit: deutsch
- Familienstand: ledig

SCHULISCHER UND AKADEMISCHER WERDEGANG

– 1993	Glocksee-Schule, Hannover
1993 – 1996	Karl-Friedrich-Gauß Schule, Hemmingen
	Abschluss: Abitur
1996 – 1997	Zivildienst im Kinderkrankenhaus auf der Bult, Hannover
1997 – 2002	Studium der Geowissenschaften an der Gottfried Wilhelm Leibniz Universität Hannover
	Abschluss: Diplom-Geowissenschaftler
	Thema der Diplomarbeit: Genese von Plagiograniten in Hochtemperatur-Scherzonen – Aufschmelzexperimente an gabbroiden Gesteinen aus den ODP-Legs 176 und 153
2002 –	Promotion und wissenschaftlicher Mitarbeiter am Institut für Mineralogie der Gottfried Wilhelm Leibniz Universität Hannover